NUMERICAL AND EXPERIMENTAL STUDIES ON MULTIPHASE FLOWS IN
MICROCHANNELS

A Thesis

Submitted to the Graduate School of Engineering and Natural Sciences

By

Abdolali Khalili Sadaghiani

In Partial Fulfillment of the

Requirements for the Degree

of

Master of Science in Mechatronics Engineering

July 2015

Sabanci University

NUMERICAL AND EXPERIMENTAL STUDIES ON MULTIPHASE FLOWS IN MICROCHANNELS

APPROVED BY:

Assoc. Prof. Ali Koşar
(Thesis Supervisor)
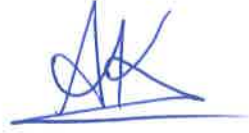
Assoc. Prof. Mehmet Yıldız

Prof. Dr. Yoav Peles

Assist. Prof. Gözde Ince

Assoc. Prof. Burç Mısırlıoğlu

DATE OF APPROVAL: 24/08/2015

Believe nothing, no matter where you read it, or who said it, no matter if I have said it, unless it agrees with your own reason and your own common sense.

ABSTRACT

NUMERICAL AND EXPERIMENTAL STUDIES ON MULTI-PHASE FLOWS IN MICROCHANNELS

ABDOLALI KHALILI SADAGHIANI

M.Sc. Thesis, July 2015

Supervisor: Associate Professor Ali Koşar

Keywords: Flow boiling, Nanofluid, Surface characteristics, Microchannel, Modeling

Microchannels are considered as one of the key elements in thermal management of microsystems. Despite the advantages of the microchannels, understanding of the fundamental hydrodynamic and thermal transport mechanisms in multiphase flows in them is far from satisfactory. Therefore, in this thesis using numerical and experimental approaches, it is aimed to focus on the understanding of phase change phenomena in order to be able to make use of them.

In the first study, convective heat transfer of alumina/water nanofluids in a microtube is presented using a numerical approach. The effects of nano-particle size and concentration on convective heat transfer are studied. Next, the effect of MWCNTs (multi-wall carbon nanotubes) on convective heat transfer was experimentally studied. The effect of MWCNT concentration on thermal performance is presented.

In the second study, high mass flux subcooled flow boiling of water in microtubes is investigated. Both experimental and numerical approaches are implemented to investigate high mass flux flow boiling in micro scale. Heat transfer coefficients are obtained as a function of mass flow rate, heat flux, and vapor quality.

In the third study, the effects of surface wettability and roughness on flow boiling in a rectangular microchannel are presented. Micro and nano-structured and nano-coated surfaces

are integrated into the channel to investigate the effect of surface characteristics on flow map, bubble formation and release and boiling heat transfer.

ÖZET

MİKROKANALLARDAKİ ÇOK FAZLI AKIŞ ÜZERİNE SAYISAL VE DENEYSEL ÇALIŞMALAR

ABDOLALI KHALILI SADAGHIANI

Yüksek Lisans Tezi, Temmuz 2015

Danışman: Doçent Doktor Ali Koşar

Anahtar Kelimeler: Akış Kaynaması, Nanoakışkan, Yüzey Karakteristikleri, Mikrokanal, Modelleme

Mikrokanallar mikrosistemlerin soğutulmasında anahtar unsurlardan biri olarak kabul edilmektedir. Mikrokanalların birçok avantajına karşılık, içerisindeki çok fazlı akışlarda temel hidrodinamik ve ısı transferi mekanizmaları tatmin edici düzeyde anlaşılamamıştır. Bundan duyulan motivasyonla bu tezde sayısal ve deneysel yöntemlerle faz değiştirme mekanizmalarının anlaşılması amaçlanmıştır.

İlk çalışmada mikrotüp içerisinde bulunan aluminyum/su nanoakışkanların taşınımlı ısı transferi sayısal olarak ele alınmıştır. Nano-parçacık boyutu ve konsantrasyonunun taşınımlı ısı transferi üzerindeki etkileri üzerinde durulmuştur. Daha sonra, çok katmanlı karbon nanotüp içeren nanoakışkanların taşınımlı ısı transferi ele alınmıştır. Çok katmanlı karbon nanotüplerin konsantrasyonunun termal performansa etkileri de işlenmiştir.

İkinci çalışmada, mikrotüpteki yüksek kütle akışlı ve doymamış koşullarda akış kaynaması araştırılmıştır. Hem deneysel hem de sayısal yaklaşımlarla mikro boyutta yüksek kütle akışlı kaynama ısı transferi incelenmiştir. Kütle akış hızı, ısı akısı ve buhar kalitesinin fonksiyonu olarak ısı transferi katsayıları elde edilmiştir.

Üçüncü çalışmada, dikdörtgen mikrokanaldaki akış kaynamasında yüzey ıslatılabilirliği ve pürüzlülüğünün etkisi sunulmuştur. Mikro ve nano yapılı ve nano kaplamalı yüzeyler kanal

içerisine entegre edilip, yüzey özelliklerinin ve yapısının akışa, baloncuk olması ve yüzeyden kopması ile birlikte kaynama ısı transferine etkileri araştırılmıştır.

ACKNOWLEDGEMENTS

TABLE OF CONTENTS

LIST OF TABLES

LIST OF FIGURES

NOMENCLATURE

A	area (m^2), constant number (-)
d, D	Diameter (m)
c$_p$	Specific heat capacity (J kg^{-1} K^{-1})
C_D	drag coefficient
d_p	nanoparticles diameter (m)
D_B	Brownian diffusivity, (m s^{-1})
D_h	hydraulic diameter of microchannel (m)
D_T	thermophoresis coefficient (m s^{-1})
f	Friction factor (-), frequency (s^{-1})
F	Force (N)
G	Mass flux (kg m^{-2}s^{-1}), term in the turbulent kinetic energy equation (kg m^{-1} s^{-3}), particle – particle interaction modules (Pa)
G_p	viscosity coefficient (Pa s)
h	convective heat transfer coefficient (W m^{2}K^{-1}), specific enthalpy (J kg^{-1})
h_p	fluid-particle heat transfer coefficient (W m^{-2} K^{-1})
H	Enthalpy (J)
h$_{fg}$	Latent heat of vaporization (kJ kg^{-1})
k	Conductivity(W m^{-1}K^{-1}), turbulence kinetic energy (J kg^{-1})
K	Projected area of bubbles (m^2)
k_B	Boltzmann constant (J K^{-1})
L	Length (m)

$\dot{m}$	Mass flow rate (kg s^{-1})
N_a	Active nucleation site density (-)
Nu	Nusselt number (-)
P	Pressure (Pa), Power (W)
Pr	Prandtl number (-)
Q,q	Heat (W)
$\dot{q}$	heat flux (W m^{-2})
q$'$	Volumetric heat generation (W m^{-3})
$\dot{Q}, \dot{q}$	Heat flux (W m^{-2})
R	Interaction force (N m^{-3})
R_{col}	particle–particle interaction force (N)
R_d	drag force (N)
R_{vm}	virtual mass force (N)
R_{pq}	interaction force (N)
Re	Reynolds number (-)
S	Source term
St	Stanton number (-)
T	Temperature (K)
t	Time (s)
u, v, w	Velocity components (m s^{-1})
V	Volume (m^3)
$\vec{V}$	Velocity vector (m s^{-1})

Greek

α	Volume fraction (-), thermal diffusivity (m^2 s^{-1})
β	Angle (degree), interphase drag coefficient (Pa s^{-1})
$\theta, \theta*$	non-dimensional temperatures
ε	Turbulence dissipation rate (J Kg^{-1} s^{-1})
τ	Shear tensor (Pa)
λ	Bulk viscosity (kg $m^{-1}s^{-1}$), mean free path (m)
μ	Dynamic viscosity (kg $m^{-1}s^{-1}$)
υ	Specific volume (m^3 kg^{-1})
ρ	Density (kg m^{-3})
τ	shear stress (Pa)
φ	volume fraction
σ	Surface tension (N m^{-1})
Ω	Portion of wall that is that is covered by vapor (-)

Subscripts

b	Bubble
c	Cross sectional
col	collision of particles
eff	Effective
f	Fluid
FC	Forced convection
g	Gas
h	Heated
i	inner, inlet, interfacial, phase index (=fluid, particle)

in	inlet
k	Related to turbulence kinetic
l	Liquid
lift	Lift force
LO	Entire flow as liquid
loss	Loss
ls	Liquid side
m	Mean, mixture
nf	nanofluid
0	Outer, outlet
ONB	Onset of nucleate boiling
p	particle
td	Turbulence dispersion
sp	Single phase
sat, s	Saturation
SB	Subcooled
t	Turbulence
tc	Fraction that is in contact with the liquid
tp	Two-phase
v	Vapor
vs	Vapor side
vm	Virtual mass
vw	Vapor and close to wall
vl	Wall lubrication

W	Wall
x	Location (m), vapor quality
ε	Related to turbulence dissipation
υ	Related to bubble shear

CHAPTER 1. INRODUCTION

1.1   Background and motivation

Miniaturization of the electronics systems has led to integration of more components in an electronic system. According to Moore's law (Moore 1965), the number of transistors integrated on a chip doubles every 2 years, such that the number of integrated transistors on a chip has been increased from 10000 in 1967 to more than 2 billion in 2014. Apparent consequences of Moore's law are the reduced size and increased performance of a microprocessor. Due to this electronics miniaturization the chip power densities have increased dramatically, so that much higher heat fluxes are needed to dissipate from microelectronic systems. Generated heat flux in microelectronics have reached hundreds of walls per centimeter square and it will continue to thousands in the near future. This amount of energies exceeded the based cooling limits. Practically, the ineffective cooling of high heat flux devices is a major constraint in dense packaging of microelectronics and has to be resolved in order to nurture the miniaturization process. Therefore, novel technologies for thermal management need to be developed in order to promote the miniaturization process.

Microchannels have received attention from scientific community and industry. One of the pioneer work in this area was done by Tuckerman and Pease (Tuckerman and Pease 1981) in mid 80s. They showed that the microchannels can be considered as an effective tool for heat dissipation due to their very promising and effective cooling potential. The use of microchannels in heat exchangers makes them compact (due to high surface area to volume ratio), lightweight and thermally efficient. The surface temperature of microchips has to be kept low enough to make sure about the reliable operation of them. Multiphase flows can maintain the require temperature of such systems. As an example latent heat associated with phase change of the fluids during the boiling process dictates the temperature of the fluid to the saturation temperature. Also the use of dispersed nano-particles in the fluid may allow the design of compact heat exchange devices using the less fluid inventory, for the same heat transfer performance, in comparison to the cases when single phase liquid is used as a coolant.

Although miniaturization of the microelectronics was one of the first motivations for microchannel work, the applications of microchannels are not limited to electronics industry. There are other science and engineering areas that benefit from several advantageous offered by microchannels. Micro channel heat exchangers may be used in automotive industry to reduce the refrigerant charge significantly as compared to conventional sized heat exchangers for the same effectiveness and heat transfer performance, great design flexibility may be achieved and space constraints can be overcome due to compactness of the heat exchanger. Few other application areas of micro channels which may be mentioned here are: fuel cells, chemical processing industry, microfluidics devices, separation and modification of cells in bio applications etc.

Despite the attractive and motivating advantages of the micro channels, the understanding of the fundamental hydrodynamic and thermal transport mechanisms especially in multiphase flows is far from satisfactory. Therefore, more studies are essential focusing on the understanding of governing phenomena in order to be able to use the micro channel heat sinks in appropriate fields of application.

1.1 Structure of the thesis

The current thesis is divided into several chapters as follows:

- The second chapter presents a brief introduction to multiphase flows and microchannels. Then a thorough literature survey in the field of nanofluid single phase flow, flow boiling in microchannels, and micro-scale flow boiling on structured and coated surfaces are presented.
- The third chapter is devoted to investigate nanofluid single-phase flow in microtubes using numerical and experimental approaches. Experimental studies on multi-wall carbon nanotube (MWCNT) based nanofluid, and numerical investigation of alumina (Al_2O_3) based nanofluid are presented in this chapter. At first experimental study consisting the sample preparation and characteristics, experimental setup and procedure, and thermal performance of proposed system is discussed. Next, numerical modeling is presented. Computational domain, code validation and

overning equations are given. Heat and flow characteristics in the proposed microtube are discussed in detail.

- The forth chapter presents numerical and experimental studies on high mass flux subcooled flow boiling in horizontal microtubes. In this chapter, at first experimental setup and procedure is presented and then the experimental test section is modeled numerically. The combined experimental and numerical results are presented at the end of this chapter.

- The fifth chapter is devoted to the experimental investigations on micro and nanostructured, and nano-coated surfaces. After describing the system and experimental setup, sample preparation and characteristics are presented. The effect of different surface on heat transfer performance and two-phase flow patterns is presented afterwards.

- Chapter six includes major conclusions and future work for multiphase flows in microchannel.

CHAPTER 2. MULTIPHASE FLOW IN MICRO-SYSTEMS LITERATURE REVIEW

2.1   Multiphase flows

Multiphase flow is consists of two or more separate phases, e.g. fluid or solid, and has the characteristic properties of a fluid. Multiphase transport phenomena must be considered in the design and optimization of many engineering systems, such as heat exchangers, electronics cooling devices, biotechnology, nanotechnology, and fuel cells. In each of these applications, the presence of multiple phases has a deep impact on systems' performance, and must be considered in order to achieve the system design objectives in the most efficient manner. The presence of several phases within a single system may significantly alter the performance of the system, since they increase its complexity and this effects the reliability of the system.

The flow dynamics of multiphase flow is quite different from the single phase flow. While it is much easier to derive the transport equations for a mixture, there is no general equivalent of the NS equation (Navier Stokes) for multiphase system. One way of deriving the equations of multiphase flows is using averaging procedure. Using this procedure it is possible to correctly describe the multiphase system's dynamics using general assumptions (Hiltunen and tutkimuskeskus 2009). The disadvantage of it is that the derived equations include more unknown than independent equations. Therefore, additional system dependent constitutive relations are needed.

Regarding many applications of multiphase flows e.g. fluidized bed, and nuclear and combustion reactors, it seem impossible to derive constitutive laws needed to describe interactions and materials properties of multiple phases, e.g. particle induced fluctuation motion of particle and liquid phases in a laminar flow of such system (look at 3.2.1). Even more, in a turbulence flow, averaging over this fluctuating motion leads to additional correlations. The dynamics of the turbulence flow and inter-phase interactions are difficult to solve, thus general and practical solutions are needed in this area (look at 4.2.3). A multiphase flow components may be a homogeneous mixture or clearly inhomogeneous. Since our interested multiphase flow are homogeneous rather than having inhomogeneous components (e.g. plug and stratified flows of gas and liquid in a partially filled channel), in

the rest of this section, a brief introduction on principles of modeling of such systems are presented.

Several alternative approaches can be taken in modeling of such flows. The most frequent method is to treat the multiphase fluid as a unique fluid with modified rheological characteristics that are functions of concentration of the secondary phase (look at 3.2.3.1). This approach may be used in cases where the phase's interaction effects can be adequately described using rheological variables, and/or the phases velocities are almost equal. One of the advantageous of this model is that modeling uses conventional single fluid algorithms. Single fluid approach seems to be adequate for studying simple characteristics of a particular case of multiphase flow.

Generally two different approaches have been developed for multiphase modeling (Hiltunen, Jäsberg et al. 2009). In the Eulerian model all phases are treated as fluids, obeying one phase equations of motion with appropriate boundary conditions defined at phase boundaries. The flow equations are derived from these equations of motion using an averaging procedure. There are several alternative ways of carrying this averaging procedure such as time averaging, volume averaging and ensemble averaging, or even a combination of these basic methods (Ishii 1975). Regardless of the method used, the averaging procedure leads to equations of the same form with a few extra terms. One example of these extra terms can be the interactions (change of mass, momentum etc.) at phase boundaries (see 3.2.1 and 4.2.3). Each averaging procedure may suggest different methods for solving the closure problems that are associated with the solution of these equations.

In general, the advantage of the Eulerian approach is it can be applied to any multiphase flow, regardless of the number and nature of the phases. On the other hand, the disadvantage of this model is that most of the times it leads to a complex sets of flow equations and closure conditions. In some applications such as for a relatively homogeneous suspension of dispersed phases that follows the motion of the continuous phase, it is possible to use so-called mixture model, a simplified formulation of Eulerian approach. The mixture model includes the conservation equations of the mixture as well as continuity equations for each dispersed phase. The slip velocity between the phases are calculated from approximate algebraic equations (Hiltunen and tutkimuskeskus 2009). Lagrangian approach is another

common method. In this method the fluid is treated as continuum phase while the motion of the particulate phase is obtained by integrating the equation of motion of individual particles along their trajectories. One result of such complexity related to multiphase flows is that the dynamics of these flows are still a branch of experimental fluid dynamics and yet the only key for many multiphase flow engineering problems especially at small scale models is trial and error testing (Hiltunen and tutkimuskeskus 2009).

2.2   Microchannels

The potential of using micro-systems in various fields of engineering and science along with the rapid advances in the production and use of high power micro-devices, have attracted attention of thermofluidics community. This led to widespread interest in the problems of microfluid mechanics and the need for both comprehensive and detailed treatment of the fundamental aspects of these phenomena (Yarin, Mosyak et al. 2008).

A micro channel could be one that exhibits different hydrodynamic or thermal behavior as compared to conventional channels and the physical phenomena dominant in conventional channels are no more important in micro channels. It is noted from the literature that single-phase classical theory is applicable in the case of micro channels. Conventional theory for two-phase flow is, however, not appropriate for micro channels. The terms mini and micro channel have been used in the literature without any particular criterion, although there have been some attempts to define the two terms. Some researchers define the same transition criterion between macro and micro for both single and two-phase flow in a channel while others distinguish between the two depending upon whether single or two-phase flow is prevalent in the channel.

A simple way to convey the dimensional range into consideration, is to classify the channel based on its hydraulic diameter, since it has various effects on different processes. Although criteria derivation based on the parameters of a specific process seems to be an acceptable choice, bearing in mind the number of parameters governing the macro to micro transition a classification based on dimensional characteristics of the channel is usually accepted in the literature (Kandlikar, Garimella et al. 2005).

The classification proposed by Mehendale et al. (Mehendale, Jacobi et al. 2000) divided the range from 1 to 100 (μm) as microchannels, 100 (μm) to 1(mm) as meso-channels, 1 to 6 (mm) as compact passages, and greater than 6 (mm) as conventional passages. The earlier channel classification scheme of Kandlikar and Grande (Kandlikar and Grande 2003) is slightly modified, and a more general scheme based on the smallest channel dimension is presented in Table 2.1 (Kandlikar, Garimella et al. 2005).

Table 2.1 Channel classification scheme

Channel Classification	Dimension length Limits
Conventional	$3e\text{-}3 < D_h$ (m)
Minichannels	$3e\text{-}3 > D_h > 2e\text{-}4$ (m)
Microchannels	$2e\text{-}4 > D_h > 1e\text{-}5$ (m)
Transitional Microchannels	$1e\text{-}5 > D_h > 1e\text{-}6$ (m)
Transitional Nanochannels	$1e\text{-}6 > D_h > 1e\text{-}7$ (m)
Nanochannels	$D_h < 1e\text{-}7$ (m)

Several macro-to-microscale transition criteria have been proposed by independent researchers varying from physical channel size classifications to approaches based on bubble confinement and bubble departure diameter. These criteria have so far not of proven and there exists no well-established criterion to define a threshold for transition from macro to micro scale channel. The word micro in fluid flow and heat transfer does not necessarily imply channels of micron size.

2.3   Heat and flow fields of multiphase flows in microscale

Heat transfer performance of a system is the function of working flow, fluid-solid interface and system physical properties. In this thesis, it is aimed to investigate the effects of two different fluid flows (water and nanofluid), surface characteristics (coated and roughened surfaces), and system dimensions (hydraulic diameter and length) on hydro-thermal performance of two and three-phase flows in microsystems. The structure of literature review

consists of three sections as studies related to nanofluids, subcooled flow boiling and flow boiling on structured and coated characteristics.

2.3.1 Nanofluids convective heat transfer

With fast advancements in microsystem technologies, it becomes a challenge to cool microelectromechanical systems (MEMS). As a result, many researchers have directed their efforts towards liquid coolants to improve heat transfer in micro devices. Consequently, research on heat and fluid flow in micro scale devices has rapidly progressed during this decade. Conventional fluids such as water have rather poor thermal properties. Therefore, many researchers have recently considered dispersing small particles in a base fluid to enhance cooling performances of micro and nano systems and studied thermophysical and hydrodynamic properties of such fluids (Siginer, Wang et al. 1995, Eastman, Choi et al. 2001, Das, Putra et al. 2003, Jang and Choi 2004, Tillman, Hill et al. 2006, Hwang, Jang et al. 2009, Fazeli, Hosseini Hashemi et al. 2012, Kurtoğlu, Bilgin et al. 2012, Şeşen, Tekşen et al. 2013, Kurtoğlu, Kaya et al. 2014, Turgut and Elbasan 2014). The dispersion (consisting of discrete nanosized particles and a conventional base fluid) with improved thermal properties was named as nanofluid by Choi et al. (Choi and Eastman 1995, J. A. Eastman 1996), who showed that the thermal conductivity of the base fluid could be increased up to 100 % upon adding nano-particles with a volume fraction of 1% to the base fluid.

There are many experimental studies on nanofluids in the literature (Xuan and Li 2003, Liu, Xiong et al. 2007, Jung, Oh et al. 2009, Wu, Wu et al. 2009, Ahn, Kim et al. 2010, Ahn, Kang et al. 2011, Liu and Yu 2011, Singh, Harikrishna et al. 2012, Zirakzadeh, Mashayekh et al. 2012, Narvaez, Veydt et al. 2014). Hwang et al. (Hwang, Jang et al. 2009) conducted an experimental study in order to investigate pressure drop and convective heat transfer coefficient for laminar alumina-water nanofluids in a uniformly heated tube. They discussed the effects of nanoparticles' migration due to the viscosity gradient, thermophoresis, and Brownian diffusion on the convective heat transfer enhancement in nanofluids and stated that the heat transfer enhancement cannot be contributed only by the thermal conductivity increment of nanofluids, and can also be related to the flattening of the velocity profile. Singh et al. (Singh, Harikrishna et al. 2012) investigated the effects of alumina nanoparticles' volume fraction and diameter on nanofluid convective flow in

microchannels. They stated that the main reason behind differential behavior of nanofluids may be due to shear induced migration of nanoparticles, which leads to nonuniform distribution of particles in nanofluid flow. Xuan and Lee (Xuan and Li 2003) investigated the effect of volume fraction and Reynolds number on convective heat transfer of turbulent copper-water nanofluid flows. They concluded that dispersed nanoparticles provided remarkable enhancements in heat transfer. They proposed a new convective heat transfer correlation for nanofluid flows in a tube. Jung et al. (Jung, Oh et al. 2009) experimentally studied convective heat transfer of nanofluids in a rectangular microchannel and showed that Nusselt number obtained from nanofluid with 1.8% nanoparticle volume fraction was up to 32% higher compared to the pure water case. Wu et al. (Wu, Wu et al. 2009) investigated convective heat transfer characteristics of alumina-water nanofluid laminar flows in trapezoidal microchannels. They observed that pressure drop and friction factor in nanofluids slightly increased when compared with those of pure water, while Nusselt number considerably increased. They found that the alumina nanoparticles deposited on the inner wall of microchannels more easily with increased wall temperature.

Although the majority of the studies in the literature show that adding nanoparticles to base fluid enhances heat transfer, there are also investigations stating otherwise. Liu and Yu (Liu and Yu 2011) conducted an experimental study to investigate single phase forced convection of alumina-water nanofluids. They concluded that, rather than enhancing convective heat transfer, the presence of nanoparticles caused deterioration of heat transfer in the transition and at the early stage of fully developed turbulent flows. Narvaez et al. (Narvaez, Veydt et al. 2014) investigated heat transfer characteristics of alumina nanofluid flows by designing a coolant loop apparatus to model a typical aircraft avionics cooling loop. Their results showed no evidence for heat transfer increment attribute to alumina nanoparticles additives.

From the numerical point of view, two major approaches, namely, homogeneous (single phase) and two-phase approaches have been employed to numerically investigate heat transfer characteristics of nanofluid flows (Kalteh, Abbassi et al. 2012). Most of the studies have been performed using the single phase (homogeneous) model (Khanafer, Vafai et al. 2003, Kim, Kang et al. 2004, Roy, Nguyen et al. 2004, Maïga, Palm et al. 2005, Akbarinia 2008, Choi and Zhang 2012, Fazeli, Hosseini Hashemi et al. 2012, Sakanova, Yin et al.

2014), where a homogeneous mixture of nanoparticles and the base fluid are considered as the nanofluid, whereas nanoparticles and the base fluid are considered as separate phases in the two-phase model (Fani, Kalteh et al. , Bianco, Manca et al. 2011, Mokhtari Moghari, Akbarinia et al. 2011).

Khanafer et al. (Khanafer, Vafai et al. 2003) numerically studied the effect of nanoparticle volume fraction on heat transfer. They presented an analysis based on thermophysical properties of nanofluids and proposed a heat transfer correlation for nanofluids. They found that the variants among models for the effective viscosity are pronounced. Kim et al. (Kim, Kang et al. 2004) studied convective instabilities driven by buoyancy and heat transfer characteristics of nanofluids. They showed that heat transfer was enhanced with the increase in volume fraction of nanoparticles. Roy et al. (Roy, Nguyen et al.) investigated hydrodynamic and thermal fields of alumina-water nanofluids in a radial laminar flow cooling system. They observed that inclusion of nanoparticles even with small volume fractions in a traditional coolant could provide considerable improvements in heat transfer. Maïga et al. (Maïga, Palm et al. 2005) numerically studied laminar forced convective flows of alumina-water and alumina-glycol nanofluids in a uniformly heated tube and a system of parallel, coaxial disks. They stated that although addition of nanoparticles to the base fluid produced a remarkable increase in heat transfer coefficients, it had a drastic adverse effect on the wall shear stress. Jou and Tzeng (Jou and Tzeng 2006) performed a numerical study on natural convection heat transfer enhancements of nanofluids filling a two-dimensional enclosure. They developed an empirical equation for average Nusselt numbers as a function of volume fraction and showed that increasing the nanoparticle fraction and buoyancy parameter enhance average heat transfer.

Göktepe et al. (Göktepe, Atalık et al.) numerically studied alumina-water nanofluid flows in a circular microtube for particle concentrations of 0.6%, 1% and 1.6% at a flow Reynolds number of 1050. They concluded that in comparison to the homogeneous model, the two-phase model predicted convective heat transfer coefficient and friction factor more accurately at the entry region. Kalteh et al. (Kalteh, Abbassi et al. 2011) studied water based copper nanofluid flows inside an isothermally heated micro channel and concluded that the two-phase model resulted in more heat transfer enhancement in comparison to the single

phase model. They found that heat transfer augmentation increased with the increase in nanoparticle volume concentration as well as with the decrease in the nanoparticle diameter. Fard et al. (Fard, Esfahany et al. 2010) performed a numerical investigation of convective heat transfer in laminar flows of nanofluids in order to compare the single and two-phase approaches. Their results showed that, for 2% concentration copper-water nanofluids, the average relative error between the experimental data and CFD results based on the single phase model was 16 %, while it was 8 % for the two-phase model. Nanofluid forced convection at constant heat flux and temperature conditions in developing flow through a tube was studied by Bianco et al. (Bianco, Chiacchio et al. 2009). They results showed that the difference between single-phase and two phase model becomes significant at 11% volume concentration. They used single and two-phase models considering both constant and temperature dependent properties. Behzadmehr et al. (Behzadmehr, Saffar-Avval et al. 2007) studied turbulent forced convective heat transfer of copper-water nanofluids in a circular tube. They used the two-phase mixture model and compared their results with the single phase (homogeneous) model. They stated that the two-phase model had more accurate results. Adding 1% volume fraction of nanoparticles increased the Nusselt number up to 15%, while it did not have any significant effect on the skin friction.

2.3.2   High mass flux flow boiling

Micro scale heat transfer attracted much attention of the heat transfer community because of its potential in its use in various engineering fields (Wang and Prasad 2000, Gavriilidis, Angeli et al. 2002, Nguyen and Wereley 2002, Trebotich, Zahn et al. 2002, Guo and Li 2003, Garimella, Singhal et al. 2006, Norton, Wetzel et al. 2006, Baffou, Quidant et al. 2010, Sesen, Khudhayer et al. 2010, Kaya, Ozdemir et al. 2013). With recent requirements from heat exchangers, continuous improvements in heat removal capacities of micro scale cooling systems have been taking place. Boiling in microchannels is considered as an effective method to obtain high heat removal rates (Agostini, Fabbri et al. 2007, Kosar 2012, Kaya, Demiryürek et al. 2013, Magnini, Pulvirenti et al. 2013, Çıkım, Armağan et al. 2014, Demir, Izci et al. 2014). Low critical heat flux and flow instabilities at particularly low mass velocities and low pressures restrict thermal performance of such systems involving phase change in micro scale. Since scaling laws are not applicable to two-phase flow and flow

boiling, there exists a lack of data and information about flow boiling under subcooled boiling and high flow rate conditions in micro scale (Collier and Thome).

During the last decade, fundamental differences between micro and macro scale boiling phenomena have been reported in some studies (Taitel and Dukler 1976, Mohammed Shah 1987, Hall and Mudawar 2000, Ribatski, Wojtan et al. 2006, Zhang, Hibiki et al. 2006, Cioncolini, Thome et al. 2009, Ong and Thome 2011, Ribatski 2013). Recent investigations were focused on developing new models and correlations for flow boiling in micro scale (Bertsch, Groll et al. 2009, Kosar 2009, Kandlikar 2010, Krishnamurthy and Peles 2010, Thome and Consolini 2010, Harirchian and Garimella 2012). Small scale dimensions limit experimental studies in obtaining local heat transfer and flow characteristics in micro scale. Computer based modeling is considered as a powerful tool to assess local thermal and hydrodynamic characteristics and can be utilized for design and optimization of micro devices.

High mass flux boiling is getting more and more popular, where instabilities become suppressed and higher critical heat fluxes would be achieved. Increasing flow rate changes boiling mechanism from saturated boiling to subcooled low quality boiling inside micro systems. Experimental studies on heat transfer characteristics on low quality flow boiling are already present in the literature (Pierre and Bankoff 1967, Liu and Winterton 1991, Collier and Thome 1994, Bartel 1999, Kandlikar 1999, Mudawar and Bowers 1999, Lee, Park et al. 2002, Haynes and Fletcher 2003, Ghiaasiaan 2008, Wang and Cheng 2009). Due to the importance of high mass and heat flux flow boiling studies in micro scale, the availability of reliable results and models related to local heat transfer coefficient and pressure drop are vital for researchers and engineers.

One of the first experimental investigations in subcooled flow boiling was conducted by Pierre and Bankoff (Pierre and Bankoff 1967). They measured void fraction at different cross sections in a vertical rectangular channel. Their experiments showed no evidence of void peak near the walls. This is important because implementing the wall lubrication force for adiabatic two-phase flow resulted in the void fraction peak near the wall boundaries. This was proven to be advantageous for air/water two-phase flows as well as for water flow boiling. (Bartel, Ishii et al. 2001, Končar, Kljenak et al. 2004, Lucas, Shi et al. 2004).

Bartel and Lee et al. (Bartel 1999, Lee, Park et al. 2002) studied radial flow characteristics in vertical tubes. Their measurements showed that the local void fraction decreased from the heated surface to the subcooled liquid core. They also observed that the liquid velocity profiles generally deviated from the profiles of single-phase flow due to the non-uniform void fraction and vapor velocity distributions. Lie and Lin (Lie and Lin 2006) experimentally investigated channel size affects subcooled flow boiling heat transfer and associated bubble characteristics of refrigerant R-134a in a horizontal narrow annular duct. They found that subcooled flow boiling heat transfer coefficient increased with a reduction in the gap size, but decreased with an increase in the inlet liquid subcooling for subcooled boiling of R-134a. Furthermore, in the light of a visualization study, they concluded that the bubble growth was suppressed so that smaller and fewer bubbles emerged with the increase in refrigerant mass flux and inlet subcooling. Wang and Cheng (Wang and Cheng 2009) investigated subcooled flow boiling and microbubble emission boiling (MEB) phenomena of deionized water in a partially heated Pyrex glass microchannel. Their results indicated that a vapor bubble in contact with a highly subcooled liquid could break up into many microbubbles due to condensation and instability of bubble interface between vapor and subcooled water. They concluded that occurrence of MEB in microchannel can remove a large amount of heat flux with only a moderate rise in wall temperature.

Martín-Callizo et al. (Martín-Callizo, Palm et al. 2007) investigated subcooled flow boiling heat transfer for refrigerant R-134a in vertical cylindrical micro- and mini-tubes. They found that the wall superheat at ONB (onset of nucleate boiling) was essentially higher than that predicted with correlations for larger tubes. They concluded that an increase in mass flux leads to early subcooled boiling resulting in an increase in heat transfer coefficient, whereas for fully developed subcooled boiling, an increase in mass flux only resulted in a slight improvement of the heat transfer. Furthermore, higher inlet subcooling, higher system pressure and smaller channel diameter led to better boiling heat transfer. Yuan et al. (Yuan, Wei et al. 2009) conducted experiments to study subcooled flow boiling heat transfer of FC-72 in micro pin fin microchannel. Their results showed that flow boiling curves for the micro-pin-finned surfaces in the nucleate boiling region are only slightly affected by fluid velocity and subcooling, but shifted towards a smaller wall temperature compared to that of the pool boiling case. They concluded that micro-pin-finned surfaces generated a considerable heat

transfer enhancement compared to smooth surfaces. Suzuki et al. (Suzuki, Kokubu et al. 2005) studied subcooled flow boiling of water in a horizontal rectangular channel for large heating surfaces. They concluded that heat transfer enhancement in boiling could be achieved with highly subcooled flow boiling via microbubble emission boiling and microbubble emission boiling occured in transition boiling.

Haynes and Fletcher (Haynes and Fletcher 2003) investigated heat transfer in subcooled flow boiling of refrigerants R11 and HCFC123 inside a microtube. They claimed that both convective and nucleate boiling heat transfer contributions were important in subcooled boiling heat transfer. Mudawar and Bowers (Mudawar and Bowers 1999) studied high mass flux subcooled flow boiling of water in microtubes. They reported that the maximum critical heat flux for flow boiling in a microtube was achieved at a specific small heated length, and further decrease in heated length would be impractical. Kaya et al. (Kaya, Ozdemir et al. 2013) studied critical heat flux in flow boiling of deionized water at high mass fluxes in microtubes for different heated lengths and developed new CHF (critical heat flux) prediction correlations. They concluded that CHF had a stronger relationship with mass flux unlike the weaker trend in previous macro scale studies in the literature. Their results indicated that CHF decreased with increasing length/diameter ratio.

Besides experimental studies on flow boiling in microchannels, recent advances in computational fluid dynamics (CFD) allow numerical modeling and would provide valuable insight into local characteristics of flow boiling (Cheung, Vahaji et al. 2014, Yeoh, Vahaji et al. 2014). Among multiphase models of flow boiling, the Eulerian model is one of the widely used approaches (Aminfar, Mohammadporfard et al. 2013). There are some studies numerically investigating subcooled boiling (Luo and Svendsen 1996, Roy, Kang et al. 2002, Tu and Yeoh 2002, Zhuan and Wang 2010, Rui and Wen 2011, Wei, Pan et al. 2011, Zhuan and Wang 2012, Ganapathy, Shooshtari et al. 2013, Magnini, Pulvirenti et al. 2013). Tu and Yeoh (Tu and Yeoh 2002) conducted a numerical study for modeling low pressure flow boiling using the CFX-4.2 code. They studied important modeling issues and parameters of subcooled flow boiling such as partitioning of the wall heat flux, mean bubble diameter, and bubble departure diameter. It was shown that the void fraction increased along the channel and with respect to increasing subcooling.

Koncar et al. (Končar, Kljenak et al. 2004) performed multidimensional modeling of vertical upward subcooled flow boiling using a two-fluid approach and calculating local two-phase flow parameters (void fraction and bubble size). They modeled the evolution of cross-sectional distributions of two-phase flow parameters along the flow at low-pressure conditions using a two-fluid model. Yun et al. (Yun, Splawski et al. 2012) examined a mechanistic bubbles size model to enhance the prediction capability in subcooled flow boiling of a CFD code. They applied advanced subcooled boiling models such as new wall boiling and two-phase logarithmic wall function models for an improvement of energy partitioning and two-phase turbulence models, respectively. Their results indicated that the velocity wall function for flow boiling can improve the prediction capability of phase velocity. Yeoh and Tu (Yeoh and Tu 2004) employed population balance equations combined with a three-dimensional two-fluid model to predict bubbly flows with the presence of heat and mass transfer processes. In their model, the range of bubble sizes in subcooled flow boiling was distributed according to the division of 15 diameter groups through the formulation of a MUSIG model.

Narumanchi et al. (Narumanchi, Troshko et al. 2008) numerically studied turbulent jet impingement involving nucleate boiling using the CFD code FLUENT. For nucleate boiling, the Eulerian multiphase model was used. They implemented a mechanistic model of nucleate boiling in a user-defined function (UDF) in FLUENT. Xu et al. (Xu, Wong et al. 2006) developed a one-dimensional, non-equilibrium two-fluid model for the predictions of low-pressure subcooled flow boiling. Their results indicated that at low pressure the void fraction was insensitive to the fraction of the heating surface covered by the fluid. They concluded that buoyancy force plays an important role on the void fraction evolvement, especially at low velocity for vertical downward-flows. Basu et al. (Basu, Warrier et al. 2005, Basu, Warrier et al. 2005) developed a mechanistic model for subcooled flow boiling for prediction of wall heat flux as a function of wall superheat considering bubble dynamics on the heater surface. Their model proposed that all the wall energy was first transferred to the superheated liquid layer adjacent to the wall, whereas the evaporative component was independently found.

Roy et al.(Roy, Kang et al. 2002) numerically investigated turbulent subcooled flow boiling of refrigerant R-113 in a vertical channel. Their results were compared with the experimental studies, and a reasonably good agreement was obtained. Končar et al. (Koncar, Krepper et al. 2005) numerically modeled subcooled flow boiling using CFD code CFX-5 for pressure range of 3 to 11 (MPa), mass flow rate of about 1000 (kg/m^{2}s) and heat fluxes up to 1.2 (MW/m^2). They concluded that it is necessary to model the effects of bubble induced turbulence and non-drag forces for realistic simulation of the two-phase flow field. Wang and Zhuan (Zhuan and Wang 2010, Rui and Wen 2011, Zhuan and Wang 2012) modeled flow boiling in mini and microchannels. They investigated bubble characteristics and flow regimes for various flow patterns and compared liquid-gas flow patterns to the experimental results. Their results indicated that both bubble growth and coalescence lead to early occurrence of flow pattern transitions at high heat flux and mass velocity. At low mass velocity and high heat flux, action of bubble expanding is apparent in the flow pattern evolution. Magnini et al. (Magnini, Pulvirenti et al. 2013) numerically investigated bubble behavior in two-phase flows. They proposed a transient heat conduction based boiling heat transfer model for the liquid film region.

Ganapathy et al. (Ganapathy, Shooshtari et al. 2013) performed a numerical study on two-phase flows inside a single microchannel. Their simulated condensation flow regimes were qualitatively compared to those available in the experimental visualization database, and a favorable agreement was obtained. Wei et al. (Wei, Pan et al. 2011) numerically investigated bubble dynamics in subcooled flow boiling using the VOF (Volume of Fluid) method. Bubble coalescence, sliding, detachment from the heated wall, and bubble shape variation during lifetime were examined. They claimed that the fluctuation of mass flow rate caused by swing motion significantly affected hydrodynamic pressure, drag and shear lift forces, which would further influence bubble sliding and detachment, and would change heat transfer near the heated wall. Their results indicated that pressure drop of flow boiling fluctuated around that of the single phase flow, and the amplitude of fluctuations was increased with wall heat flux. Li et al. (Li, Wei et al. 2009) modeled bubble departure characteristics with the CFX commercial software. Comparison of the numerical results with the experimental data demonstrated that surface tension was crucial in modeling bubble departure diameter and active nucleate site density.

2.3.3 Flow boiling on structured and coated surfaces

It has long been known that surface characteristics have a significant effect on nucleate boiling heat transfer. Several investigations have focused on developing methods of enhancing heat transfer rates. Subcooled flow boiling heat transfer enhancement using enhanced surfaces is one of the state-of-the-art studies for heat flux dissipation from confined spaces or small area in different applications such as compact heat exchangers, heat sinks, cooling of small electric devices and engine cooling system design (Torregrosa, Broatch et al. 2014). Mechanical sanding is one way for changing the roughness of surface. Piasecka (Piasecka 2014) investigated the use of single-sided enhanced foil surface with various depressions for a heating element for an FC-72 laminar flow in a rectangular minichannel. According to this study, beside typical shape of boiling curves, untypical boiling curves with several stepped courses of nucleation hysteresis in the region of developed nucleate boiling were found and also gradual increase in the void fraction and heat flux were occurred. Porosity on the surface is another parameter which affects the subcooled flow boiling heat transfer, especially in the case of micro-porosity as can studied by Zhang et al. (Sun, Zhang et al. 2011)

Messina and Park (Messina and Park 1981) by changing surface micro geometry by etching Cu plate surface with pit arrays, sanding and mirror by polishing with Freon-113 at 1 bar pressure reported CHF enhancement in pool boiling. In another study, Ferjancic and Golobic (Ferjančič and Golobič 2002) improved Ra by etching the Fe ribbon and changing roughness by sanding and using water and FC-72 as working fluids at atmospheric pressure investigated roughness effect and reported CHF enhancement in pool boiling. On the other hand, using special materials for coating surface of the plate is another way for changing surface morphology and researching on this type of enhanced surface on flow boiling heat transfer. Kumar et al. (Kumar, Suresh et al. 2014) investigated effects of coating material such as vertically aligned CNT on cupper substrate on CHF and enhancement of 20% was observed at desired mass flux during this experimental study. Yang et al. (Yang, Dai et al. 2014, Yang, Dai et al. 2014) showed enhancement up to 300% of flow boiling CHF by using superhydrophilic Si nanowires inner walls.

Hwang and Kaviany (Hwang and Kaviany 2006) investigated the effects of porous coatings on critical heat flux. They found 80% enhancement in critical heat flux (CHF). Sarwar et al. (Sarwar, Jeong et al. 2007) introduced Al_2O_3 microporous coatings on samples in flow boiling. They concluded that particles having sizes smaller than 10 (μm) and coating thicknesses of 50 (μm) increases CHF up to 25%. Khanikar et al. (Khanikar, Mudawar et al. 2009) performed experiments on carbon nanotube coated surfaces and found have higher critical heat fluxes. They concluded that CNT coated surfaces can be considered as an alternative for augmentation for boiling heat transfer.

Jeong et al. (Jeong, Sarwar et al. 2008) used surfactant solutions (trisodium phosphate (TSP, Na3PO4, 12H2O)) for surface modification. CHF enhancement up to 50% achieved in their study. Kim and Kim (Kim and Kim 2009) used different nanoparticles (TiO_2, Al_2O_3, and SiO_2) to investigate critical heat flux of aqueous nanofluids. Their experiments showed enhancement in CHF. They claimed that the main reason was deposition of nano-particles on the heating surface. In other words, deposited nanoparticles on the heating surface changed the surface properties such as surface wettability, surface roughness, and maximum capillary wicking height.

Sesen et al. (Şeşen, Khudhayer et al. 2010) investigated pool boiling on a plate having an array of copper nanorods with an average diameter 100 (nm) and length 500 (nm) was integrated. They found that nanostructured surfaces have the potential to be an effective method for micro-cooling systems and heat generators. They showed 100% enhancement in heat transfer coefficient. To observe the effects of nano-sheets, Park et al. (Park, Lee et al. 2010) used graphene/graphene-oxide nano-sheets as an additive in nanofluids. Their results showed that these nano-sheets extended boiling curves. They claimed that the reason was attributed to formation of self-porous surface structure of nano-sheets.

The effect of silica nanoparticle coatings on critical heat flux was studied by Forrest et al. (Forrest, Williamson et al. 2010) and showed 100% enhancement in CHF. They concluded that surface wettability was severely changed with silica nanoparticle thin film coating.

Morshed et al. (Morshed, Yang et al. 2012) conducted flow boiling experiments on copper nanowire coatings in microtubes. Their experiments showed 56% increment in heat transfer coefficients using the copper nanowire coatings. The effect of surface wettability on critical heat flux was studied by Phan et al. (Phan, Caney et al. 2012). They concluded that surface with the lower contact angles could extend the boiling curves. Ahn et al. (Ahn, Kang et al. 2012) studied critical heat flux of flow boiling using micro/nanostructured surfaces. They showed that under the annular flow regime the CHF is dramatically enhances. They concluded that this may related to high wettability of such surfaces, which enhances the liquid replacement and liquid film stability. Betz et al. (Betz, Jenkins et al. 2013) investigated pool boiling on superhydrophobic to superhydrophilic surfaces. They concluded that hydrophilic surfaces have higher heat transfer coefficients due to their higher surface wettability.

The effect of aluminum nanostructured surfaces on pool boiling was investigated by Saeidi and Alemrajabi (Saeidi and Alemrajabi 2013). It was found 8% increment in CHF and 160% in heat transfer coefficient for structured aluminum plates in comparison to untreated plates. Tang et al. (Tang, Tang et al. 2013) performed experiments of nucleate pool boiling heat transfer on nanoporous copper surface. For low heat fluxes, lower wall superheats and higher heat transfer coefficients was observed for structured surfaces. The effect of hydrophobic titania coatings on pool boiling was investigated by Yongwei et al. (Cai, Liu et al. 2013). Their results indicated that thinner coatings have higher heat transfer coefficients.

CHAPTER 3. NANOFLUID CONVECTIVE FLOW IN HORIZONTAL MICROTUBES

Nanofluid is considered as new type of fluid consisting of suspension of nano sized particles in a base fluid (e.g. copper/ethylene glycol, and copper oxide/water nanofluids) (Saidur, Leong et al. 2011). Nanoparticles (metal or metal oxide) increase thermal conductivity of the base fluid, and augment heat transfer removal from the coolant (Siginer, Wang et al. 1995). Nanofluids have following advantages in comparison to conventional solid liquid suspensions (Siginer, Wang et al. 1995):

- More heat transfer surface due to high specific surface area.
- High dispersion stability due to Brownian motion of particles.
- Lower pumping power in comparison to pure liquids.
- Adjustable properties such as surface wettability and thermal conductivity using particle concentration.

In chapter 3, numerical and experimental investigations on hydro-thermal characteristics of nanofluid single phase convective flow in horizontal microtubes is presented. At first, experimental study on multi-wall carbon nanotubes (MWCNTs) based nanofluid is studied. Then, alumina (Al_2O_3) based nanofluid is investigated numerically in horizontal microtubes.

3.1   Description of the experiments

3.1.1   Nanofluid

Hydro-thermal characteristics of nanofluids are functions of the size, type, and hydro-thermal properties of the nanoparticle. Multi-walled carbon nanotube was used in the experiments, where base fluid was considered as distilled water. Nanofluids were prepared using two-step method, where produced dry MWCNT powder (first step) is mixed in the base fluid (second step). In order to prevent aggregation 2500 ppm Sodium Dodecyl Sulfate (SDS) was added to base fluid as surfactant. Outer diameter of multi wall carbon nanotubes is 10-20 nm and length of them is 1-2 µm. Stirring and sonication were done for 1 hour in the sonication bath. Fig. 3.1 shows the SEM images of the multi-wall carbon nanotubes.
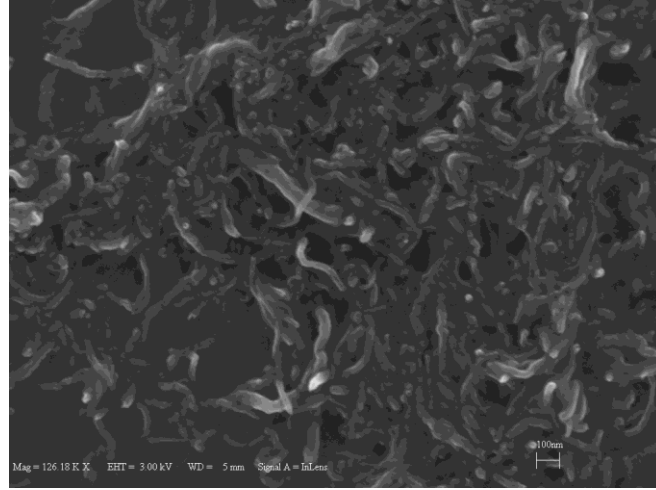
Fig. 3.1. SEM image of MWCNT.

The thermophysical properties of nanofluids such as density, viscosity, heat capacity, and conductivity were calculated using widely used correlations. These correlations calculate the properties of nanofluid using base fluid and nano-particle properties (Maxwell 1881, Pak and Cho 1998, Khanafer, Vafai et al. 2003, Selvakumar and Suresh 2012):

$$\rho_{nf} = (1-\varphi)\rho_{bf} + \varphi\rho_{np} \tag{3.1}$$

$$\mu_{nf} = \rho_{bf}(1-2.5\varphi) \tag{3.2}$$

$$c_{p,nf} = (1-\varphi)c_{p,bf} + \varphi c_{p,np} \tag{3.3}$$

$$k_{nf} = \frac{2k_{bf} + k_{np} + 2\varphi(k_{np} - k_{bf})}{2k_{bf} + k_{np} - \varphi(k_{np} - k_{bf})}k_{bf} \tag{3.4}$$

Here nf, bf and np refers to the nanofluid, base fluid and nanoparticle, respectively. In these equations, φ is the volume fraction ratio, ρ is the density, μ is the viscosity, c_p is the specific heat, and k is the thermal conductivity.

3.1.2 Experimental setup and procedure

Convective heat transfer of distilled water-based multi-walled carbon nanotubes in microtubes with 889 and 1067 μm inner and outer diameters, respectively was investigated. Nanofluids with 0.25%, 0.5% and 1% weight fractions and inlet temperatures of 22.5 and 26 ºC were studied.

The experimental setup consists of a syringe pump, a stainless steel tube as the test section, a pressure sensor, and a DC power supply. The schematic of the test section is showed in Fig. 3.2. Wall heat flux was applied using Joule heating. As it is seen, the experimental setup is an open loop system, where the working fluid is collected at the outlet via a reservoir. Volumetric flow rate was fine controlled via syringe pump with fixed inlet temperatures.
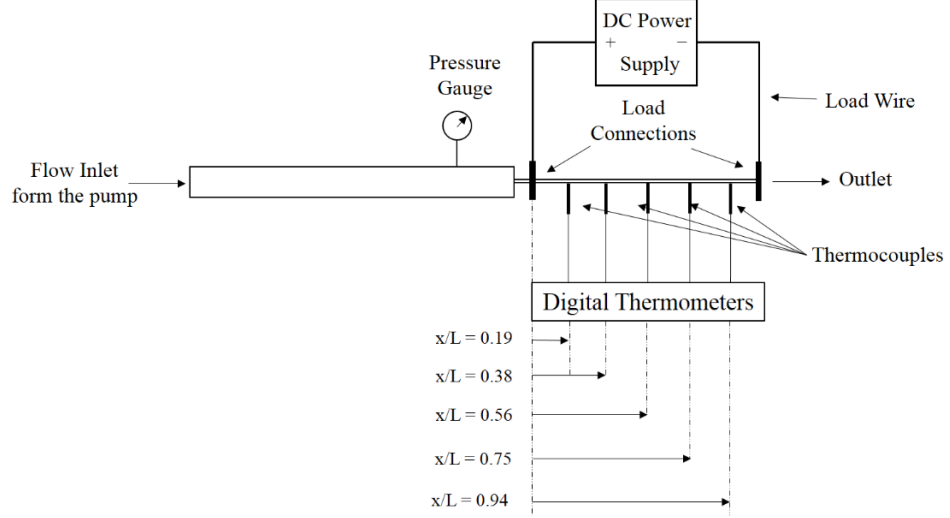
Fig. 3.2. Schematic of the test section

3.1.3 Data reduction

Obtained temperature, pressure, and heat flux data are used for calculating the fiction factor, heat transfer coefficient, and Nusselt number. Friction factor of the system is calculated as:

$$f = \frac{2\Delta P \, D_i}{L_t \, \rho_{nf} \, u_{nf}^2} \quad (3.5)$$

Here, ΔP is the pressure drop, D_i is inner diameter of the microtube, L_t is the microtube length, and u is the flow velocity. 1-D steady state radial heat conduction with constant properties and uniform volumetric heat generation is assumed for temperature analysis due to the ratio of tube length to tube thickness.

As a result, the local inner surface temperature of the microchannel, $T_{w,i}$, is expressed in terms of the measured local outer surface temperature, $T_{w,o}$, as

$$T_{w,i} = T_{w,o} + \frac{\dot{q}_{net}}{4k_{ss}}\left(\frac{D_o^2}{4} - \frac{D_i^2}{4}\right) - \frac{\dot{q}_{net}}{2k_{ss}}\frac{D_o^2}{4}\ln\left(\frac{D_o}{D_i}\right), \text{ where } T_{w,o} \text{ is the outlet wall temperature,}$$

22

$\dot{q}_{net}$ is the volumetric net heat flux, k_{ss} is the stainless steel thermal conductivity, and D_o and D_i are microtube inner and outer diameters, respectively.

Fluid temperature is calculated by using the following energy balance equation as $T_f = T_{in} + \dfrac{(P - Q_{loss}) x_{th}}{\dot{m} c_{p,nf} L_h}$. Here T_f and T_{in} are the fluid and inlet temperatures, respectively,

P is the electrical power, $\dot{m}$ is the mass flow rate, Q_{loss} is the heat loss, and x_{th} is the thermocouple location. Nanofluid heat transfer coefficient is calculated as:

$$h = \frac{(P - Q_{loss})}{A_s (T_{w,i} - T_f)} \quad (3.6)$$

For average heat transfer coefficient, $T_{w,i}$ is taken as the average inner wall temperature, and T_f is taken as the average fluid temperature obtained from exit and inlet fluid temperatures. Thus mean average temperature difference was used for average heat transfer coefficient calculations as $T_{w,i} - T_f = \dfrac{1}{4}(T_{w,2} + T_{w,3} + T_{w,4} + T_{w,5}) - \dfrac{1}{2}(T_{in} - T_{out})$[13].

The maximum uncertainties in experimental parameters are given in Table 3.1. They were provided by the manufacturer's specification sheets or were obtained using the propagation of uncertainty method presented in Coleman and Steele (Coleman and Steele 2009) study.

Table 3.1.Estimated uncertainties

Parameter	Uncertainties
Electrical power (P)	$\pm\,0.32\%$
Flow rate ($\dot{m}$)	$\pm\,0.4\%$
Friction factor (f)	$\pm 1.4\%$
Inner diameter (D_i)	$\pm\,2\mu m$
Fluid Temperature (T)	$\pm\,0.1^oC$
Outer diameter (D_o)	$\pm\,1\mu m$
Heat transfer coefficient (h)	$\pm\,3.2\%$

3.1.4 Validation

Single-phase water flow experiments were conducted in order to validate the test setup and data reduction. Obtained results are shown in figure. As it is seen, a good agreement between obtained results and predicted by correlations achieved.
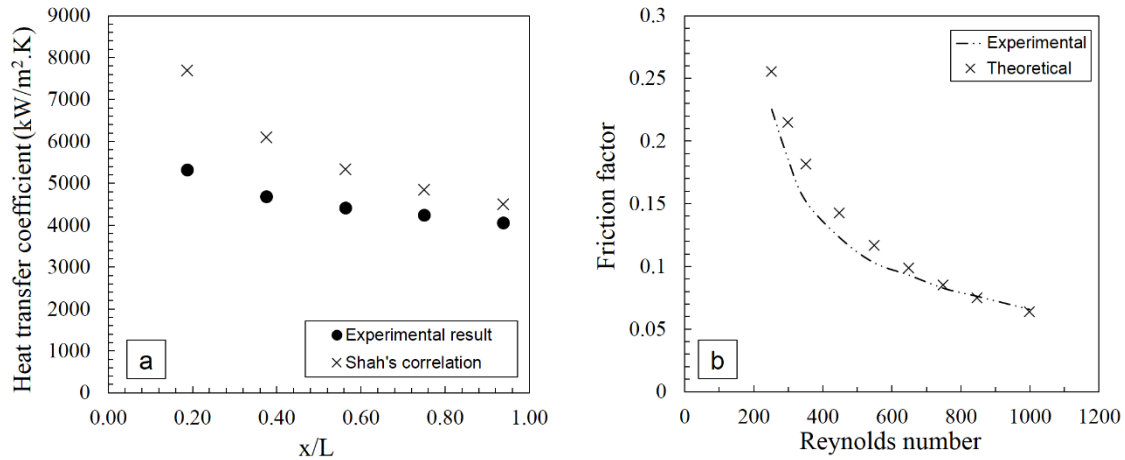
Fig. 3.3. System validation, comparison between obtained friction factor (a) and heat transfer coefficient for 1000 Reynolds number flow (b)

Validations are friction factors for laminar flow for Reynolds numbers ranging from 200 to 1000, and heat local transfer coefficient for flow with 1000 Reynolds number.

3.1.5 Results and discussion

The experiments were divided to two sets of Reynolds numbers, namely 500 and 1000 and three sets of weight fractions of 0.25, 0.5 and 1%. Local heat transfer coefficients of CNT nanofluids for different weight fractions and Reynolds numbers are shown in Fig. 3.4. Obtained results indicate that at low Reynolds number (Re=500), the ratio of nanofluid and pure water heat transfer coefficients is close to the unity. It means that heat transfer with the introduction of nanotubes to the base fluid for all of the chosen fractions. Therefore, at low Reynolds number fraction ratio has no considerable effect on heat transfer coefficients (Fig. 3.4-a). The effect of CNT weight fraction for the experimental heat flux range is shown in Fig. 3.4-b. It can be inferred that CNT fraction has no promising effect on heat transfer coefficient at Reynolds number of 500.
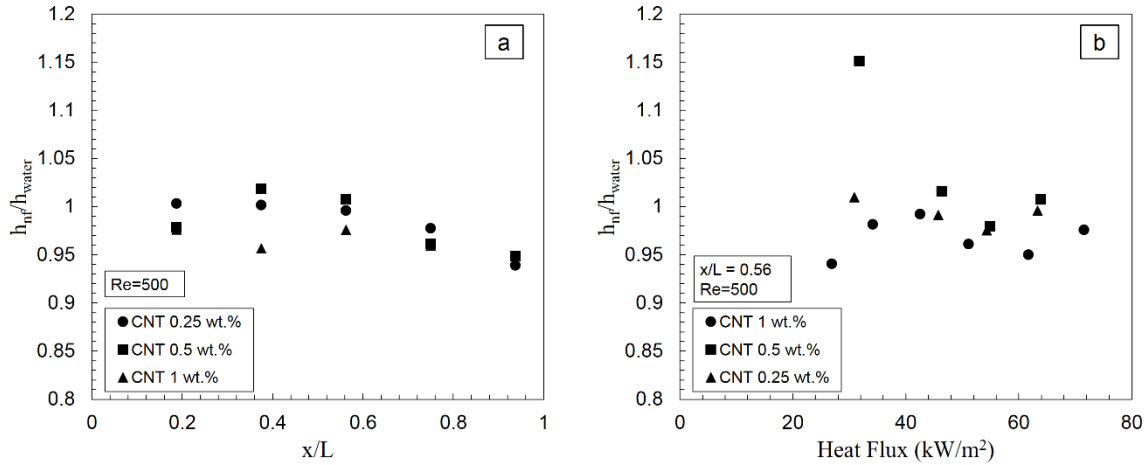
Fig. 3.4. Ratio of MWCNT nanofluid over water convective heat transfer coefficient at Re = 500 a) local heat transfer coefficient ratio b) effect of heat flux at non-dimensional location of x/L=0.56

Local heat transfer coefficients for higher Reynolds number (Re=1000) are displayed in Fig. 3.5-a. Similar to low Reynolds number (Re=500) results, there is no considerable enhancement in heat transfer. This is due to the laminar flow conditions, where no significant effects of nanoparticles on heat transfer were also reported in the literature (Haghighi, Saleemi et al. 2013). Because of the lack of mixing of nanoparticles with respect to the base fluid, no heat transfer enhancement is present under these conditions. Fig. 3.5-b shows the obtained local (three locations of x/L = 0.19, 0.56 and 0.96 along the microtube) heat transfer coefficient for the 1 wt. % nanofluid over a wide range of heat fluxes. According seen in Fig. 3.5-c, at Re=1000 as heat flux increases the heat transfer coefficient ratio (h_{nf}/h_{water}) increases. This is associated with decreased viscosity of the fluid, which leads to better mixing of nanoparticles inside the base fluid. Furthermore, it can be observed that almost for all of the experiments, the obtained heat transfer coefficients at the non-dimensional location of x/L=0.56 are higher those at other locations.
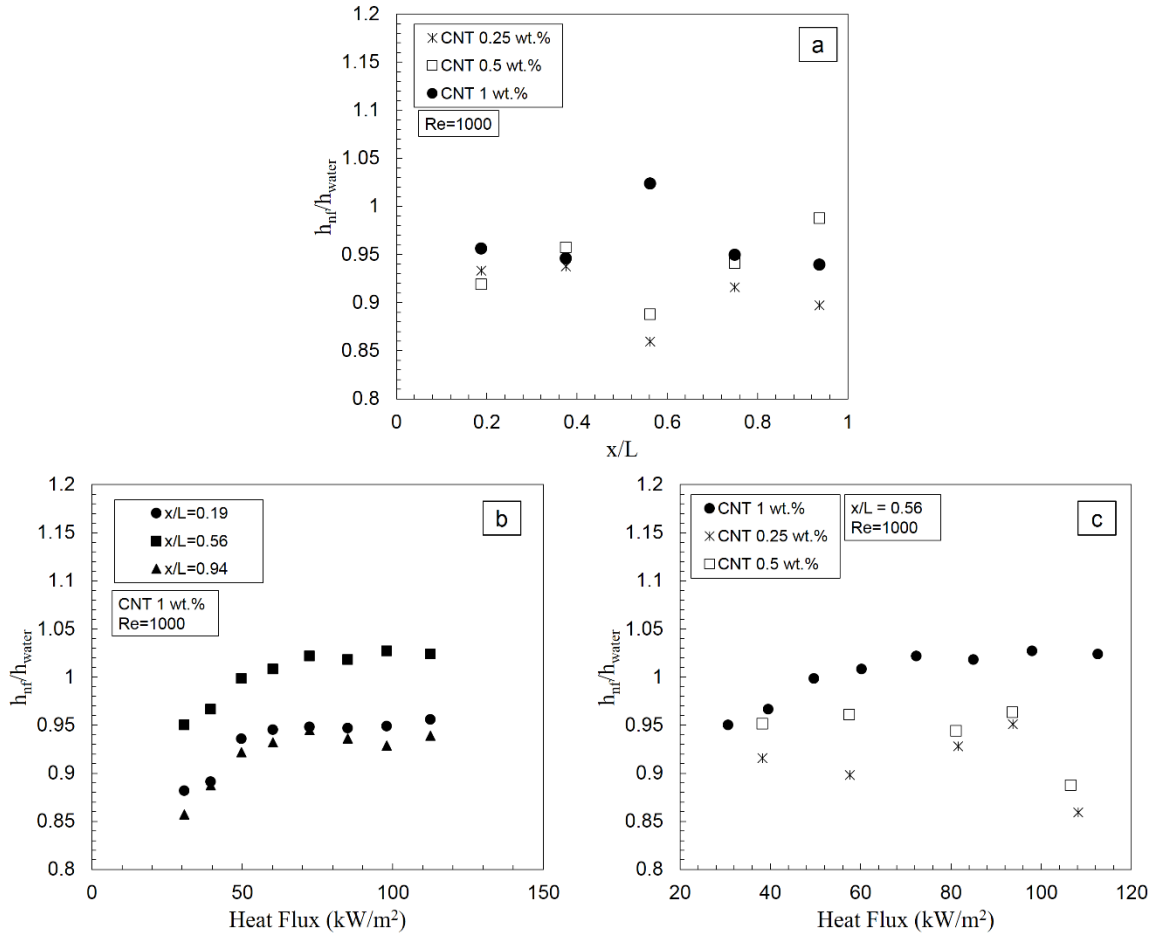
Fig. 3.5. Ratio of MWCNT nanofluid over water convective heat transfer coefficient at Re = 1000 a) local heat transfer coefficient ratio b) effect of heat flux on local heat transfer coefficient ratio for 1% wt. MWCNT nanofluid c) effect of nanofluid concentration on heat transfer coefficient ratio at nondimensional location of x/L=0.56

The potential deposition of CNT on the microtube surface is one of the parameters affecting the heat transfer performance. Heat transfer experiments are performed to investigate the effect of CNT deposition. The obtained results are illustrated in Fig. 3.6. In these sets of experiments, firstly pure water is pumped into the clean microtube before performing the experiments with CNT. Then, CNT nanofluid with desired fraction ratio is pumped for coating the inner surface of microbe with CNT and is heated. Finally, the second experiment set of pure water is performed with the coated microtube. As can be observed from Fig. 3.6, coating the inner surface of the microtube with CNT slightly affects heat transfer coefficient for both Reynolds numbers. Heat transfer coefficients of pure water decrease after coating

26

the microtube with CNT, and this might cause the slight the heat transfer deterioration of CNT nanofluids. Of course, this should be studied in detail by cutting the microtube longitudinally and getting the SEM images or XRD results and get more detailed results by looking at the material surface characteristics, which is left as the future work.
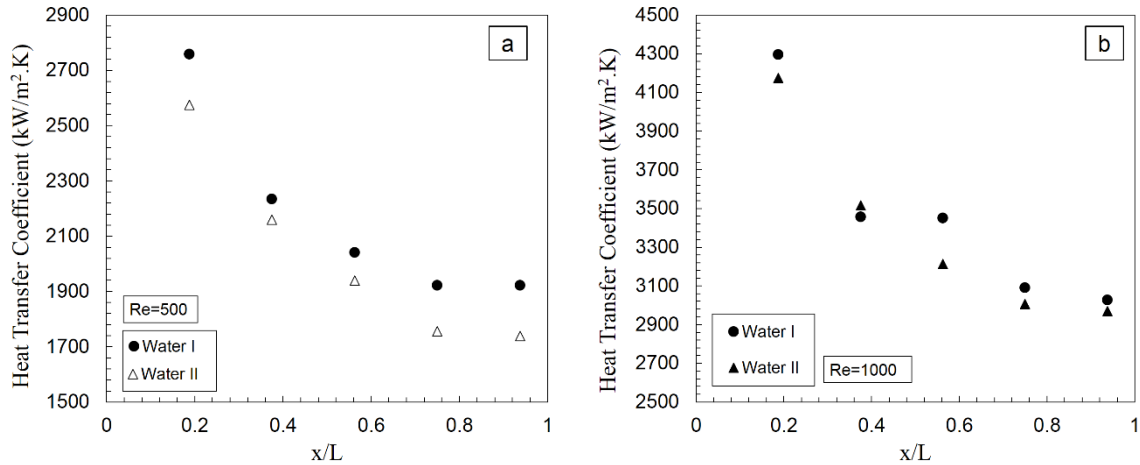
Fig. 3.6. Local heat transfer coefficients of pure water before CNT experiment (Water I) and after MWCNT experiment in the same microtube (Water II) for: (a) Re=500 and (b) Re=1000.

The obtained heat transfer coefficients for 0.25 and 0.5 wt. % MWCNT nanofluids for 26 C inlet temperature are shown in Fig. 3.7. As it is seen, local heat transfer coefficients of water after experiments with MWCNT nanofluid (water II) are lower than nanofluid heat transfer coefficients, which is mainly due to CNT deposition on microtube walls.

Furthermore, results indicate that MWCNT fraction enhances heat transfer coefficients. The amount of enhancement is more pronounced at higher Reynolds number.
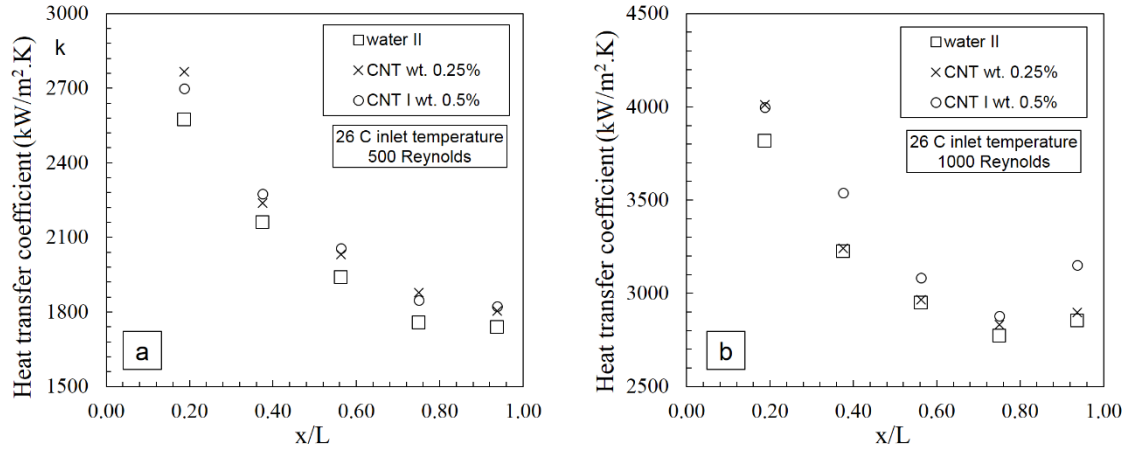
Fig. 3.7. Obtained local heat transfer coefficients for 0.25 and 0.5 wt. % nanofluid and water convective flow after MWCNT experiments at 26 C inlet temperature a) Re=500 b) Re=1000

3.1.6 Summary

Multi-walled carbon nanotube nanofluid with 0.25, 0.5 and 1 wt. % were used to study the effects of nanotubes on convective heat transfer in a microtube. 14 cm long microtube with ~900 and ~1100 μm inner and outer diameters, respectively were used and water was considered as base fluid. The main findings are as following:

i-) It can be concluded that as Reynolds number increases, the effect of particle concentration becomes pronounced. At low Reynolds number, particle concentration has no effect on local heat transfer coefficient.

ii-) Obtained wall temperatures for water flow before and after nanofluid tests showed that wall temperatures increase after nanofluid tests. This may due to deposition of carbon nanotubes on the heating surface.

iii-) It was found that nanofluids has no considerable effect on convective heat transfer in a microtube under the experimental conditions.

3.2 Numerical modeling

There are two major approaches, namely, homogeneous (single phase) and two-phase approaches have been employed to numerically investigate heat transfer characteristics of nanofluid flows. At homogeneous model, thermo-physical characteristics of working fluid

e.g. density, viscosity are modified using available correlations. On the other hand, at two-phase approach the presence of nano-particles modify the multi-phase flow.

3.2.1   Formulation and governing equations

Hydrodynamic and heat transfer characteristics of nanofluid flow in a microtube are numerically investigated utilizing a finite volume based commercial tool, namely Fluent 14, wherein the Eulerian model was used to solve mass, momentum and energy conservation equations. The Eulerian multiphase model in ANSYS Fluent allows for modeling of multiple separate, yet interacting phases.

The continuity equation for phase q is given as:

$$\nabla \cdot \left(\varphi_q \rho_q \vec{\mathrm{v}}_q \right) = S_q \quad (3.7)$$

where φ_q, ρ_q and $\vec{\mathrm{v}}_q$ are volume fraction, density, and velocity vector of phase q, respectively. Here for a dilute system, the source term for particle phase is assumed as $S_q = \nabla \cdot \vec{\mathrm{J}}_p$ and calculated as $\vec{\mathrm{J}}_p = \vec{\mathrm{J}}_{p,B} + \vec{\mathrm{J}}_{p,T}$ where $\vec{\mathrm{J}}_{p,B} = -D_B \nabla \varphi_p$ (Fani, Kalteh et al.) and $\vec{\mathrm{J}}_{p,T} = -D_T \nabla T / T$ (Buongiorno 2006). Here $D_B = \dfrac{k_B T}{3\pi \mu_f d_p}$ is Brownian diffusion coefficient, $D_T = \beta \nu \varphi_p$ is thermophoresis coefficient, k_B is Boltzmann constant, T is temperature, μ_f is fluid viscosity, d_p is particle diameter, β is a proportionality factor and is defined by McNab and Meisen (McNab and Meisen 1973) as $\beta = 0.26\dfrac{k_l}{2k_l + k_p}$, k_p and k_l are thermal conductivity of particle and base fluid, respectively, ν is fluid's dynamic viscosity and φ_p is particle concentration.

The momentum balance for phase q is stated as:

$$\nabla \cdot \left(\varphi_q \rho_q \vec{\mathrm{v}}_q \vec{\mathrm{v}}_q \right) = -\varphi_q \nabla p + \nabla \cdot \underline{\underline{\tau}}_q + \vec{\mathrm{R}}_{pq} + \vec{\mathrm{R}}_{vm,q} + \vec{\mathrm{R}}_{col,q} \quad (3.8)$$

where $\underset{=q}{\tau}$ is the qth phase deviatoric stress-strain tensor, p is the pressure shared among all the phases, $\vec{R}_{pq}$ is an interaction force between p^{th} and q^{th} phases, $\vec{R}_{vm,q}$ is virtual mass force, and $\vec{R}_{col,q}$ is particle interaction force.

The qth phase deviatoric stress-strain tensor is given as follows:

$$\underset{=q}{\tau} = \varphi_q \mu_q \left[\left(\nabla \vec{v}_q + \nabla \vec{v}_q^T \right) - \frac{2}{3} \left(\nabla \cdot \vec{v}_p \right) I \right] \quad (3.9)$$

where μ_q is shear viscosity of phase q. The shear viscosity of particle phase is based on Miller and Gidaspow (Miller and Gidaspow 1992) and Gidaspow (Gidaspow 1994), and particle viscosities were taken as $\mu_p = G_p \varphi_p$. Here G_p ranges from 0.5 to 2, where larger values apply for coarser particles. A sensitivity analysis was performed to explore the effect of nanoparticle viscosity on Nusselt number for a Reynolds number of 500 and a particle concentration of $\varphi_p = 0.01$ by varying nanoparticle viscosity between the values of 5×10^{-3} to 2×10^{-2} with the increment of 10^{-3} sequentially. It was seen that the values tried in the given range provide rather similar results in terms of Nusselt number, and therefore, the G_p coefficient for nanoparticle viscosity is chosen to be 0.5 (Pa.s) in this study following the stated work above.

 The interaction force between phases is calculated as:

$$\vec{R}_{pq} = K_{pq} \left(\vec{v}_p - \vec{v}_q \right) \quad (3.10)$$

Here, K_{pq} is the fraction coefficient. For a two phase flow with volume fraction ratios higher than 0.8 ($\varphi_p < 20\%$), the fraction coefficient is calculated from (Syamlal and Gidaspow 1985):

$$K_{pq} = \frac{3}{4} C_D \frac{\varphi_p \varphi_f \left(\vec{v}_f - \vec{v}_p \right)}{d_p} \varphi_f^{-2.687} \quad (3.11)$$

where C_D is drag coefficient and is expressed as:

$$C_D = \begin{cases} 24/\text{Re}_p \ (1+0.15\text{Re}_p^{0.687}) & \text{Re} < 1000 \\ 0.44 & \text{Re} > 1000 \end{cases} \quad (3.12)$$

where the particle Reynolds number is defined as $\text{Re}_p = \left(\varphi_f \rho_f |\vec{v}_f - \vec{v}_p| d_p\right)/\mu_f$. Here subscripts 'f' and 'p' refer to the fluid and particle phases, respectively.

$\vec{R}_{vm,q}$ is virtual mass force, which is defined as (Drew and Lahey 1993):

$$\vec{R}_{vm,q} = 0.5\rho_q \varphi_q \left(\frac{D\vec{v}_f}{Dt} - \frac{D\vec{v}_p}{Dt}\right) \quad (3.13)$$

where the term $\dfrac{D}{Dt}$ stands for the phase material time derivative.

The particle-particle interaction force is calculated as (Bouillard, Lyczkowski et al. 1989):

$$\vec{R}_{col,q} = G(\varphi_f)\vec{\nabla}\varphi_f \quad (3.14)$$

Here G is the particle-particle interaction modulus and it is calculated by $G = \exp\left(-600(\varphi_f - 0.376)\right)$.

To state the conservation of energy in the Eulerian multiphase model, separate equations can be written for each phase as:

$$\nabla \cdot \left(\varphi_q \rho_q \vec{v}_q C_{p_q} T_q\right) = -\underline{\underline{\tau}}_q : \nabla\vec{v}_q - \nabla \cdot \vec{q}_q + Q_{pq} \quad (3.15)$$

where Q_{pq} is the intensity of heat exchange between p^{th} and q^{th} phases. The colon (:) indicates the inner product between two tensors. The heat exchange between phases must comply with the local balance condition $Q_{pq} = -Q_{qp}$. The amount of exchanged heat between two phases is calculated by equation $Q_{pq} = h_v(T_f - T_p)$. Here h_v is volumetric interphase heat

31

transfer coefficient and can be calculated for micro-dispersed spherical particles from (Minkowycz, Sparrow et al. 2006, Das, Choi et al. 2007):

$$h_v = \frac{6(1-\varphi_f)}{d_p}h_p \quad (3.16)$$

where h_p is the fluid particle heat transfer coefficient and calculated from the Ranz-Marshall (Ranz and Marshall 1952) correlation:

$$Nu_p = \frac{h_p d_p}{k_f} = 2.0 + 0.6\,\mathrm{Re}_p^{0.5}\,\mathrm{Pr}_f^{1/3} \quad (3.17)$$

Here, Pr_f and k_f are the base fluid conductivity and Prandtl number, respectively. The effective thermal conductivities for phases are considered as follows based on the work done by Kuipers et al (Kuipers, Prins et al. 1992):

$$k_{eff,f} = \frac{\left(1-\sqrt{(1-\varphi_f)}\right)}{\varphi_f}k_f \quad (3.18)$$

$$k_{eff,p} = \frac{\sqrt{(1-\varphi_f)}\left(\omega A + (1-\omega)\Gamma\right)}{\varphi_p}k_f \quad (3.19)$$

Here, $\Gamma = \dfrac{2}{\left(1-\dfrac{B}{A}\right)}\left[\dfrac{B(A-1)}{A\left(1-\dfrac{B}{A}\right)^2}\ln\left(\dfrac{A}{B}\right) - \dfrac{(B-1)}{\left(1-\dfrac{B}{A}\right)} - \dfrac{(B+1)}{2}\right]$, and A, B and ω are $\dfrac{k_p}{k_f}$,

$1.25\left(\dfrac{1-\varphi_f}{\varphi_f}\right)^{10/9}$ and 7.26×10^{-3} for spherical particles, respectively.

The description of multiphase flow as interpenetrating continua necessitates the concept of phasic volume fractions. The volume of phase q, V_q, is defined as:

32

$$V_q = \int_V \varphi_q dV \quad (3.20)$$

where $\varphi_p + \varphi_f = 1$. Mean fluid temperature for flow is calculated using the following equation (Boulet and Moissette 2002, Kalteh, Abbassi et al. 2011):

$$T_m = \frac{\iint \rho_f u_f c_{p,f} T_f dA}{\iint \rho_f u_f c_{p,f} dA} \quad (3.21)$$

Local heat transfer coefficient and Nusselt number at a location along the channel are calculated as:

$$h_x = \frac{\dot{q}}{(T_w - T_m)} \quad (3.22)$$

$$Nu_x = \frac{h_x D_h}{k_f} \quad (3.23)$$

Here, the subscripts of "w", "f", and "m" indicate wall, fluid and mean, respectively. Average Nusselt number is expressed as:

$$Nu = \frac{1}{L} \int_0^L Nu_x dx \quad (3.24)$$

Here L is the length of microtube

In the single phase approach, it is assumed that nanoparticles are well dispersed within the base fluid. Thus, the effective properties of nanofluids can be evaluated using some classical formulas as (Rea, McKrell et al. 2009, Khanafer and Vafai 2011)

$$\rho_{nf}(\varphi_p, T) = (1 - \varphi_p)\rho_f(T) + \varphi_p \rho_p \quad (3.25)$$

$$c_{p,nf}(\varphi_p, T) = \frac{(1-\varphi_p)(\rho c_f)_f + \varphi_p (\rho c_p)_p}{\rho_{nf}} \quad (3.26)$$

$$\mu_{nf}(\varphi_p, T) = \mu_f(T) e^{(4.91\varphi_p/0.2092-\varphi_p)} \quad (3.27)$$

$$k_{nf}(\varphi_p, T) = k_f(T)(1 + 4.5503\varphi_p) \quad (3.28)$$

Here subscripts " nf ", " f " and " p " refer to nanofluid, base fluid and particle, respectively. Conservation equations for single phase flow are as follows:

The continuity equation:

$$\nabla \cdot (\rho \vec{v}) = 0 \quad (3.29)$$

Here ρ and $\vec{v}$ are respectively density and the velocity vector.

The momentum balance:

$$\nabla \cdot (\rho \vec{v} \vec{v}) = -\nabla p + \nabla \cdot \underline{\underline{\tau}} \quad (3.30)$$

The conservation of energy:

$$\nabla \cdot (\rho \vec{v} C_{P_{nf}} T) = \underline{\underline{\tau}} : \nabla \vec{v} - \nabla \cdot \vec{q} \quad (3.31)$$

In order to analyze hydrothermal properties of two phase flow, dimensionless temperatures and velocity were defined as $\theta = \dfrac{T_f - T_w}{T_{in} - T_w}$, $\theta^* = \dfrac{T_w - T_m}{\dot{q} D_h / k_f}$ and $U = \dfrac{u_f}{u_{in}}$, where w, f and m represent inlet, wall, fluid phase and mean, respectively. Here u_l and u_{in} are velocities in x direction. In order to compare the hydrodynamic performance of single and two phase approaches, friction factor is defined and calculated as:

34

$$f = \frac{8\tau_w}{\rho_{nf} u_{in}^2} \quad (3.32)$$

Here, τ_w is the wall shear stress and u_{in} is the flow inlet velocity in x direction. Here ρ_{nf} is calculated from modified thermophysical properties of nanofluid using equation (2.20).

3.2.2 Numerical model

3.2.2.1 Computational domain

The computational domain consisting of a microtube with a length of 12 (cm) and inner and outer diameters of ~500 and ~700 μm is displayed in Fig. 3.8. The Finite Volume method is used to discretize the governing equations. The coupled algorithm and second order schemes are used for pressure-velocity coupling and the approximation of convection terms, respectively. Uniform axial inlet velocities are considered as the hydrodynamic inlet boundary condition for both phases, while a constant inlet temperature of 293 K is imposed as the thermal boundary condition for the inlet. Thermophysical properties of the working fluid are considered as temperature dependent. The pressure at the outlet is kept at atmospheric level. No-slip condition is enforced for the velocity at wall boundaries, and constant heat flux ranging from 25 to 300 (kW/m^2 is applied on the walls. The diameter of alumina nanoparticles is taken as 20 and 40 nm.
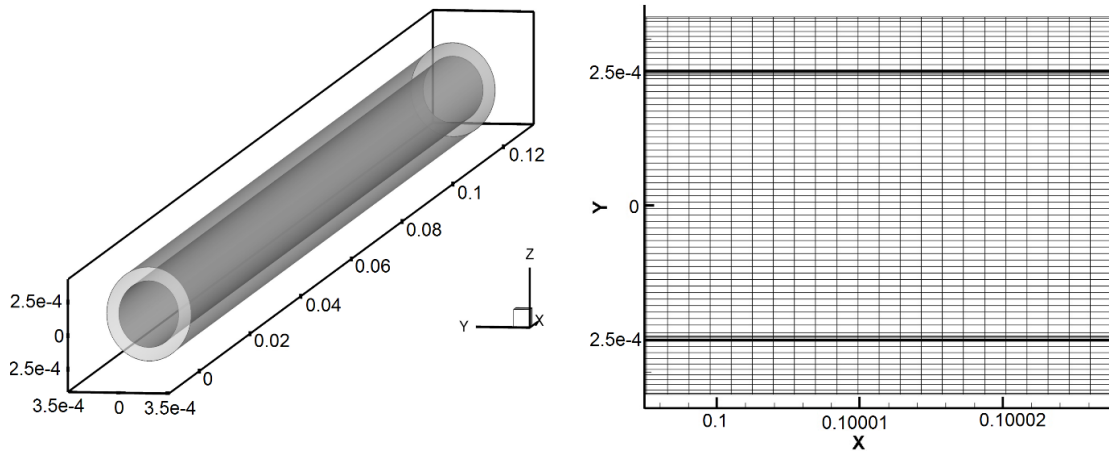
Fig. 3.8. The computational domain (all dimensions are in meter)

3.2.2.2 Grid independency and code validation

In order to obtain grid size independent solutions, a series of numerical simulations with different grid sizes ranging from 4 μm to 24 μm (namely fine and coarse levels, respectively) are conducted at a fixed flow rate. Wall average temperatures obtained from the configurations with six difference grid sizes at a Reynolds number of 1000 are presented in Fig. 3.9.
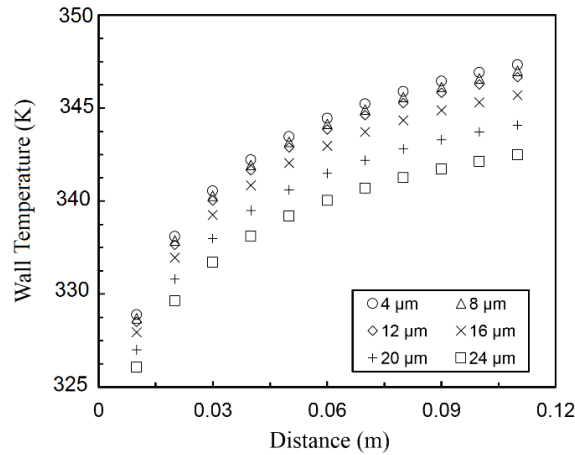
Fig. 3.9. Grid independency tests with different grid sizes

The average difference in wall temperatures between the cases with 4 and 8 μm grid sizes is less than 1% implying grid independency. For the rest of numerical study, grid size of 8 μm is used. The total number of generated mesh elements in the computational domain was about 8×10^5 and the normal growth rate in the wall boundaries in the mesh generation process was chosen as 1.1.

Nusselt numbers for flow with the base fluid (pure water) at different Reynolds numbers are compared with those obtained from an available correlation by Shah and London

$$\left(Nu_x = 4.363 + 8.68\left(10^3 x^*\right)^{-0.506} \exp\left(-41 x^*\right) \quad , \quad x^* = \frac{x}{D_h \operatorname{Re} \operatorname{Pr}} \right) \quad \text{(Shah} \qquad \text{and}$$

London 1978) recommended for laminar flows at constant heat flux. Table 3.2 shows the obtained results. As can be seen, the accuracy of the numerical model is in a good agreement with the predictions of the correlation. As a result, the grid size is taken as 8 μm for the simulations in the rest of this study.

Table 3.2. Comparison between obtained average Nusselt numbers and predictions of Shah and London (Shah and London 1978) for pure water ($\varphi_p = 0\%$)

Reynolds number	Current study	Correlation	Deviation (%)
500	5.429376	5.416917	0.23
750	5.97012	5.943375	0.45
1000	6.539061	6.469833	1.07
1250	7.09354	6.996292	1.39

Proposed model was examined by previous numerical and experimental work by Kalteh et al. (Kalteh, Abbassi et al. 2012) and Karimzadehkhouei et al.(Karimzadehkhouei, Yalcin et al. 2014). Viscous dissipation, Brownian and thermophoresis diffusion source terms in particle phase was disabled in order to have the same mathematical conditions as those in the first reference (Kalteh, Abbassi et al. 2012) and to provide a basis for comparison. The obtained enhancements in average Nusselt number for laminar flow of nanofluids with 1 percent nanoparticle volume fraction for Reynolds number ranging from 50 to 250 are presented in Fig. 3.10. As can be seen, there is a good agreement between the results of the model and numerical and experimental results of Kalteh et al. (Kalteh, Abbassi et al. 2012). Moreover, in order to show the effects of viscous dissipation, Brownian and thermophoresis diffusion on average Nusselt number, the results of the model for this case are also plotted in this figure.
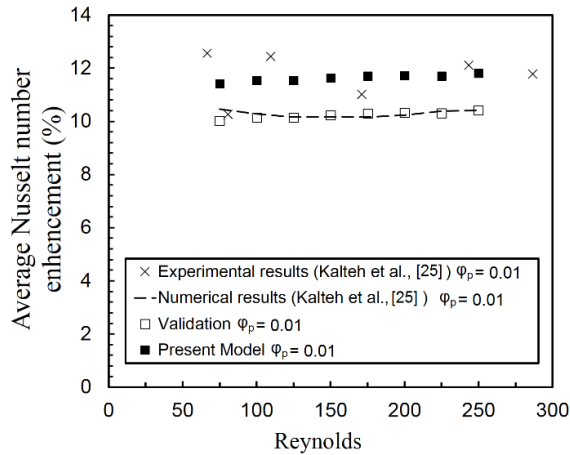
Fig. 3.10. Validation and comparison between calculated results and results available in the literature (Kalteh, Abbassi et al. 2012)

In Fig. 3.11, the results of numerical simulation for a nanofluid with the weight fraction (wt.%) of 1 % and water are presented in terms of average Nusselt number-Reynolds number profile and are also compared with the experimental results reported by Karimzadehkhouei et al.(Karimzadehkhouei, Yalcin et al. 2014). As can be seen, the obtained results are in agreement with the available data in the literature. The existing differences may be attributed to the change in the apparent viscosity of nanofluid which is directly related to its microstructure (the spatial distribution and arrangements of particles in continuous media). Depending on hydrodynamic forces which may lead to order or disorder/clustering in arrangements of particles, and colloidal interactions (particle-particle, and particle-fluid owing to physicochemical effects) (Ozel, Orum et al. 2014), the particles might be individually well dispersed, or form cluster thereby leading to chain like larger structures. Hence, when the microstructure changes, so does the viscosity and in turn the heat transfer characteristic of suspension. It is worth mentioning that since continuum level large scale simulations are not able to include the effect of microstructure on the flow with their current formulations. These deviations might be further caused by the uncertainties in the experimental results.
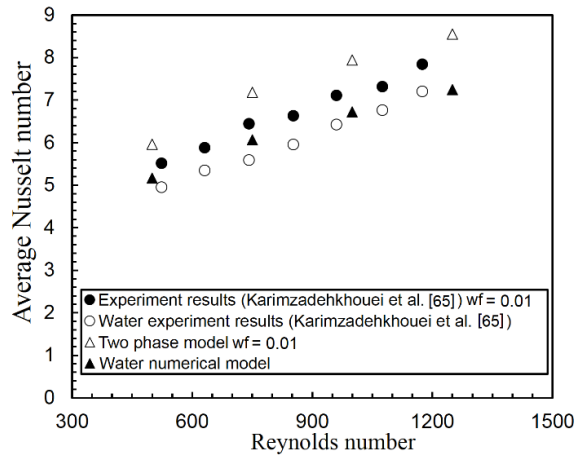
Fig. 3.11. Validation and comparison between calculated results and available in the literature (Karimzadehkhouei, Yalcin et al. 2014).

3.2.3 Results and discussion

3.2.3.1 Single phase model

The effect of different approaches on thermophysical properties of nanofluids were studied in the literature (Li, Zhou et al. 2009, Khanafer and Vafai 2011, Mahbubul, Saidur et al. 2012, Sundar, Sharma et al. 2013). Most of these correlations were proposed for a specific particle diameter, particle concentration, and fluid temperature. In the homogeneous model, it is assumed that base fluid and nanoparticles have the same temperature and velocity fields. Effective properties of single phase nanofluid flows are functions of nano particle size, concentration, material, shape, and base fluid temperature and type. The effect of different correlations on heat transfer characteristics of nanofluid flows was studied in the literature for the single phase model (Khanafer and Vafai 2011, Khaleduzzaman, Mahbubul et al. 2013, Sohel, Saidur et al. 2013, Sundar, Sharma et al. 2013, Wu and Zhao 2013, Göktepe, Atalık et al. 2014).

There are also other studies dedicated to the comparison of single phase model with different correlations to the two-phase model (Haghshenas Fard, Esfahany et al. 2010, Lotfi, Saboohi et al. 2010, Akbari, Galanis et al. 2011, Göktepe, Atalık et al. 2014). In this study, four sets of correlations are investigated, where first three sets are obtained through curve fitting to the available experimental data, while the last set is the widely used theoretical correlations

of Hamilton and Crosser (Hamilton and Crosser 1962) and Einstein. All the correlations are used for the nanoparticle concentration of 1 % in order to investigate the effect of different correlations on the convective heat transfer.

Case 1:

$$\mu_{nf}(0.01,T) = 2.910^{-7}T^2 - 2.10^{-4}T + 3.410^{-2}$$ (Palm, Roy et al. 2006)

$$k_{nf}(0.01,T) = 0.003352T - 0.3708$$ (Palm, Roy et al. 2006)

Case 2:

$$\mu_{nf}(\varphi_p,T) = -0.4491 + \frac{28.837}{T} + 0.574\,\varphi_p - 0.1634\varphi_p^2 + 23.053\frac{\varphi_p^2}{T^2} + ...$$

$$... 0.0132\varphi_p^2 - 2354.735\frac{\varphi_p}{T^3} + 23.498\frac{\varphi_p^2}{d_p^2} - 3.0185\frac{\varphi_p^3}{d_p^2}$$ (Khanafer and Vafai 2011)

$$1\% \le \varphi_p \le 9\% \qquad 20 \le T(^oC) \le 70 \qquad 13\,nm \le d_p \le 131\,nm$$

$$k_{nf}(\varphi_p,T) = k_f(T)\left(\begin{array}{c} 1.0 + 1.0112\varphi_p + 2.4375\,\varphi_p\left(\dfrac{47}{d_p}\right) - ... \\[2ex] ...0.0248\,\varphi_p\left(\dfrac{k_p}{0.613}\right) \end{array} \right)$$ (Khanafer and Vafai 2011)

Case 3:

$$\mu_{nf}(\varphi_p,T) = \mu_f(T)\, e^{(4.91\varphi_p/0.2092-\varphi_p)}$$ (Rea, McKrell et al. 2009)

$$k_{nf}(\varphi_p,T) = k_f(T)\left(1 + 4.5503\varphi_p\right)$$ (Rea, McKrell et al. 2009)

Case 4:

$$\mu_{nf} = \mu_f\left(1 + 2.5\varphi_p\right)$$ (Einstein 1906)

$$k_{nf} = k_f \left(\frac{k_p + 2k_f + 2\varphi_p(k_p - k_f)}{k_p + 2k_f - \varphi_p(k_p - k_f)} \right)$$

(Hamilton and Crosser 1962)

The numerical results obtained with above correlations are presented in Fig. 3.12. As can be seen, compared to the first three cases, the case 4 underestimates the overall heat transfer performance. Nusselt number profile for case 3 is in good agreement with the cases 1 and 2. Given that cases 1 and 2 are only applicable to a mixture with the volume fraction of 1 % and the fluid temperatures in the range of 20 to 70, respectively, the expressions of case 3 (correlations proposed by (Rea, McKrell et al. 2009)) were employed in this study for calculating the thermophysical characteristics of the nanofluid.
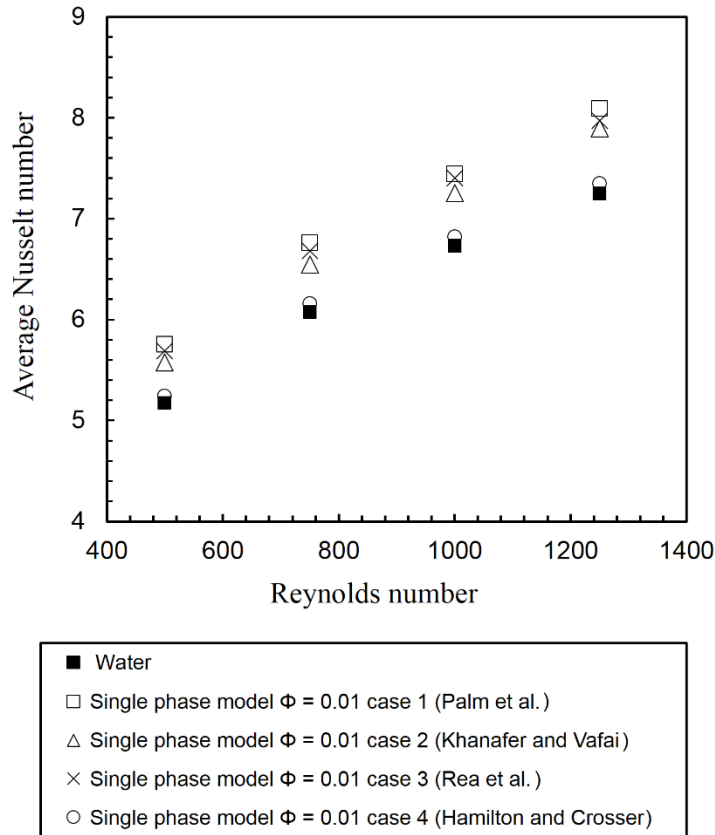
Fig. 3.12. Comparison of the average Nusselt number using different single phase models

3.2.3.2 Flow field

Fig. 3.13-a shows friction factor as a function of Reynolds numbers in the range of 500 to 2000. One can note that the numerically obtained results agree well with the theoretical friction factors $(f = 64/\text{Re})$ for laminar single phase flows (Bergman and Incropera 2011). It can be further seen from the figure that under the considered conditions in numerical simulations, the addition of nanoparticles to the base fluid has minor effect on friction factor, which agrees with the available data in the literature (Wu, Wu et al. 2009). In Fig. 3.13-b, pressure drops calculated using single and two-phase modeling approaches are presented for a fixed particle volume fraction ($\varphi_p = 3\%$). The pressure drops computed using the single phase model are slightly higher than those of the pure fluid, whereas the calculated pressure drops using the two phase model are higher than those of the single phase model. In the two phase model, the particle motion and the related change in fluid viscosity contribute to the pressure drop, and this is more pronounced at higher Reynolds numbers, where fluid regime changes from laminar to transitional.
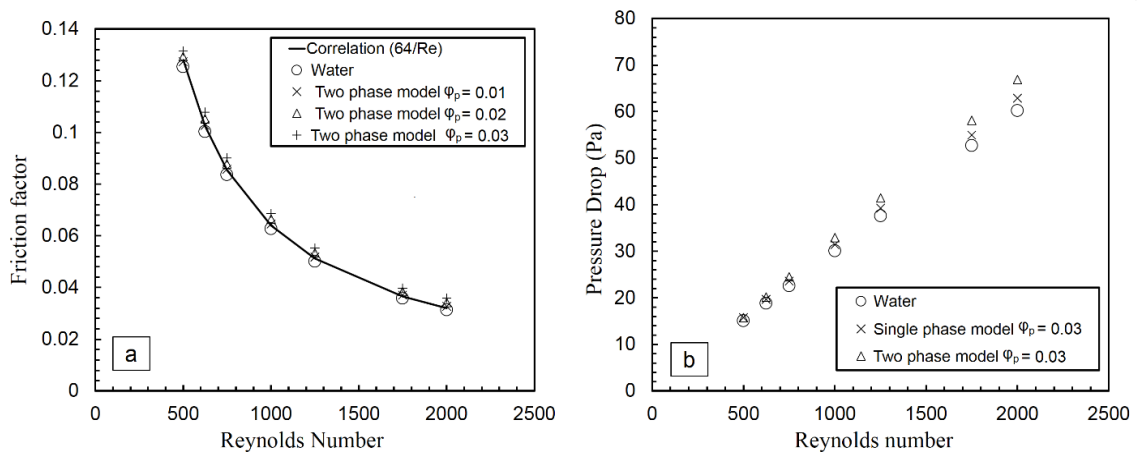
Fig. 3.13. Friction factors and pressure drops obtained from the single and two phase models

In Fig. 3.14, wall shear stress along the microtube at a Reynolds number of 1000 is shown for nanofluids with different particle volume fractions. As the nanoparticle concentration increases, so does the wall shear stress, and the average velocity decreases as shown in Fig. 3.14 and Fig. 3.15. As a result, the effect of wall shear stress on the friction factor is

42

compensated by the decrease in velocity, whereby the friction factor remains almost unaffected by the volume fraction as seen in Fig. 3.13-a.
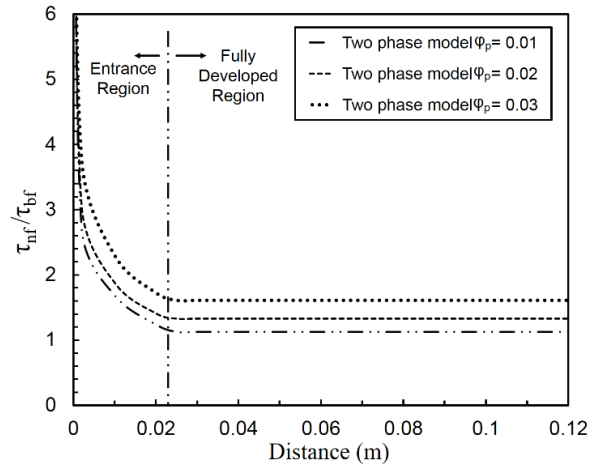
Fig. 3.14. Wall shear stress profile at Re=1000

Fig. 3.15 demonstrates dimensionless velocity and temperature profiles for Reynolds number of 1000 at the distance of x = 0.1 (m) from the inlet. The presence of nanoparticles in the base fluid alters the fluid properties. Namely, as the particle concentration increases, the viscosity of the nanofluids increases. Therefore, the vicinity of maximum velocity in the velocity profile becomes flatter compared to that of the pure fluid, which was also reported in the literature (Kalteh, Abbassi et al. 2012). Due to a flatter profile, the velocity gradient near the wall increases leading to larger wall shear stresses (Fig. 3.14). The flatter velocity profile results in larger velocity values near the wall. Consequently, the rate of heat transfer between bulk of the fluid and wall boundary is enhanced, and a uniform thermal distribution is obtained as shown in Fig. 3.15-b. Moreover, as the nanoparticle volume concentration increases, bulk temperature increases leading to a decrease in temperature difference between wall and bulk fluid and consequent enhancement in the heat removal capacity of nanofluids.
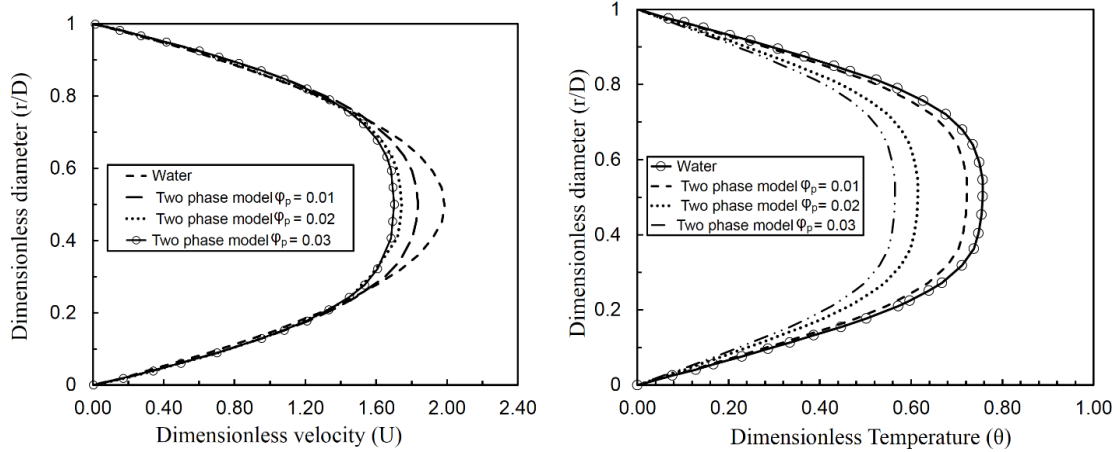
Fig. 3.15. Non-dimensional velocity (a) and temperature profile (b) at the location of x=0.1 m for a Reynolds number of 1000

3.2.3.3 Heat transfer

Fig. 3.16 shows the average Nusselt number at different Reynolds numbers for water and alumina-water nanofluids of three different volume fractions (i.e., 1, 2 and 3%). It is obvious that Nusselt number increases with an increase in nanoparticle volume concentration as well as with Reynolds number. The increase in Nusselt number with Reynolds number can be attributed to the thermal developing effects at the inlet since the thermal entry length varies $\left(L/D_h = 0.05\,\mathrm{Re}_f\,\mathrm{Pr}\right)$ (for the base fluid) between 5.77×10^{-2} m and 2.31×10^{-1} m in this study corresponding to a significant portion of entry region over the entire channel. Moreover, at a fixed Reynolds number, the increase in the particle volume concentration leads to an increase in Nusselt number thereby indicating the effectiveness of nanofluid as a cooling liquid. Quantitatively, at a Reynolds number of 1250, nanofluids with 1, 2 and 3% particle volume concentrations result in an increase in Nusselt number up to 15, 25, and 40%, respectively.

Heat transfer enhancement of nanofluids was attributed to several reasons, namely mixing effect of nanoparticles inside the base fluid near the wall, Brownian motion of particles, thermal conductivity increment, particle migration (Williams, Buongiorno et al. 2008) and thermophoresis effect. As stated before, flattening of velocity profile is a possible mechanism for heat transfer enhancement. Mixing effects with nanoparticle motions within the flow have an additional contribution particularly at higher Reynolds numbers. There is no evidence of

saturation in heat transfer enhancement, which also agrees with the studies in the literature performed at the same nanoparticle volume concentrations (Kurtoğlu, Kaya et al. 2014).
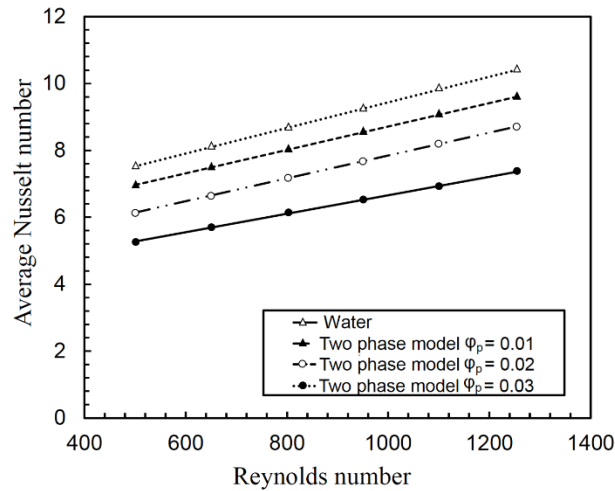
Fig. 3.16. The variation of the average Nusselt number as a function of Reynolds number

The average Nusselt number of nanofluids computed using the single and two phase approaches are presented in Fig. 3.17. It can be noted that when the nanofluid is treated as a single phase (homogenous) fluid, the average Nusselt number is lower than that calculated by the two-phase approach, which indicates that the single phase model underestimates heat transfer enhancement of nanofluids. When the single phase model is implemented, Nusselt number is calculated via modified thermal properties of nanofluids without considering particle motion, while particle motion is also taken into account in the two phase approach. Particle dynamics has a significant effect on energy transfer contribution for enhancing the thermal conductivity of nanofluids and promoting mixing as stated in the literature (Kalteh, Abbassi et al. 2011).
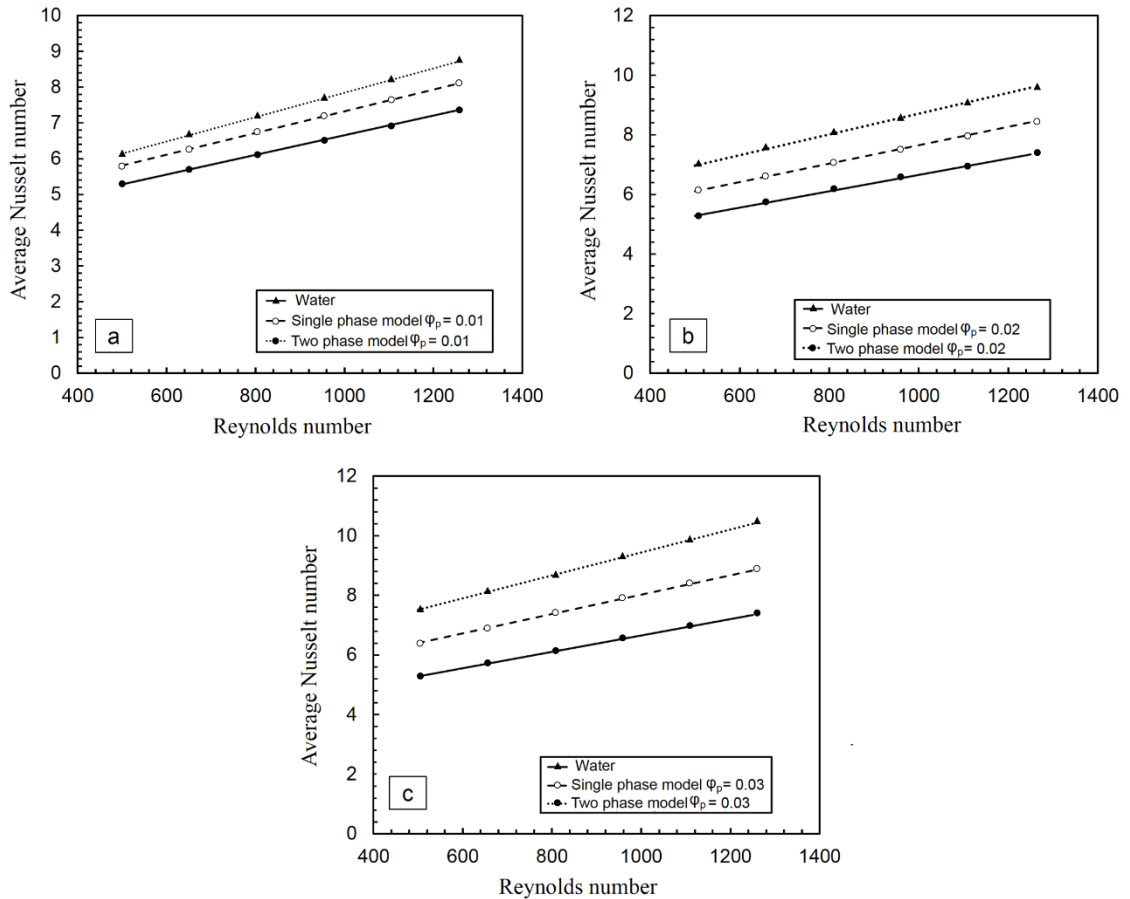
Fig. 3.17. The comparison of calculated average Nusselt number for single and two phase modeling approaches for nanofluids with a) $\varphi_p = 1\%$, b) $\varphi_p = 2\%$ and c) $\varphi_p = 3\%$.

Fig. 3.18-a and Fig. 3.18-b show local Nusselt numbers of nanofluids at Reynolds numbers of 1750 and 2000 for different particle volume concentrations, respectively. As can be seen, local Nusselt number decreases along the microtube indicating lessening of entrance effects. In addition, at a higher Reynolds number, Nusselt number has a larger value, which is due to enhancement of nanoparticle mixing at higher Reynolds number. Comparing the results of Fig. 3.16 and Fig. 3.14 to each other, it can be clearly observed that particle volume concentration effect is more pronounced at higher Reynolds numbers, which is consistent with the available literature (Kumaresan, Mohaideen Abdul Khader et al. 2013). For example, addition of nanoparticles with a volume fraction of 3% to the flow at a Reynolds number of 500 increases the local Nusselt number up to 25%, while the nanofluid with the same particle volume concentration at a Reynolds number of 2000 results in a local Nusselt

number increase up to 50%. The values of heat transfer enhancements in this study overlap with those reported in the literature for alumina nanoparticles (Heris, Esfahany et al. 2007, Godson, Raja et al. 2010, Moraveji and Ardehali 2013).
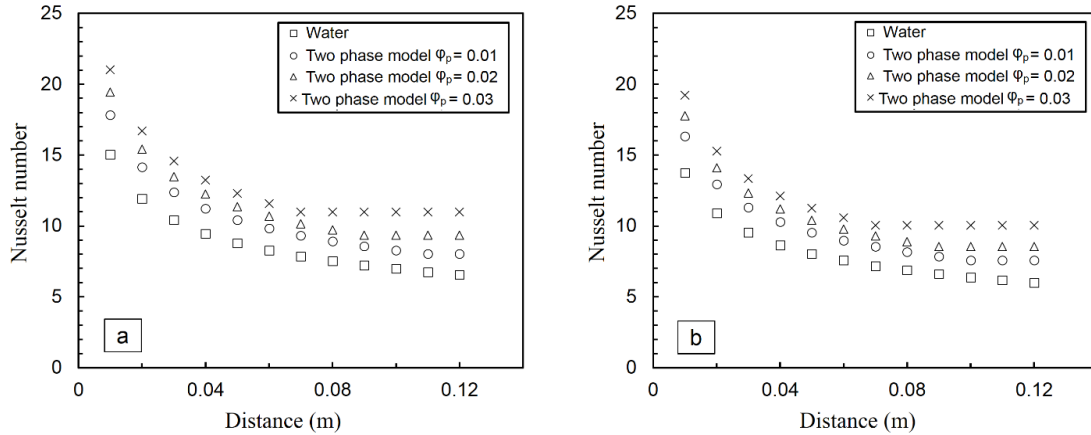
Fig. 3.18. Local Nusselt number for flow at a) Reynolds number 1750 b) Reynolds number 2000

Local non-dimensional temperature of three nanofluids with different inlet and wall boundary conditions are shown in Fig. 3.17. As can be seen in Fig. 3.17-a, non-dimensional thermally developing lengths (L/D_h) for water with Reynolds numbers 500 and 1000 and wall heat fluxes of 25 and 95 kW/m^2, are almost 110 and 170, respectively, which are in agreement with analytical predictions $\left(L/D_h = 0.05\, \text{Re}_f\, \text{Pr}_f\right)$ (Mills 1992). It can be observed that the flow at a Reynolds number of 2000 does not reach thermally fully developed conditions over the whole channel. Non-dimensional temperature is proportional to temperature difference between wall and fluid mean temperatures. Lower amount of non-dimensional temperature represents higher heat transfer rate from walls to fluid. Fig. 3.19 shows the effect of particle on thermally developing length. Nanoparticles increase thermally boundary layer thickness by enhancing the thermal conductivity of flowing fluid. Consequently, two phase flow reaches to thermally developed condition within a shorter distance from inlet in comparison to the base fluid flow. This is shown in Fig. 3.17, where circled points are endpoints of the thermal entry length. As an example, at a Reynolds number

of 2000, the pure fluid flow is thermally developing, while the flow of nanofluid with $\varphi_p = 3\%$ reaches thermally developed condition at a dimensionless location of $L/D_h = 150$.
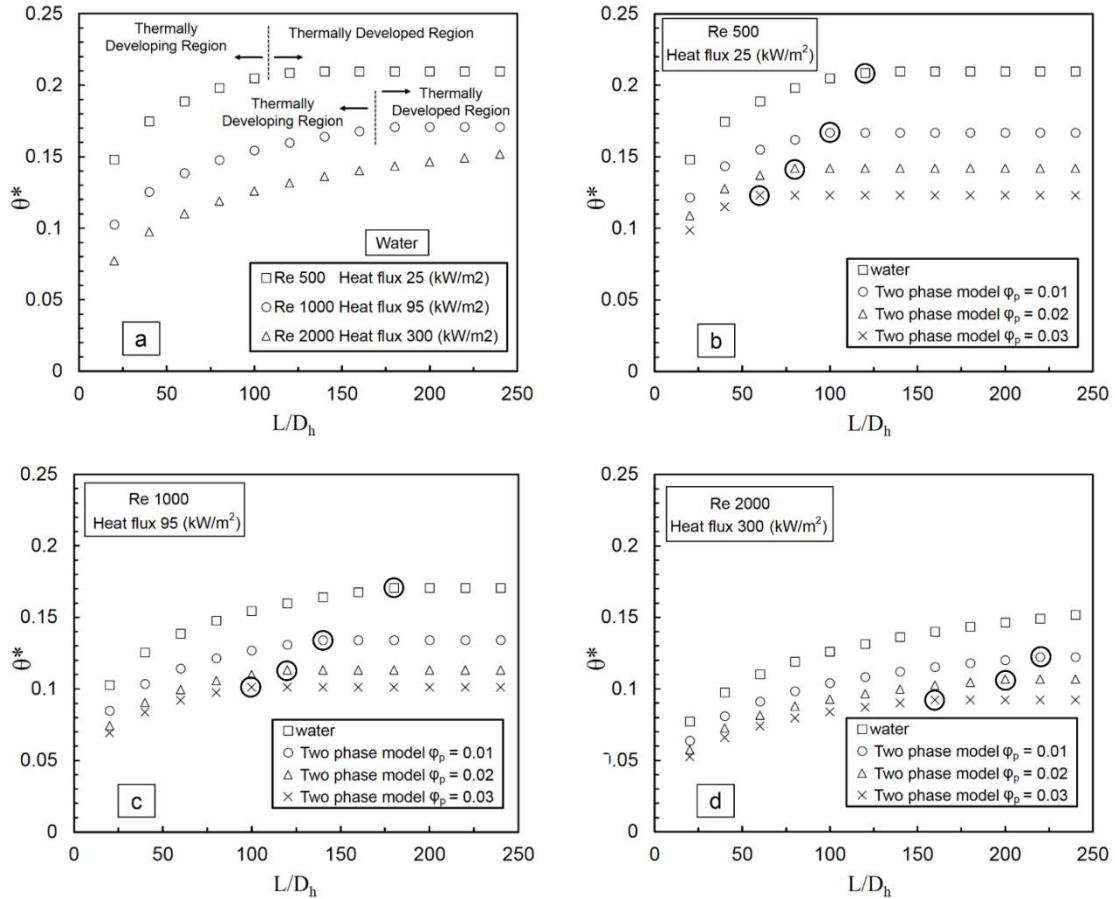
Fig. 3.19. Local dimensionless temperature as a function of length to diameter ratio

Cross-sectional temperature distribution of water and nanofluid flow for Re=1000, heat flux of 95 kW/m² at non-dimensional location of L/D$_h$=50 is shown in Fig. 3.20-a and Fig. 3.20-b. As expected, nanofluid temperature distribution is more uniform and temperature gradient is lower than water convective flow (more convective heat transfer). Also water temperature is higher than nanofluid temperature, which is also shown in Fig. 3.19-c. According to Fig. 3.20-c and Fig. 3.20-d local wall temperature of nanofluid flow is much lower than water convective flow. This indicates that for a fixed wall heat flux nanofluid has more heat dissipation rate that water convective flow.
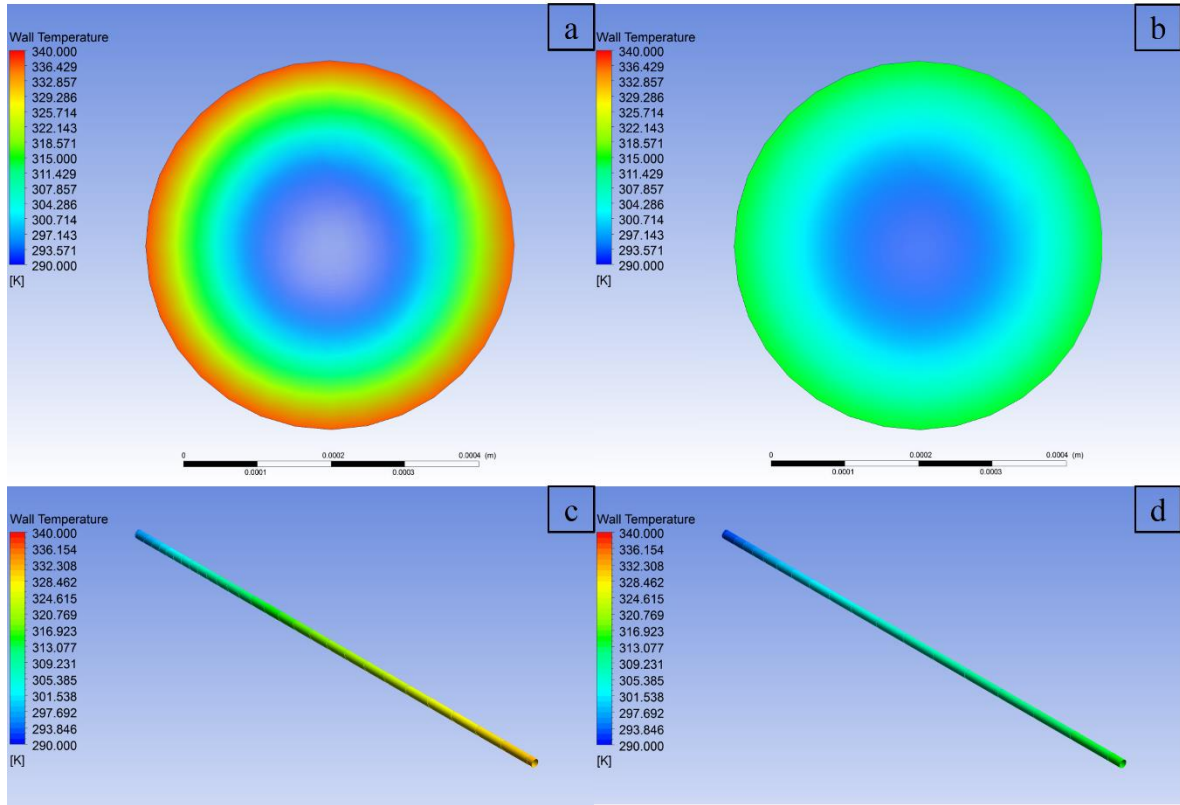
Fig. 3.20. Cross sectional temperature distribution for water and 3% volume fraction alumina nanofluid a) water b) nanofluid c) wall temperature distribution of water flow d) wall temperature distribution of nanofluid convective flow

In order to study the effect of the particle size on heat transfer, a particle size of 40 nm was also considered. Fig. 3.21 shows average Nusselt numbers for particles with 20 and 40 nm diameter at different Reynolds numbers. The nanoparticle size has an adverse effect on heat transfer, which is consistent with the literature (Anoop, Sundararajan et al. 2009). Since heat transfer between particles and the fluid takes place at the particle-fluid interface, nanofluid thermal conductivity increases at the same particle concentration, as particle size decreases (Teng, Hung et al. 2010). Increased thermal conductivity is not the only mechanism responsible for heat transfer enhancement. Additionally, small particles have higher velocities in comparison to bigger ones, which increases the collision effect of nanoparticle motion and further increases heat transfer (Akbarinia and Laur 2009).

49
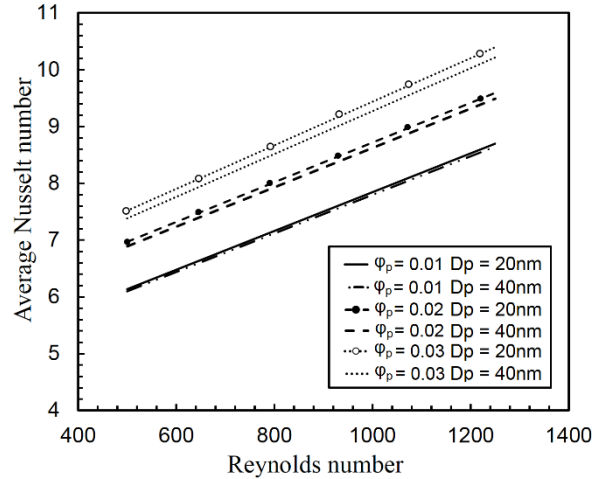
Fig. 3.21. Average Nusselt numbers for nanofluids with different nanoparticle sizes

3.2.4 Summary:

In this study, forced convective heat transfer characteristics of alumina-water nanofluid with different volume fractions in a horizontal microtube have been numerically investigated using both homogeneous and Eulerian multiphase models. The following major conclusions are drawn from the results:

i-) The single phase model underestimates the hydrodynamic and heat transfer characteristics of nanofluid flows. Unlike the two-phase approach, the single phase approach does not take particle motions into account in computations. Given that particle dynamics has a significant effect on the energy transfer contribution for enhancing thermal conductivity of nanofluids and particle mixing at higher Reynolds numbers, the existence of differences in the results of both approaches is highly intuitive and perceptive.

ii-) Heat transfer is augmented with nanoparticle volume concentration as well as with Reynolds number. At higher Reynolds numbers, this effect is more pronounced, and no saturation in heat transfer enhancement was observed upon reaching a certain (3%) nanoparticle concentration.

iii-) The results on friction factor of nanofluids showed that adding nanoparticle has a minor effect on friction factor compared to Nusselt number thereby highlighting the potential of nanofluids for increasing the thermal hydraulic performance.

iv-) Smaller nanoparticles result in more enhanced heat transfer compared to bigger ones, which is attributed to increased thermal conductivity and increased collision effects of nanoparticle motion.

v-) Thermal entry length is shortened with nanoparticle volume fraction.

CHAPTER 4. HIGH MASS FLUX FLOW BOILING IN HORIZONTAL MICROTUBES

Flow boiling heat dissipation rate is much higher that a single-phase liquid coolant. This is mainly because flow boiling systems can carry larger amounts of thermal energy through the latent heat of vaporization, whereas single-phase systems rely only on the sensible heat (Kandlikar 2006). Boiling is the process in which heat transfer leads to a phase change of a substance from a liquid to a gas. Boiling will not occur if the wall temperature is below the saturation temperature. Saturation flow boiling occurs when the bulk liquid reaches saturation temperature and sub-cooled flow boiling exists when the bulk liquid temperature remains below its saturation value but the surface is hot enough for bubbles to form. Bubbles formed at the wall will condense as they move out of the developing saturation boundary layer, but the appearance of these bubbles will affect the heat transfer between the wall and the fluid. Subcooled flow boiling has been of particular interest as a mean of providing high heat flux cooling. At the present time, one of the simplest ways to achieve high heat flux cooling in microelectronics is with a subcooled flow boiling process (Carey 2007). There are three different boiling heat transfer mechanisms:

I) Nucleate boiling, where steam bubbles form at the heat transfer surface and then break away to be carried into the main stream of the fluid.

II) Convective boiling, where heat is conducted through the liquid which evaporates at the liquid-vapor interface.

III) Film boiling, where the heat is transferred by conduction and radiation through a film of vapor that covers the heated surface and the liquid vaporizes at the vapor-liquid interface.

Experimental observations and physical arguments indicate that the basic phenomenology of flow boiling in microchannels is similar to that in large channels as long as there are defects on the heated surface that have characteristic sizes that are smaller than the flow channel cross sectional dimensions. Therefore, bubbles nucleate on the heated wall crevices in such small channels, leading to the onset of nucleate boiling and further downstream the bubbles are released into the bulk flow and lead to the development of a two-phase flow field. The confinement resulting from the small size channel can affect the bubble dynamics.

The confinement of bubbles in microchannels leads to a different growth pattern of bubbles between conventional and small channels. 21 Flow boiling in microchannels can be affected by superficial tension forces, boundary conditions that behave differently in comparison with macrochannels (e.g. jump wall temperature, wall velocity slip at Knudsen number much bigger than 1; $Kn \gg 1$), or even continuity is not valid and rarefied gas dynamics theory is needed. Studies on microscale flow regime maps have increased greatly in recent years but most of these studies are focused on adiabatic conditions rather than on diabetic two-phase flows.

In chapter 3, high mass flux flow boiling in horizontal microtubes is presented using numerical and experimental methods. At first, experimental part of study is presented. Then experimental study was modeled using ANSYS-Fluent 14 commercial software.

4.1   Description of the experiments:

4.1.1   Experimental setup

The experimental setup consists of a storage cylinder, an Omega® turbine flow meter, thermocouples, pressure sensors, proper tubing, fittings and test section. The schematic of the experimental test setup is presented in Fig. 4.1. In order to provide Joule heating, a DC power supply is used to supply current and voltage using alligator clips to the desired sections of 6 and 12 cm long stainless steel hypodermic round tubes of ~600 and ~900 μm inner, and ~900 and ~1100 μm outer diameters. Thermocouples are attached to the heated length with a prescribed distance on the microtube surface. The obtained data from power supply, pressure sensors and thermocouples are used to calculate local heat transfer coefficients, pressure drops, and vapor qualities in microtubes.
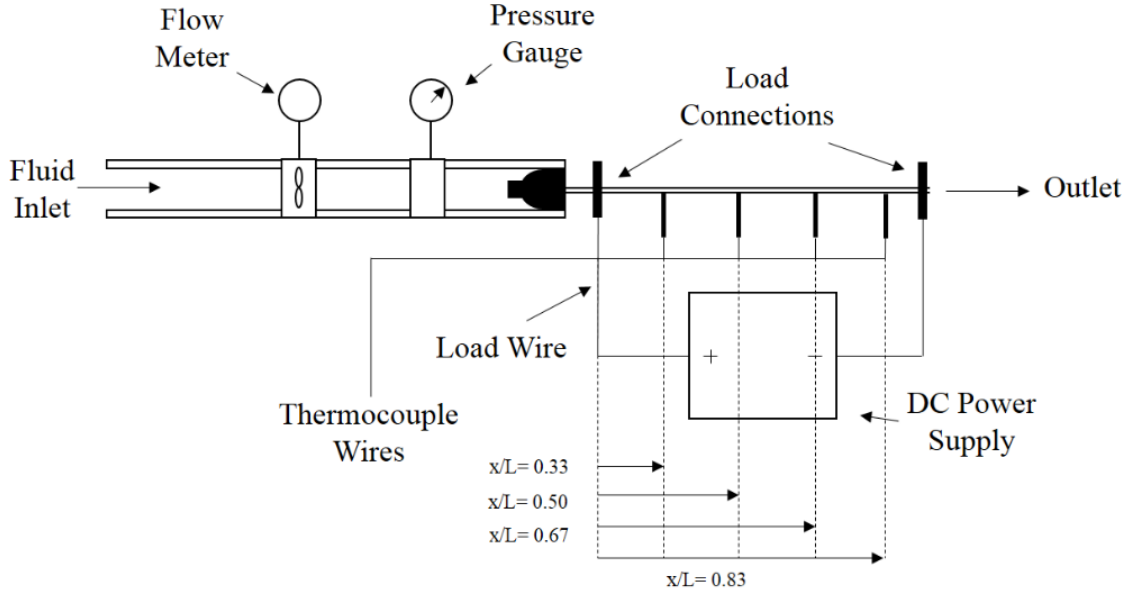
Fig. 4.1. Schematic of the experimental setup

4.1.2   Data reduction

The experimentally measured quantities were inlet pressure, flow rate, voltage, current, temperature of fluid at the inlet of test section, outer surface temperatures at specified locations. The local inner wall temperature was obtained from the outer wall temperature with a 1-D heat conduction model assuming steady-state radial conduction through the wall with uniform heat generation, and constant material properties:

$$T_{w,i} = T_{w,o} + \frac{q'}{16k_w}\left(D_o^2 - D_i^2\right) - \frac{q'}{2k_w}r_o^2 \log\left(\frac{D_o}{D_i}\right) \quad (4.1)$$

Here k_w is the thermal conductivity of the wall, D_o and D_i are outer and inner diameters of the microtube, respectively, and q' is the volumetric heat generation, which is expressed as a function of net power, inner and outer radiuses and heated length of microtube:

$$q' = \frac{4(P - Q_{loss})}{\pi(D_o^2 - D_i^2)L_h} \quad (4.2)$$

Heat loss (Q_{loss}) was estimated by carrying out single-phase experiments and comparing the applied heat to the sensible heat gain of the fluid. The heat loss was calculated as a

54

function of the difference between wall temperature and ambient temperature. The heat loss was taken into account while calculating the effective heat flux transferred to the fluid. Single-phase friction factor is obtained from adiabatic tests and is given by:

$$f = \frac{2 D_i \, \Delta P \, \rho_f}{L G^2} \quad (4.3)$$

Here D_i is inner diameter of microtube, ΔP is pressure drop, L is microtube length, ρ is density and G is mass flux and is calculated as $G = \dot{m}/A_c$. Here $\dot{m}$ is mass flow rate and A_c is the cross sectional area of microtube. Reynolds number is expressed as $\mathrm{Re} = G D_i / \mu_f$, where μ_f is fluid viscosity.

Two-phase heat transfer coefficient is obtained using the inner wall temperature and the net power as:

$$h_{tp} = \frac{(P - Q_{loss})}{A_s \, (T_{w,i} - T_f)} \quad (4.4)$$

Here P is electrical power, Q_{loss} is heat loss and A_s is inner surface area, which is expressed as $A_s = \pi D_i L_h$, where L_h is heated length.

Two different heat fluxes were used for partial subcooled and developed subcooled boiling heat fluxes. Kandlikar (Kandlikar) proposed the following correlation for subcooled and low quality flow boiling:

$$\dot{q}_w = \left[1058 \left(G h_{fg} \right)^{-0.7} F_{fl} \, h_{LO} \, \Delta T_{sat} \right]^{1/0.3} \quad (4.5)$$

The correlation of Petukhov and Popov (Ghiaasiaan 2008) can also be used for the ranges of $0.5 < \mathrm{Pr}_l < 2000$ and $10^4 < \mathrm{Re}_{LO} < 5 \times 10^6$:

$$Nu_{LO}^* = \frac{\left(\mathrm{Re}_{LO} \right) \left(f/8 \right) \mathrm{Pr}_l}{1 + 12.7 \left(\mathrm{Pr}_l^{2/3} - 1 \right) \left(f/8 \right)^{0.5}} \quad (4.6)$$

Here, f is friction factor and calculated as follows:

$$f = \left(0.79 \ln(\mathrm{Re}_{LO}) - 1.64\right)^{-2} \quad (4.7)$$

h_{LO} can be calculated using the following equation:

$$h_{LO} = Nu_{LO}^{*}\left(\frac{k_f}{D_i}\right) \quad (4.8)$$

For heat flux in partial boiling, Bergles (Ghiaasiaan 2008) proposed the following correlation

$$\dot{q}_w = \dot{q}_{FC}\sqrt{1 + \left(\frac{\dot{q}_{SB} - \dot{q}_{ONB}}{\dot{q}_{FC}}\right)^2} \quad (4.9)$$

Here $\dot{q}_{FC}$ is the forced convection heat flux. The heat flux $\dot{q}_{SB}$ is the heat flux in the subcooled boiling correlation. $\dot{q}_{ONB}$ is the onset of nucleate boiling heat flux. Forced convective and onset of nucleate boiling heat fluxes are expressed as:

$$\dot{q}_{FC} = h_{sp}(T_{w,i} - T_f) \quad (4.10)$$

$$\dot{q}_{ONB} = \frac{k_l h_{fg}}{8\sigma v_{fg} T_{sat}} \Delta T_{sat,ONB}^2 \quad (4.11)$$

$$\Delta T_{sat,ONB} = \frac{4\sigma T_{sat} v_{fg} h_{sp}}{k_l h_{fg}}\left[1 + \sqrt{1 + \frac{k_l h_{fg} \Delta T_{sub}}{2\sigma T_{sat} v_{fg} h_{sp}}}\right] \quad (4.12)$$

Here, σ is surface tension, v is specific volume, h_{sp} is single phase heat transfer coefficient, h_{fg} latent heat of vaporization, and k is thermal conductivity. The enthalpy at different axial locations was determined by a simple energy balance given by $H_x = H_{in} + \dfrac{\dot{q}}{\dot{m}}\dfrac{x}{L_h}$. Here, H_x is the local enthalpy at a given axial location, H_{in} is the inlet enthalpy, and x is the axial distance from the inlet. The fluid temperature was determined

at different locations with the local enthalpy and pressure as the independent variables. The equilibrium vapor quality was determined as follows:

$$x_{eq} = \frac{H_x - H_{f,sat}}{H_{fg}} \quad (4.13)$$

Here $H_{f,sat}$ is the saturated fluid enthalpy and H_{fg} is the enthalpy of vaporization at the saturation temperature.

The uncertainties in the measured values were whether provided by the manufacturer's specification sheet or were obtained using the propagation of uncertainty method developed by Coleman and Steele (Coleman and Steele 2009). The typical uncertainties were estimated as demonstrated in Table 4.1.

Table 4.1.Estimated uncertainties

Parameter	Uncertainties
Electrical power (P)	±0.35%
Mass flux (G)	±3%
Inner diameter (d_i)	±2 μm
Outer diameter (d_o)	±1 μm
Quality (x_{eq})	±3%
Pressure drop (ΔP)	±2%
Nusselt number (Nu)	±5%
Friction factor (f)	±4%
Two phase heat transfer coefficient (h_{tp})	±8%

4.2 Numerical simulation

4.2.1 Computational Domain:

Finite volume method was used to discretize the governing equations. The Coupled algorithm and second order schemes were used for pressure-velocity coupling and the approximation of convection terms, respectively. Water was used as the working fluid. Mass fluxes changed

from 4000 to 8000 kg/m^2.s, and inlet temperatures were kept as 295 and 305 K. Thermophysical properties of working fluid has been considered as temperature dependent. The outlet boundary condition was considered as atmospheric pressure at the exit of the microchannel. Applied heat flux to wall boundaries was in the range of 100 to 1300 W/cm^2. The computational domains consisted of microtube configurations with lengths of 6 and 12 cm and inner diameters of 596 and 900 μm, and outer diameters of 889 and 1066 μm. The schematic of a typical computational domain for a microtube with a length of 12 cm and inner and outer diameters of 596 and 889 μm, respectively, is shown in Fig. 4.2.
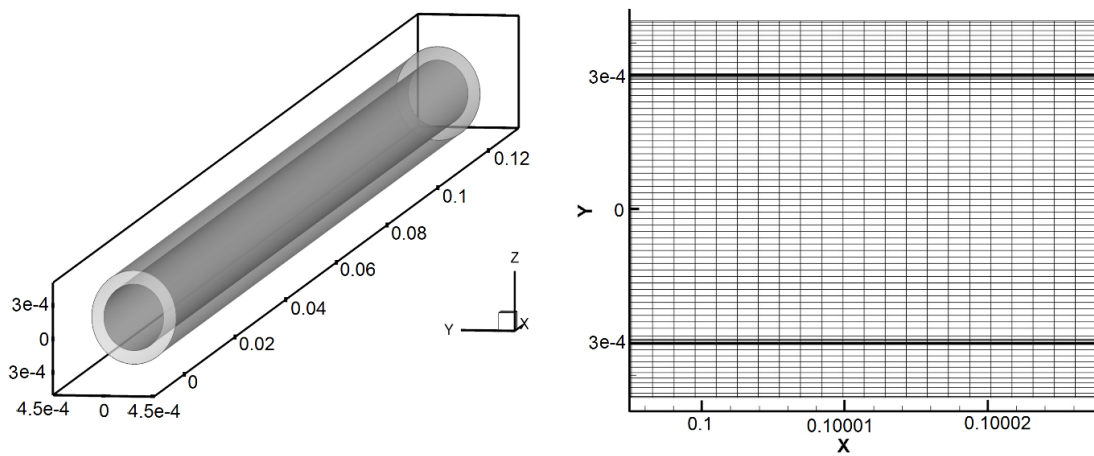
Fig. 4.2. Numerical domain a) 3D view of microtube b) mesh structure at the middle of microtube (all dimensions are in meter)

4.2.2 Grid independency of the model

To ensure grid independency, four different grids with grid sizes ranging from 4 to 16 μm (namely fine and coarse levels, respectively) were tested, and the corresponding Nusselt numbers were obtained. Figure 3-a shows the variation of Nusselt number with the minimum grid size at the mass flux of 4000 kg/m^2.s for a microtube of the diameter of ~600 μm and the length of 12 cm.

The average difference in Nusselt number between the cases with grid sizes of 4 and 8 μm is less than 1%. Therefore, for the rest of the simulations, the minimum grid size of 8 μm (673162 nodes) is used. Moreover, Richardson extrapolation as well as the grid convergence index (GCI for minimum grid sizes of 8 and 12 μm) was utilized to obtain an estimate of the value of the Nusselt number and friction factor at zero grid spacing, and the error band of

these parameters is plotted in Fig. 3-b. Based on these results, the friction factor and Nusselt number recoveries are estimated to be 0.039 and 31.81 with an error band of 0.52% and 1.03%, respectively.
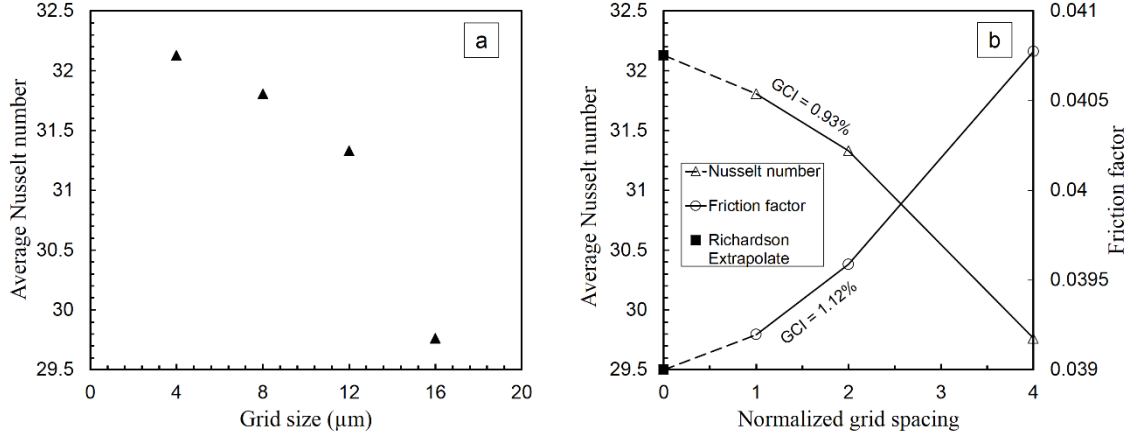
Fig. 4.3. (a) Grid independence test for a case at the mass flux of 4000 kg/m^2.s and (b) Richardson Extrapolation and grid convergence index.

4.2.3 Governing equations

Simulations were done using the Finite Volume Method in the commercial CFD software ANSYS Fluent 14.0. The Eulerian model was used to solve transport equations. The Eulerian multiphase model in ANSYS Fluent allows for modeling of multiphase flows with multiple separate yet interacting phases. The multiphase flow given below must be supplemented by additional relationships of state equations, constitutive equations, boundary and initial equation to achieve the closure.

4.2.3.1 Conservation equations

The continuity equation for phase q is given as:

$$\frac{\partial}{\partial t}\left(\alpha_q \rho_q\right)+\nabla \cdot \left(\alpha_q \rho_q \vec{v}_q\right)=\sum_{p=1}^{n} \dot{m}_{pq} \quad (4.14)$$

Here $\vec{v}_q$ is the velocity of phase q and $\dot{m}_{pq}$ stands for the mass transfer from p[th] to q[th] phase. The momentum balance for phase q is expressed as:

59

$$\frac{\partial}{\partial t}\left(\alpha_q \rho_q \vec{v}_q\right) + \nabla \cdot \left(\alpha_q \rho_q \vec{v}_q \vec{v}_q\right) = -\alpha_q \nabla p + \nabla \cdot \underline{\underline{\tau}}_q + \sum_{p=1}^{n}\left(\vec{R}_{pq} + \dot{m}_{pq}\vec{v}_{pq}\right)$$
$$+\left(\vec{F}_{lift,q} + \vec{F}_{vm,q} + \vec{F}_{vl,q} + \vec{F}_{td}\right) \quad (4.15)$$

Here $\underline{\underline{\tau}}_q$ is the qth phase stress-strain tensor and is given by the following equation:

$$\underline{\underline{\tau}}_q = \alpha_q \mu_q \left[\left(\nabla \vec{v}_q - \nabla \vec{v}_q^T\right) + \alpha_q\left(\lambda_q - \frac{2}{3}\mu_q\right)\nabla \cdot \vec{v}_q \ I\right] \quad (4.16)$$

Here, μ_q and λ_q are shear and bulk viscosities of phase q, respectively. In equation (4.15), $\vec{R}_{pq}$ is interaction force between phases, p is the pressure shared among all phases, $\vec{v}_{pq}$ is the interphase velocity, $\vec{F}_{lift,q}$ is the lift force, $\vec{F}_{vl,q}$ is the wall lubrication force, $\vec{F}_{vm,q}$ is virtual mass force, and $\vec{F}_{td}$ is the turbulent dispersion force.

To describe the conservation of energy in Eulerian multiphase model, a separate enthalpy equation can be written for each phase as:

$$\frac{\partial}{\partial t}\left(\alpha_q \rho_q h_q\right) + \nabla \cdot \left(\varphi_q \rho_q \vec{v}_q h_q\right) = -\underline{\underline{\tau}}_q : \nabla \vec{v}_q - \nabla \cdot \vec{q}_q + \sum_{p=1}^{n}\left(Q_{pq} + \dot{m}_{pq}h_{pq}\right) + S_q \quad (4.17)$$

Here, h is the specific enthalpy, $\vec{q}$ is the heat flux vector, S is a source term, Q is the heat exchange between phases, and h_{pq} is the interphase enthalpy.

4.2.3.2 Turbulence modeling:

The turbulence $k - \varepsilon$ model for the mixture phase is described as follows:

$$\frac{\partial}{\partial t}\left(\rho_m k\right) + \nabla \cdot \left(\rho_m \vec{v}_m \ k\right) = \nabla \cdot \left(\frac{\mu_{t,m}}{Pr_k}\nabla k\right) + G_{k,m} - \rho_m \varepsilon + S_k \quad (4.18)$$

$$\frac{\partial}{\partial t}(\rho_m \varepsilon) + \nabla \cdot (\rho_m \vec{v}_m \, \varepsilon) = \nabla \cdot \left(\frac{\mu_{t.m}}{Pr_\varepsilon} \nabla \varepsilon \right) + \frac{\varepsilon}{k}(C_{1\varepsilon} G_{k,m} - C_{2\varepsilon} \rho_m \varepsilon) + S_\varepsilon \quad (4.19)$$

Here k is the turbulent kinetic energy, ε is the dissipation rate, G is the turbulent production rate, C_1 and C_2 are constants, S_k and S_ε are the bubble induced turbulent and dissipation respectively. The turbulent viscosity and production of turbulent kinetic energy are obtained from the following expression:

$$\mu_{t.q} = C_\mu \, \rho_q \, \frac{k^2}{\varepsilon} \quad (4.20)$$

$$G_{k.q} = \mu_{t.q} \left(\nabla \vec{u}_q - (\nabla \vec{u}_q)^T \right) : \nabla \vec{u}_q \quad (4.21)$$

$\mu_{eff} = \mu_l + \mu_{t.m}$ correlation is used to calculate the effective viscosity. Here $C_{1\varepsilon}$, $C_{2\varepsilon}$ and C_μ are considered as 1.44, 1.92 and 0.09, respectively (Launder and Spalding).

Grid independent solution on dense grids was obtained by using adequate near-wall treatment. In order to modify the k-ε model for wall boundaries, some assumptions are made.

Launder and Spalding (Launder and Spalding 1974) model was used for standard wall function, where a semi-empirical correlation links the solution variables at the near wall cells to the corresponding quantities on the wall, $\frac{u_P C_\mu^{1/4} k_P^{1/2}}{\tau_w / \rho} = \frac{1}{\kappa a} \ln \left(A \frac{\rho \, C_\mu^{1/4} k_P^{1/2} y_P}{\mu} \right)$.

Here κa is the Von Karman constant, A is a constant number (9.79), u_p is the fluid mean velocity at the wall adjacent cell, k_p is the wall adjacent cell turbulent kinetic energy and y_p is the wall to adjacent cell distance. The logarithmic law for the mean velocity is suitable for $11.225 \leq \frac{\rho \, C_\mu^{1/4} k_P^{1/2} y_P}{\mu} \leq 300$. When the mesh is such that $\frac{\rho \, C_\mu^{1/4} k_P^{1/2} y_P}{\mu} \leq 11.225$ at the wall-adjacent cells, laminar stress-strain relationship can be applied as $\frac{u_P C_\mu^{1/4} k_P^{1/2}}{\tau_w / \rho} = \frac{\rho \, C_\mu^{1/4} k_P^{1/2} y_P}{\mu}$. In the k-$\varepsilon$ models, the k equation is solved in the whole domain

including the wall-adjacent cells. The boundary condition for k imposed at the wall is

$\dfrac{\partial k}{\partial n} = 0$, where n is the local coordinate normal to the wall and ε_p is found as $\varepsilon_p = \dfrac{C_\mu^{3/4} k_p^{3/2}}{\kappa \mu}$.

The ε equation is not solved at the wall adjacent cells.

4.2.3.3 Mass Transfer rates

The transferred mass from liquid to gas at the wall boundary is is calculated from:

$$\dot{m}_{pq} = \frac{A_i}{L} \left[h_{ls}(T_l - T_s) + h_{vs}(T_v - T_s) \right] + \frac{\dot{q}_E\, A_w}{L + C_{pl}(T_s - T_l)} \quad (4.22)$$

In this equation boiling happens when heat is applied to the interface and condensation happens when heat is removed from the interface. Here, the liquid side interfacial heat transfer coefficient (h_{ls}) is calculated from the correlation proposed by Ranz and Marshall (Ranz and Marshall 1952) as follows:

$$Nu_p = \frac{h_{ls} d_v}{k_v} = 2.0 + 0.6\,\mathrm{Re}_v^{0.5}\,\mathrm{Pr}_l^{1/3} \quad (4.23)$$

Here $h_{vs} = 10^5 \left(W/m^2.K \right)$ is the vapor side interfacial heat transfer coefficient (it is assumed that vapor temperature is equal to saturation temperature), $\dot{q}_E$ is the evaporative heat flux from the RPI model (Podowski, Drew et al. 1997), L is the latent heat per unite mass ($L = h_{vs}^0 - h_{ls}^0$), A_w is interfacial area density of wall surface ($A_w = \delta(\vec{x} - \vec{x}_w)$), and d_v is the diameter of vapor phase. In these equations subscripts l, v and s stand for liquid, vapor and saturation, respectively (Narumanchi, Troshko et al. 2008). In discretization, A_w is the ratio of the cell face area constituting the wall to the volume of the cell next to this face. The interfacial area density (A_i) and for small void fractions is calculated by $\dfrac{6\alpha_{vs}(1-\alpha_v)}{d_v}$, where $\alpha_{vs} = \min(\alpha_v, 0.25)$. For a large amount of vapor volume fraction, the Ishii and Mishima (Ishii and Mishima 1980) correlation is utilized:

$$A_i = \frac{4.5}{D} \frac{\alpha_v - \alpha_{vs}}{1 - \alpha_{vs}} + \frac{6\alpha_v}{d_b} \frac{1 - \alpha_v}{1 - \alpha_{vs}} \quad (4.24)$$

Here α_{vs} is the void fraction in the small bubble region. Kurul and Podowski (Kurul and Podowski 1990) recommended the following expression for vapor side volume fraction :

$$\alpha_{vs} = \begin{cases} \alpha_v & 0 < \alpha_v \leq 0.25 \\ 0.3929 - 0.5714\alpha_v & 0.25 < \alpha_v \leq 0.6 \quad (4.25) \\ 0.05 & 0.6 < \alpha_v \end{cases}$$

4.2.3.4 Interphase momentum transfer

The interfacial drag force per unit volume is calculated as:

$$\vec{R}_{lv} = 0.75 C_D \, A_i \, \varphi_l \left| \vec{v}_l - \vec{v}_v \right| \cdot (\vec{v}_l - \vec{v}_v) \quad (4.26)$$

Here the drag coefficient C_D is calculated as:

$$C_D = \begin{cases} \dfrac{24}{Re_b} 1 + 0.1 Re_b^{0.75} & 0 < \alpha_v \leq 0.1 \\ \dfrac{2}{3} d_b \sqrt{\dfrac{g \, \Delta P}{\sigma}} \left[\dfrac{1 + 17.67 \left(1 - \alpha_v\right)^{1.238}}{18.67 \left(1 - \alpha_v\right)^{1.5}} \right] & 0.1 < \alpha_v \leq 0.25 \quad (4.27) \\ 9.8(1 - \alpha_v) & 0.25 < \alpha_v \end{cases}$$

The lift force arises from a velocity gradient of continuous phase and is calculated as:

$$\vec{F}_{lift} = C_l \, \rho_l \, \alpha_v \, (\vec{v}_l - \vec{v}_v) \times \left(\nabla \times (\vec{v}_l - \vec{v}_v) \right) \quad (4.28)$$

Here lift coefficient is found using the expression recommended by Moraga et al. (Moraga, Bonetto et al. 1999) as follows:

$$C_l = \begin{cases} 0.07667 & \text{Re}_b\,\text{Re}_v \leq 6000 \\ -\left(0.12 - 0.2\exp\left(-\dfrac{\text{Re}_b\,\text{Re}_v}{36000}\right)\right)\exp\left(\dfrac{\text{Re}_b\,\text{Re}_v}{3e7}\right) & 6000 < \text{Re}_b\,\text{Re}_v < 1.9e5 \quad (4.29) \\ -0.002 & \text{Re}_b\,\text{Re}_v \geq 1.9e5 \end{cases}$$

This coefficient combines the opposing actions of two lift forces. Here $\text{Re}_b = \dfrac{d_v\left|\vec{v}_1 - \vec{v}_v\right|}{v_1}$ is

bubble Reynolds number and $\text{Re}_v = \dfrac{d_v^2\left|\nabla \times \vec{v}_1\right|}{v_1}$ is the bubble shear Reynolds number.

The lubrication force is calculated as:

$$\vec{F}_{\text{lub}} = \rho_l\,\alpha_v\,\frac{\left|\vec{v}_1 - \vec{v}_v\right|^2}{d_b}\,n_w\,\max\left\{0, C_{w,1} + C_{w,2}\frac{d_b}{y_w}\right\} \quad (4.30)$$

The coefficients $C_{w,1}$ and $C_{w,2}$ are considered as -0.01 and 0.05 as suggested by Alajbegovic et al. (Alajbegovic, Drew et al. 1999).

Turbulence diffusion force is calculated as following (Podowski, Drew et al. 1997):

$$\vec{F}_{td} = -C_{td}\rho_l k\nabla\alpha_v \quad (4.31)$$

Here the value for the turbulent dissipation force coefficient (C_{td}) is 0.1 as recommended by Kurul and Podowski (Kurul and Podowski 1990).

4.2.3.5   Wall boiling model

In general, the energy balance at the infinitely thins wall separating fluid and solid cells is stated as:

$$h_{solid,w}\cdot\left(T_{solid} - T_w\right) = \alpha_l\,[\dot{q}_E + \dot{q}_Q + \dot{q}_L] + \alpha_v\,[h_{vw}\cdot(T_w - T_v)] \quad (4.32)$$

Here the left hand side of the equation is solid side heat flux due to the conduction, the first and second terms on the right hand side are the components of heat flux delivered to the liquid and vapor phases, respectively.

Heat flux from wall to liquid phase is partitioned into three components: $\dot{q}_W = \dot{q}_L + \dot{q}_Q + \dot{q}_E$ which are liquid convective heat flux, quenching heat flux, and evaporation heat flux, respectively. Under subcooled flow boiling conditions, the wall surface is subdivided into the region Ω $(0 \leq \Omega \leq 1)$, covered by nucleation bubbles, and the region $1 - \Omega$, covered by fluid. Accordingly, convective heat flux is expressed as:

$$\dot{q}_L = St\, \rho_l\, C_{p,l}\, u_l \left(1 - A_{tc}\right) \cdot \left(T_w - T_l\right) \quad (4.33)$$

Here, u_l, $St = \dfrac{Nu}{\mathrm{Re}\,\mathrm{Pr}}$, Re and Pr are adjacent liquid velocity, Stanton, Reynolds and Prandtl numbers, respectively.

Quenching heat flux includes additional energy transfer related to liquid filling the wall vicinity after the bubble detachment:

$$\dot{q}_Q = \left(\frac{2}{\sqrt{\pi}} \sqrt{k_l\, \rho_l C_{p,l}}\, \sqrt{f}\right) A_{tc} \left(T_w - T_l\right) \quad (4.34)$$

Here f is the bubble departure frequency, k is thermal conductivity, c_p is the specific heat capacity, and ρ is density. Here A_{tc} is the fraction of the wall area in contact with the fresh liquid and is cooled down by transient conduction. This area is calculated as following:

$$A_{tc} = N_a \left(K \frac{\pi D_b^2}{4}\right) \quad (4.35)$$

Evaporation heat flux is given as:

$$\dot{q}_E = N_a\, f \left(\frac{\pi D_b^3}{6}\right) \rho_g\, h_{fg} \quad (4.36)$$

Here N_a, f, D_b and h_{fg} are the active nucleation site density, bubble frequency, departing bubble diameter and the latent heat of vaporization, respectively.

Active nucleation site density is calculated by the correlation proposed by Lemmert and Chwalas (Lemmert and Chawla 1977)

$$N_a = \left[185(T_w - T_{sat})\right]^{1.805} \quad (4.37)$$

Bubble departure diameter in microchannel with high flow rate is considered as (Kocamustafaogullari and Ishii 1983):

$$d_b = 2.496 \times 10^{-5} \left(\frac{\rho_l - \rho_g}{\rho_l}\right)^{0.9} \beta \left(\frac{\sigma}{g(\rho_l - \rho_g)}\right)^{0.5} \quad (4.38)$$

Here β is the contact angle in degree and is calculated according to (Rogers and Li 1994). Correct prediction of bubble departure diameter is important because evaporation heat rate strongly depends on this parameter. It is worth to note that since there are few correlations for bubble departure diameter in microchannels (Lee, Tseng et al. 2004, Li, Tseng et al. 2004, Thome 2004, Kuo, Kosar et al. 2006, Krishnamurthy and Peles 2010) , after comparing several correlations, it was observed that the recommended correlation of Kocamustafaogullari and Ishii (Kocamustafaogullari and Ishii 1983) for bubble departure diameter presents acceptable results for high mass flux flow boiling in microtube.

The bubble departure frequency is calculated by a simple estimation of the terminal rise velocity over the bubble departure diameter as (Cole 1960):

$$f = \sqrt{\frac{4g(\rho_l - \rho_v)}{3d_b \, \rho_l}} \quad (4.39)$$

4.2.3.6   Restrictions

The following restrictions are imposed on interfacial mass, momentum and energy interfacial exchange:

$$\begin{cases} \dot{m}_{pq} = -\dot{m}_{qp} & \dot{m}_{pp} = 0 & \vec{R}_{pq} = -\vec{R}_{qp} & \vec{R}_{pp} = 0 \quad (4.40) \\ \vec{F}_{vl} = -\vec{F}_{lv} & Q_{pq} = -Q_{qp} & Q_{pp} = 0 \end{cases}$$

The description of multiphase flow as interpenetrating continua incorporates the concept of phasic volume fractions. The volume of phase q, V_q, is defined as $V_q = \int_V \alpha_q dV$ where

$$\sum_{q=1}^{n} \alpha_q = 1.$$

A function was defined in the code to calculate the local heat transfer coefficient as $h_{tp,sub|x} = \dfrac{\dot{q}}{(T_{w|x} - T_{f|x})}$. Here x notation is used to indicate the local quantity at a given point x, and $\dot{q}$ is the applied heat flux.

4.3   Results and discussion

4.3.1   Single phase study

A single-phase heat transfer study was performed to validate the experimental setup and data reduction procedures. The experimental Nusselt numbers and friction factors for a wide range of Reynolds numbers were compared to the following available correlations (Gnielinski 1976, Swamee and Jain 1976, Shah and London 2014) :

$$f = (64/\mathrm{Re}) \text{ Laminar flow} \tag{4.41}$$

$$f = 0.25 \left[\log_{10} \left(\frac{\varepsilon/D_h}{3.7} + \frac{5.74}{\mathrm{Re}^{0.9}} \right) \right]^{-2} \text{ Turbulent flow} \tag{4.42}$$

$$Nu_x = 4.363 + 8.68 \left(\frac{10^3 x}{\mathrm{Re}\,\mathrm{Pr}\,D_h} \right)^{-0.506} \exp \left(\frac{-41x}{\mathrm{Re}\,\mathrm{Pr}\,D_h} \right) \text{ Laminar thermally} \tag{4.43}$$

developing flow

$$Nu_D = \frac{(f/8)(\mathrm{Re}-1000)\,\mathrm{Pr}}{1 + 12.7(f/8)^{0.5}(\mathrm{Pr}^{2/3}-1)} \text{ Turbulent flow} \tag{4.44}$$

Obtained results are shown in Fig. 4. The comparison of the experimental data with the theory and existing correlations was accomplished through the mean absolute error (MAE), defined as:

$$\text{MAE}(\%) = \frac{1}{M_t} \sum_{j=1}^{M_t} \frac{\left| U_{exp} - U_{theoretical} \right|}{U_{exp}} \times 100 \quad (4.45)$$

where M_t is the total number of data points.

A good agreement between the experimental results and predictions of the correlations is present with mean absolute errors of ~13.1% and ~21.6% for friction factor and Nusselt number, respectively. In standard heat transfer textbooks such as Incropera et al. (Incropera and DeWitt 1981), it was stated that the errors as large as 25% might be obtained in the comparisons with widely used correlations. This is a result of the effect of variable thermophysical properties as well as lack of correlations for thermally developing flows and lack of complex correlations recommended for laminar and turbulent flows. Therefore, these values of mean absolute errors are expected in basic heat transfer experiments.
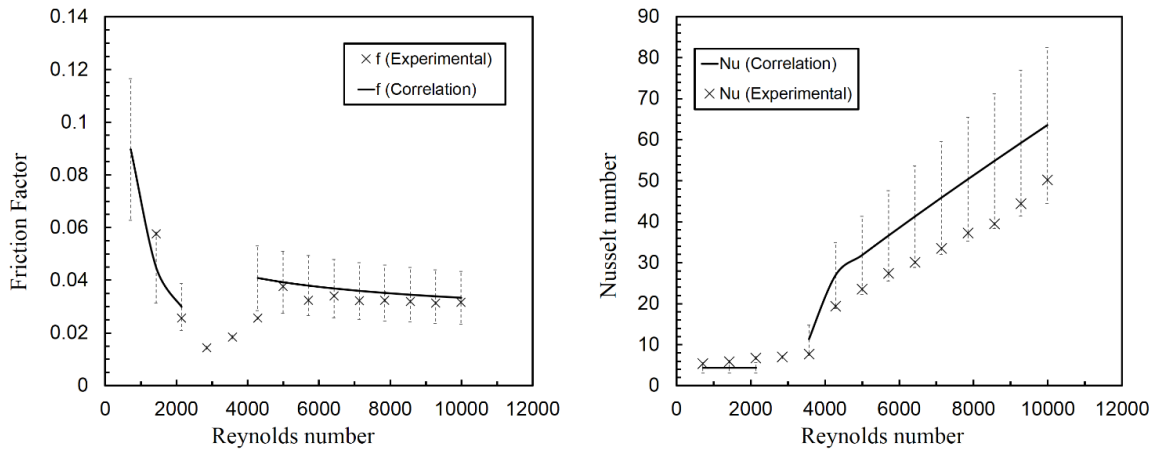
Fig. 4.4. Experimental results of the single phase study a) friction factor b) Nusselt number

4.3.2   Pressure drop

Experimental and numerical pressure drops are shown in Fig. 4.5. Fig. 4.5-a shows experimental pressure drop for the mass flux of 6000 kg/m2.s. As seen, pressure drop first decreases with applied heat flux under single phase flow conditions. This is mainly related to viscosity reduction during the heating process. Beyond the onset of nucleate boiling (ONB), this trend changes and pressure drop starts to increase. Beyond ONB, the pressure drop increases but is still small enough and comparative to single phase pressure drop, which was also reported by Lee and Mudawar (Lee and Mudawar 2008). It can be concluded that two-phase pressure drop is rather small in subcooled flow boiling and close to single phase

pressure drop. The increase in wall heat flux leads to an increase in both two-phase frictional and accelerational components of pressure drop resulting in an increasing trend with heat flux.
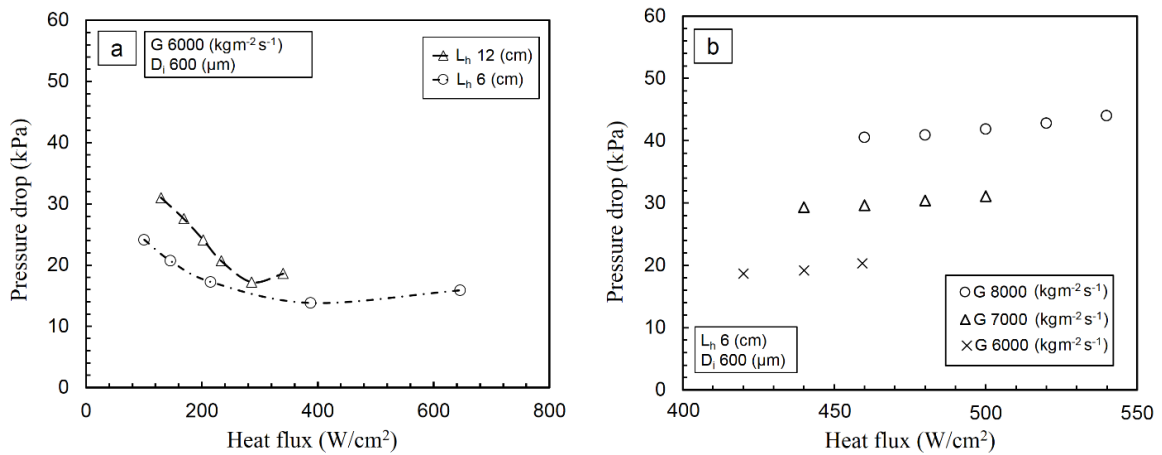
Fig. 4.5. Effect of heat flux on subcooled flow boiling pressure drop in the microtube with inner diameter of ~ 600 μm a) Experimental results at the mass flux of 6000 kg/m^2.s for the heated lengths of 6 and 12 cm b) Numerical results at different mass fluxes for the microtube with the heated length of 6 cm

Furthermore, Fig. 4.5-a displays experimental pressure drops for two different heated lengths. The longer microtube has a higher pressure drop, and the minimum pressure drop for smaller microtube is achieved at a higher heat flux. As stated before, the minimum of the curve is related to the onset of nucleate boiling (ONB), where bubbles start to grow on the wall surface. As the number of bubbles increase, the pressure drop increases as seen in the figure. When the pressure drop curves are compared, ONB occurs at higher heat flux for the shorter microtube, which is consistent with the literature (Rafet Özdemir, Kaya et al. 2011).

From the numerical point of view Fig. 4.5-b presents calculated subcooled flow boiling pressure drop results for mass fluxes ranging from 6000 to 8000 kg/m^2.s. As can be seen, pressure drop increases as inlet mass flux increases. This figure allows a comparative demonstration of calculated pressure drops for subcooled boiling with the available theory results for single phase turbulent flows. There is a good agreement between numerical and experimental pressure drops with a MAE of ~12%. It can be noted that the ratio of two-phase pressure drop and single phase pressure drop ranges from 1.05 to 1.09, which is in good

agreement with the literature implying that the two-phase/single phase pressure drop ratios in subcooled boiling are not as much as saturated flow boiling *(Kandlikar 1999)*.

4.3.3 Heat transfer

Fig. 4.6 shows heat transfer coefficients at the nondimensional location of x/L=0.83 along the microtube with ~600 (μm) inner diameter. Different mass fluxes and microtube lengths are considered to show the effect of mass flux and heated lengths on heat transfer coefficient of microtube with ~600(μm) inner diameter. It is seen that at a constant heat flux, the longer microtube has higher heat transfer coefficient. For instance, at a heat flux of 300 (W/cm^2), obtained heat transfer coefficients at a mass flux of 5500 (kg/m^2.s) are 11 and 60 (W/cm^2.K) for heated lengths of 6 and 12 (cm), respectively.
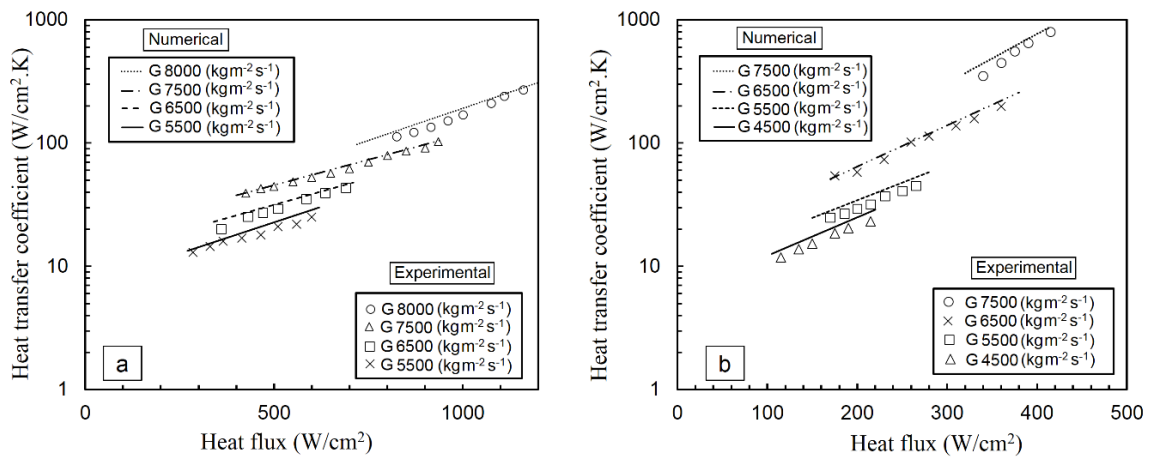
Fig. 4.6. Numerical and experimental heat transfer coefficient at the dimensionless location of x=0.83 for the microtube of inner diameter of ~600 μm a) heated length of 6 cm b) heated length of 12 cm

For high heat flux subcooled flow boiling, more heat is needed to activate the nucleation cites on the heated surface and nucleation sites operate at higher wall superheats. The onset of subcooled boiling is encountered at higher degree of subcooling and vapor bubbles may grow and collapse whilst attached or sliding along the heated surface (Collier and Thome 1994). For example, the onset of nucleate boiling occurs at the wall superheat of ~6 K for the mass flux of 5500 kg/m^2.s. As mass flux increases, higher heat flux is needed to achieve the saturation temperature at the inner wall of microtube. This shows that high mass flux

subcooled flow boiling is an effective way for high heat removal rates. It can be observed that heat transfer coefficient increases with mass flux suggesting convective heat transfer effects. . The trends in the numerical results match with the experimental results. There is a good agreement between numerical and experimental results (with a MAE of ~20%). The MAE for the microtube with the length of 6 cm is 17%, while it is 26% for the microtube of the length of 12 cm. This deviation is associated with the lack of accurate models in multiphase flows particularly for micro scale, which are used in numerical modeling (e.g. bubble departure frequency).

Fig. 4.7 shows experimental and numerical local heat transfer coefficients for different heat fluxes. As can be seen, at a fixed heat flux, as mass flux increases, heat transfer coefficient increases. As mass flux increases, heat removal capacity of working fluid increases due to more dominant convective heat transfer effects. In subcooled flow boiling, both nucleate boiling and single phase convective heat transfer effects are present. Single phase convective heat transfer effects exist at higher mass fluxes and higher subcooling, which matches with the flow conditions in this study.
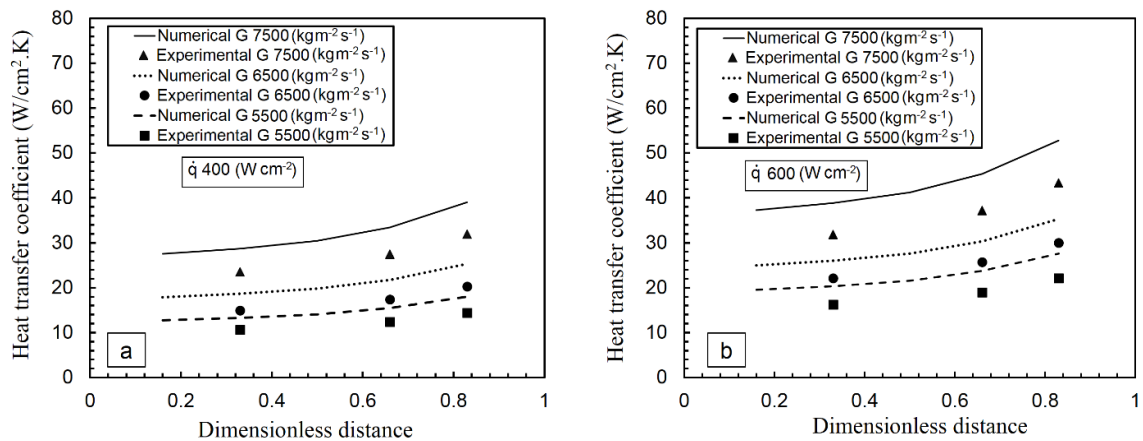
Fig. 4.7. Effect of heat flux on heat transfer coefficients in subcooled flow boiling for the microtube with inner diameter of ~600 μm and heated length of 6 cm at heat flux of a) 400 W/cm^2 b) 600 W/cm^2

Furthermore, at the heat flux of 400 (W/cm^2), maximum heat transfer coefficients achieved for mass fluxes of 5500, 6500, and 7500 (kg/m^2.s) are around 20, 25, and 40 (W/m^2.K), respectively. As illustrated in Fig. 4.7, at a fixed mass flux of 6500 (kg/m^2.s), heat transfer

71

coefficients for applied heat fluxes of 400 and 600 (W/cm^2) are around 25 and 35 (W/m^2.K), respectively, which shows that heat flux has an increasing effect on boiling heat transfer. This is due to more nucleate sites at higher heat fluxes along the microchannel and enhanced nucleate boiling. These heat transfer coefficient values are close to those reported in the experimental studies in small channels under similar experimental conditions (Rafet Özdemir, Kaya et al. 2011). When comparing the numerical results to experimental results, a reasonable agreement can be observed including similar trends in the profiles.

Fig. 4.8-a shows the effect of mass and heat fluxes on local heat transfer coefficient of microtube with an inner diameter of ~600 μm and heated length of 6 cm. According to Fig. 4.8-a, it can concluded that at subcooled flow boiling the effect of mass flux is more pronounced than the effect of heat flux. As stated before, at high mass flux subcooled flow boiling single phase convective heat transfer mechanism is dominant and nucleate boiling mechanism plays a minor role. Fig. 4.8-b presents the effect of heated length on subcooled flow boiling. It is seen that higher heat transfer coefficients are achieved with the longer microtube. The effect of mass flux on heat transfer coefficient is more for the longer microtube, while the effect of heated length is more pronounced at higher mass fluxes.
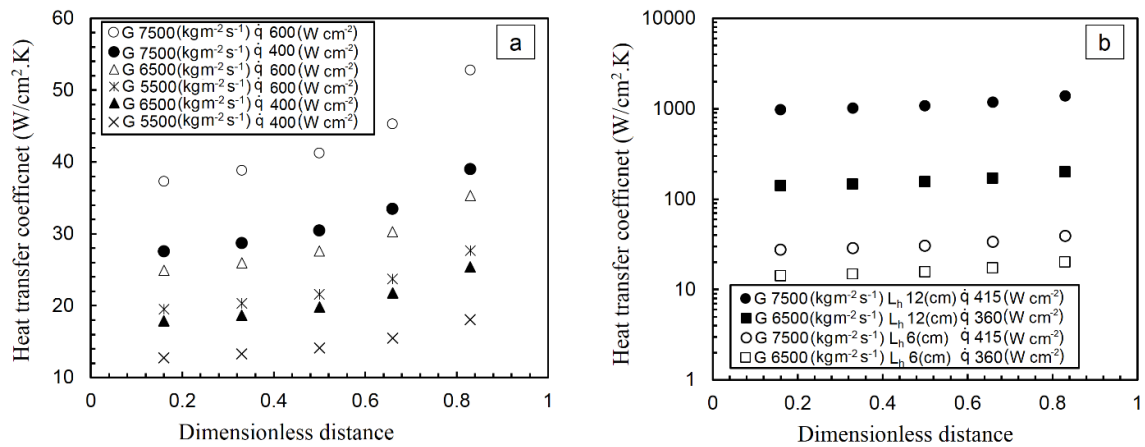
Fig. 4.8. Effect of heated length on heat transfer coefficient at fixed heat flux

The effect of microtube diameter on local heat transfer coefficient is shown in Fig. 4.9 for microtube with ~900 and ~1100 μm inner and outer diameters, respectively. As can be seen, the longer microtube results in higher heat transfer coefficients, whereas the heat fluxes are higher for the shorter microtube. Comparing Fig. 4.9 to Fig. 4.6, it can concluded that as the

diameter decreases and heated length increases, heat transfer coefficient exhibits an increasing trend. The effect of mass and heat fluxes on subcooled flow boiling is more pronounced in microtubes with smaller diameters. Again, a good agreement between the experimental and numerical results can be seen.
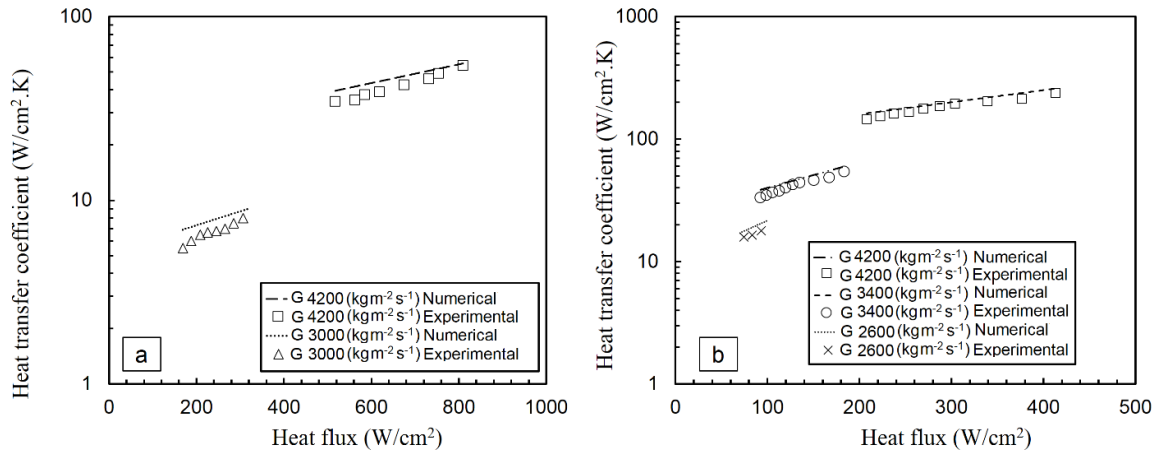
Fig. 4.9. Heat transfer coefficients for the microtube with inner diameter of ~900 μm at the dimensionless location of x=0.83 a) 6 cm heated length b) 12 cm heated length

The effect of vapor quality on heat transfer coefficient at the outlet of microchannel is shown in Fig. 4.10. It can be seen that vapor quality has an increasing effect on heat transfer coefficient, which is due to the presence of more active nucleate sites along the channel at higher heat fluxes contributing to nucleate boiling and leading to higher heat transfer coefficients. It can be seen that at a certain heat flux the void fraction curve changes its slope, which was also reported in the literature (Sami and Duong 1987). The first slope corresponds to local boiling with stationary bubbles on heated surface and high subcooling, whereas the second slope is associated with local boiling with low subcooling.
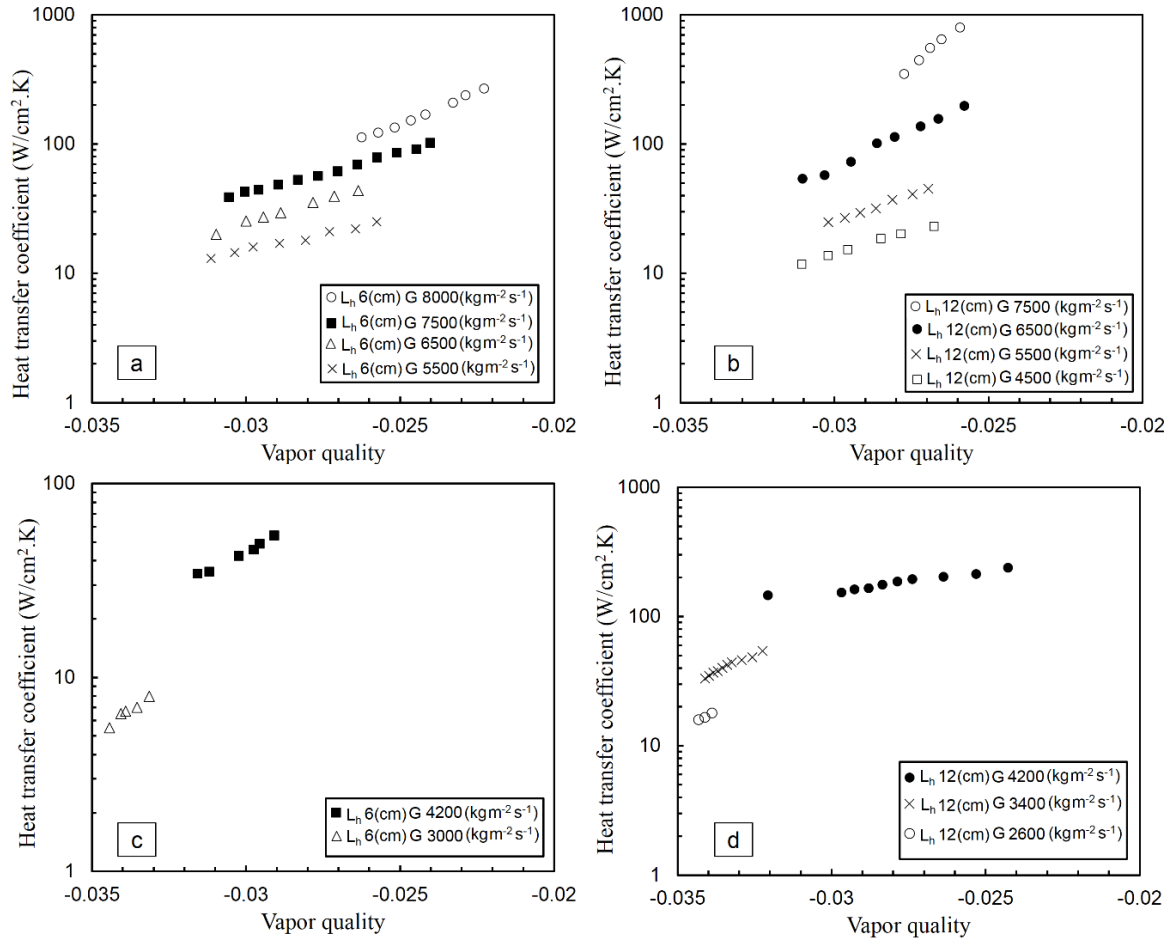
Fig. 4.10. Effect of vapor quality on heat transfer coefficient for the microtube

a) $D_i = \sim 600$ μm and $L_h = 6$ cm b) $D_i = \sim 600$ μm and $L_h = 12$ cm

c) $D_i = \sim 900$ μm and $L_h = 6$ cm d) $D_i = \sim 900$ μm and $L_h = 12$ cm

The effect of vapor quality on two-phase heat transfer coefficient for two different heated lengths at different mass fluxes is shown in Fig.4.11. As stated before, as heat flux increases, active nucleation sites increases. On the other hand, higher heat flux provides higher evaporation momentum force. Therefore, as heat flux increases, generated vapor quality increases. This trend is more pronounced at higher mass fluxes. Comparing Fig.4.11-c to Fig.4.11-d, it can be observed that as heated length increases generated vapor quality increases.
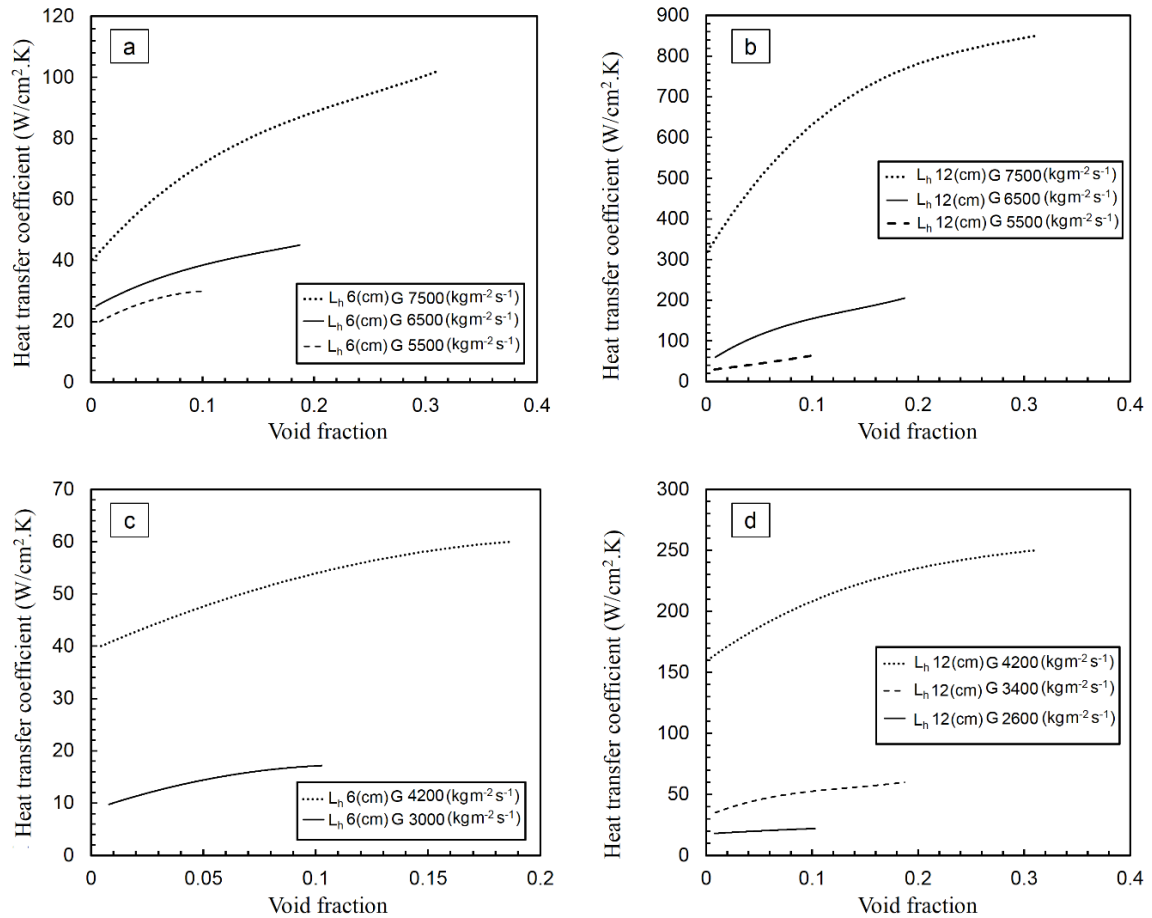
Fig.4.11. Effect of calculated numerical void fractions on heat transfer coefficient for the microtube

a) $D_i = \sim 600$ μm and $L_h = 6$ cm b) $D_i = \sim 600$ μm and $L_h = 12$ cm

c) $D_i = \sim 900$ μm and $L_h = 6$ cm d) $D_i = \sim 900$ μm and $L_h = 12$ cm

Fig. 4.12 indicates the effect of inlet subcooling on heat transfer coefficient for inlet temperatures of 295 and 305 K for microtube with 12 cm length and ~600 μm inner diameter. When subcooling decreases (by increasing the inlet temperature) the heat flux corresponding to boiling inception drops to lower values. Since at a fixed heat flux, there will be more bubbles for lower subcooling conditions, higher inlet temperature leads to higher heat transfer coefficients, which is consistent with the reported trends in the literature (Chen, Chang et al. 2009) and is attributed to more nucleation sites at lower subcooling for a fixed heat flux. For example, at a heat flux of 215 W/cm^2 and a mass flux of 6500 kg/m^2.K, heat transfer coefficient at the inlet temperature of 310 K is almost 15% higher than that at the inlet temperature of 295 K. Furthermore, it is concluded that the effect of inlet subcooling is

more pronounced at higher mass fluxes, whereas heat transfer coefficient for flow with 305 (K) inlet temperature is 15% and 10% higher than flow with 295 (K) inlet temperature for mass fluxes of 6500 and 4500 (kg/m^2.s), respectively.
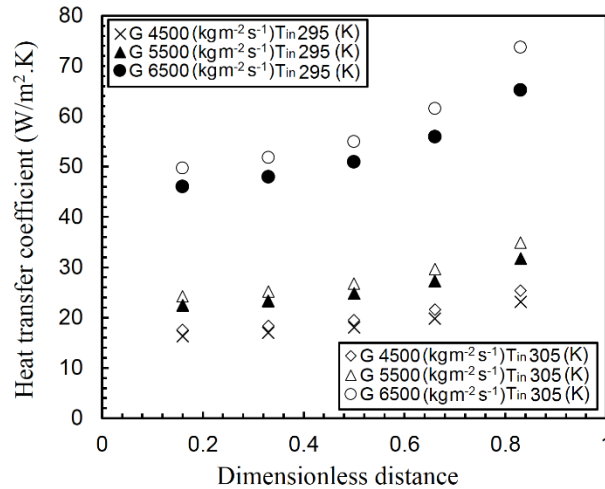
Fig. 4.12. The effect of inlet temperature on high mass flux subcooled boiling at different mass fluxes for a fixed heat flux of 215 W/cm^2

Fig. 4.13 provides a comparison between the experimental heat fluxes and those calculated using the available partial boiling correlation (4.10). Most of the experimental data could be predicted by the correlation within ±30%. As heat flux increases with increasing wall superheat, subcooled flow boiling mechanism shifts from partial subcooled flow boiling to developed subcooled flow boiling, where the correlation starts to under predict the experimental heat flux.
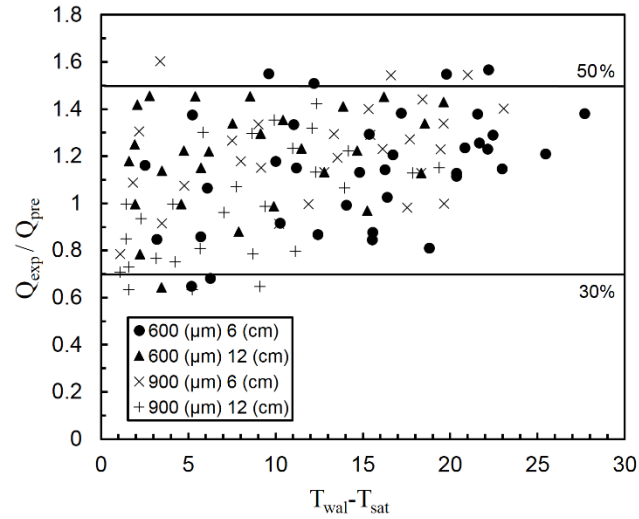
Fig. 4.13. Comparison between the experimental heat fluxes and predictions

4.4 Summary

In this study, high mass flux subcooled flow boiling was investigated both numerically and experimentally. Microtubes with heated lengths of 6 and 12 cm and inner diameters of ~600 and ~900 μm were used to investigate the effect of heated length and inner diameter on subcooled flow boiling characteristics. The following major conclusions are drawn from the results:

i-) Microtube diameter has an inverse relationship with heat transfer coefficient, while longer microtubes lead to higher heat transfer coefficients.

ii-) Subcooled boiling heat transfer is a function of the size and length of the microtube and flow conditions. As mass flux increases, higher heat fluxes can be achieved.

iii-) At high mass flux and subcooling, the convective heat transfer mechanism is more pronounced. The effect of heated length is also more visible at high mass fluxes. Furthermore, the effect of mass flux is stronger in comparison to the effect of heat flux in smaller diameter microtubes.

iv-) Heat transfer coefficient increases with vapor quality. The effect of void fraction on heat transfer coefficient is more pronounced in smaller size microtubes. Furthermore, inlet subcooling has a significant effect on heat transfer, and as inlet subcooling decreases, heat transfer coefficient becomes higher particularly in smaller microtubes (in diameter and length).

v-) The numerical results are in a good agreement with the experimental results.

CHAPTER 5. FLOW BOILING ON STRUCTURED AND COATED SURFACES

During the last decade, extensive research on flow boiling heat transfer in mini/micro channels has been conducted (Thome 2004). Most of the models for boiling in minichannels are extensions of the pool boiling nucleation model proposed by (Hsu 1962, Collier and Thome 1994). One of the main differences between conventional and mini/micro size channels is that buoyancy effects in small channels are insignificant, while viscous and capillary effects are significant (e.g. stratified flow is not observed in microchannels, effect of surface tension force predominates with diminishing length scale).

Isolated bubble, confined bubble, slug, annular/slug flow patterns are major flow boiling patterns in small passages (Cornwell and Kew 1993). The departing and growing bubbles are associated with isolated bubbly flows, which are mostly observed near the inlet region of the heated region. The bubble size grows along the channel and bubbles eventually span the entire channel cross section forming a confined bubble regime. Finally, annular flows appear downstream the channel after confined bubble/slug flow pattern. The development of diabetic flow maps is more challenging due to the coupled effects between flow dynamics and heat transfer. Important parameters affecting flow regimes are nucleation, evaporation or condensation of liquid films, dry-out condition, heat flux, mass flux, acceleration/deceleration of the flows, and thermophysical properties such as surface tension.

It has been indicated that there are some differences between conventional and micro scale nucleation criteria. As an example buoyancy in microchannels is insignificant but inertial viscous and capillary effect are crucial (e.g. stratified flow is not observed in microchannels). It is quite challenging to develop diabetic flow map in microscale. This is mainly due to the coupled effects between the flow dynamics and heat transfer, and the scale effects at the microscale level. One factor that influences these flows is surface tension.

Recently, many techniques have been proposed to predict and enhance boiling heat transfer (BHT) (Koşar, Kuo et al. 2005, Woodcock, Yu et al. 2015). In particular, the effect of heating surface characteristics on nucleate boiling heat transfer has been actively investigated. Wettability and roughness elements are key parameters for determining heating surface characteristics, since they introduce interactions among dynamics between the working

liquid, vapor, and solid surface. In this chapter, surface enhancements were accomplished by micro and nanostructures, and flow boiling experiments on coated and nano and micro structured surfaces are presented. The boiling heat transfer performances of these surfaces are compared to each other as well as a plain surface as the control sample.

5.1 Test facility and experimental procedure

The experimental setup was designed to conduct flow boiling experiments under the atmospheric conditions. The experimental setup and test section are shown in Fig.5.1 and Fig.5.2, respectively. Experimental setup consists of two water tanks/reservoir, a micro-gear pump, a pressure sensor, five thermocouples, a DC power supply, a high speed camera and a data acquisition system. De-ionized water is used as working fluid. Flow patterns are recorded with a high speed camera (T.I.M.M., ROBOT SYSTEME, 1500 FPS) for each data point. The same procedure is repeated for different flow rates.
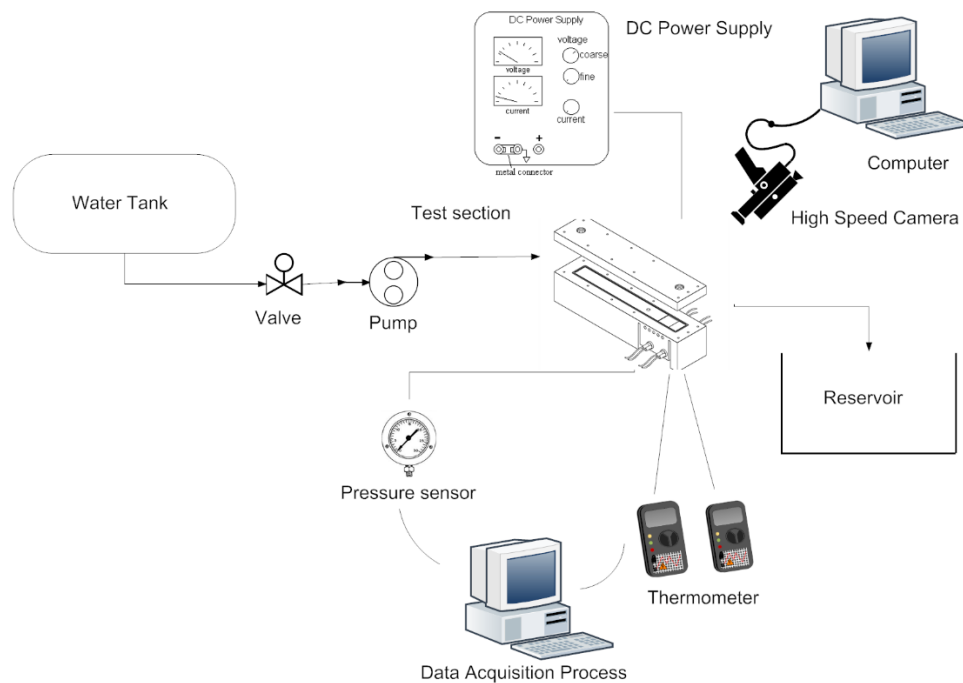
Fig.5.1. Schematic of the experimental setup

An aluminum test base contains a groove, which allows for the integration of the test plates to the system using high quality thermal grease. The test section is heated with 4 cartridge heaters placed underneath the test plate. The test section has dimensions of $14 \times 1.5 \times 0.5$

mm^3. Thermocouples are located beneath the test sample at fixed locations as well as the inlet of the test section. A sufficient distance was left between the samples and cartridge heaters to ensure a uniform heat flux distribution. The sides of the test block are covered by glass wool and air gaps are formed on the sides of the block of heaters to minimize heat losses to the ambient. An Omega pressure transducer is located downstream the heated area. The Aluminum base is connected to a transparent cover with fastening bolts and O-ring to avoid any leakage in the system. The transparent block enables flow visualization at the same time. During the experiments, electrical power is delivered to the heaters in small increments. Working fluid is propelled into the heated section using a micro gear pump at a fixed flow rate. The surface temperature values are recorded as a function of the applied voltage and current to the heaters, along with pressures from the transducer under steady state conditions.
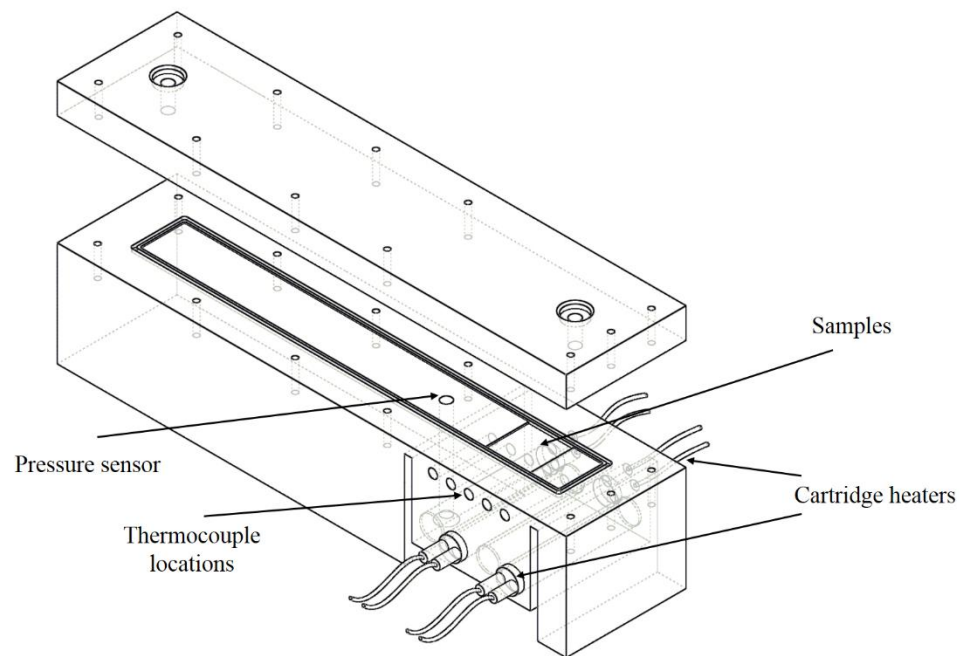
Fig.5.2. Schematic of the test section

5.2 Data reduction

The heat flux, q'', delivers to the system is obtained from:

$$q'' = \frac{P - Q_{loss}}{A} = \frac{Q_{net}}{A} \quad (5.1)$$

Here, P is the power input, Q_{loss} is the heat loss and A is the heated surface area of the aluminum base. The surface temperatures are calculated considering thermal contact resistances between the surface of the micro/nano plates and thermocouples.

$$T_S = T_{th} - q''' R_{tot} \quad (5.2)$$

Here, T_{th} is the thermocouple temperature reading above plate and R_{tot} is the total thermal resistance between plate surfaces and the thermocouples. R_{tot} is found as:

$$R_{tot} = R_{tg} + R_{plate} \quad (5.3)$$

Here, R_{tg} is the thermal resistance of the thermal grease at the interface and R_{plate} is the thermal resistance of the test plate. The heat transfer coefficient, h, for single phase flow, subcooled and saturated flow boiling are obtained from:

$$h = \begin{cases} \dfrac{q''}{T_S - T_f} & \text{single phase and subcooled boiling regions} \\ \dfrac{q''}{T_S - T_{sat}} & \text{saturated boiling region} \end{cases} \quad (5.4)$$

Here, T_S is the surface temperature and T_f is the bulk fluid temperature such that:

$$T_f = T_i + \left[\frac{(Q_{net}) x_{th}}{\dot{m} c_p L_h} \right] \quad (5.5)$$

where L_h is the heated length, T_i is the inlet fluid temperature, Q_{net} is the net power input, x_{th} is the thermocouple location, $\dot{m}$ is the mass flow rate and c_p is the specific heat of water. Boiling heat transfer data correspond to the surface temperatures greater than the saturation temperature (T_{sat}).

The enthalpy at different axial locations was determined by a simple energy balance along the heated length as:

$$H_x = H_{in} + \frac{\dot{q}}{\dot{m}} \frac{x_{th}}{L_h} \quad (5.6)$$

Here, H_x is the local enthalpy at a given axial location, H_{in} is the inlet enthalpy, and x_{th} is the axial distance from the inlet. The equilibrium vapor quality is calculated as:

$$x_{eq} = \frac{H_x - H_{f,sat}}{H_{fg}} \quad (5.7)$$

where $H_{f,sat}$ is the saturated liquid enthalpy and H_{fg} is the latent heat of vaporization.

Nusselt number for single phase flow data, where the surfaces temperatures are lower than the saturation temperature, is extracted from:

$$Nu = h D_h / k \quad (5.8)$$

where D_h is the hydraulic diameter of the channel and k is the thermal conductivity of the fluid. The flow velocity is expressed as $u = \dot{Q}/A_c$, where $\dot{Q}$ is the volumetric flow rate and A_c is the total cross sectional of the channel. The Reynolds number is given as:

$$\mathrm{Re} = \rho u \, D_h / \mu \quad (5.9)$$

Here μ is the viscosity of the working fluid.

Single-phase friction factor is obtained from adiabatic tests and is given by:

$$f = \frac{2 D_h \Delta P \rho_f}{L G^2} \quad (5.10)$$

The maximum uncertainties in experimental parameters are given in Table 5.1. They were provided by the manufacturer's specification sheets or were obtained using the propagation of uncertainty method presented in Coleman and Steele (Coleman and Steele 2009) study.

Table 5.1.Estimated uncertainties for important factors

Parameter	Uncertainties
Electrical power (P)	±0.36%
Mass flux (G)	±2.9%
Pressure drop (ΔP)	±6%
Fluid temperature (K)	±0.6%
Wall temperatures (K)	±1.2%,
Quality (x_{eq})	±8%
Nusselt number (Nu)	±7%
Two phase heat transfer coefficient (h_{tp})	±8%

5.3 System validation

A single-phase tests were conducted to validate the test setup and data reduction procedure. Since the aspect ratio of the test section is 30, the obtained results were compared with the predictions of the correlations developed for parallel plates (Bejan 2013). Fig.5.3 shows the comparison between experimental data and the predictions of the correlations. As can be seen, the prediction of the correlations are good for both friction factor and heat transfer coefficient data. All the data are predicted within ±30%.
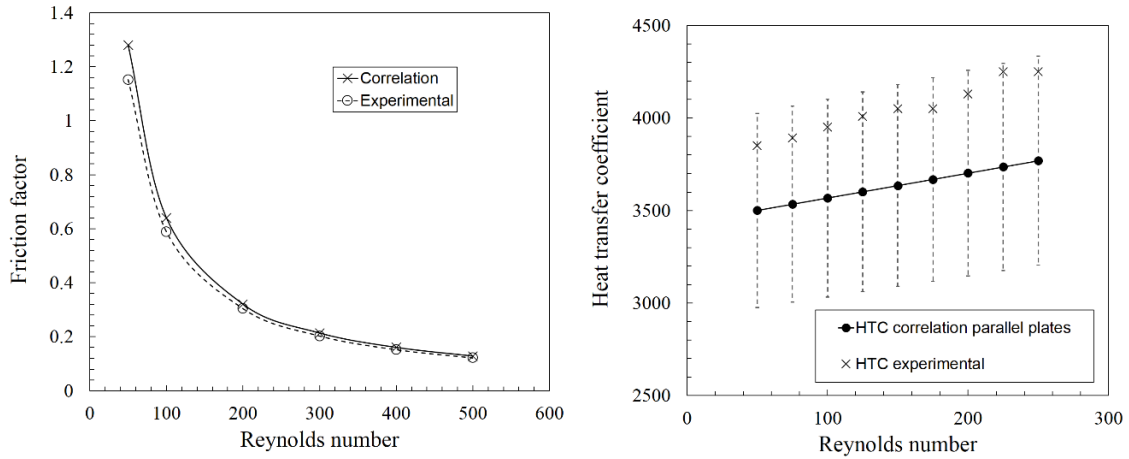
Fig.5.3. Obtained experimental friction factors and Nusselt numbers and comparison between available correlations (Bejan 2013)

5.4 Roughened surfaces

Two different materials as Aluminum alloy 2024 and Copper were chosen as substrates. Micro and nano-structures were introduced to the sample using sanding and DI-water boiling procedures, respectively. Micro-structures were formed on the aluminum surfaces, while copper samples were process to accomplish nano-roughness elements.

5.4.1 Sample preparation and characteristics

Fig.5.4 shows the schematic of the experimental procedure for sample preparation. In order to introduce the micro-structures, sandpapers with grid sizes of 36 and 1000 were used to mechanically sand the Al alloy 2024 samples. The sanding process was carried out for 20 s with an applied pressure of 3.0 ± 0.2 kg/cm^2. To introduce nanoroughness, first, Al alloy surfaces were polished with sandpapers of large grit sizes of 1500 and 3000, respectively, for removal of surface contaminants; next, the flat polished surfaces rinsed with DI water were immersed in boiling DI water for 1, 5, 20, 60, and 120 min. The micro-nano structured samples, were engineered by first sanding the surfaces with grit sizes ranging from 36 to 1000, and then immersion in boiling DI water for different times of 1, 5, and 120 min. Ultimately, the roughened surfaces were ultrasonicated with acetone, isopropanol, and DI water for 10 min each and purged with nitrogen gas.
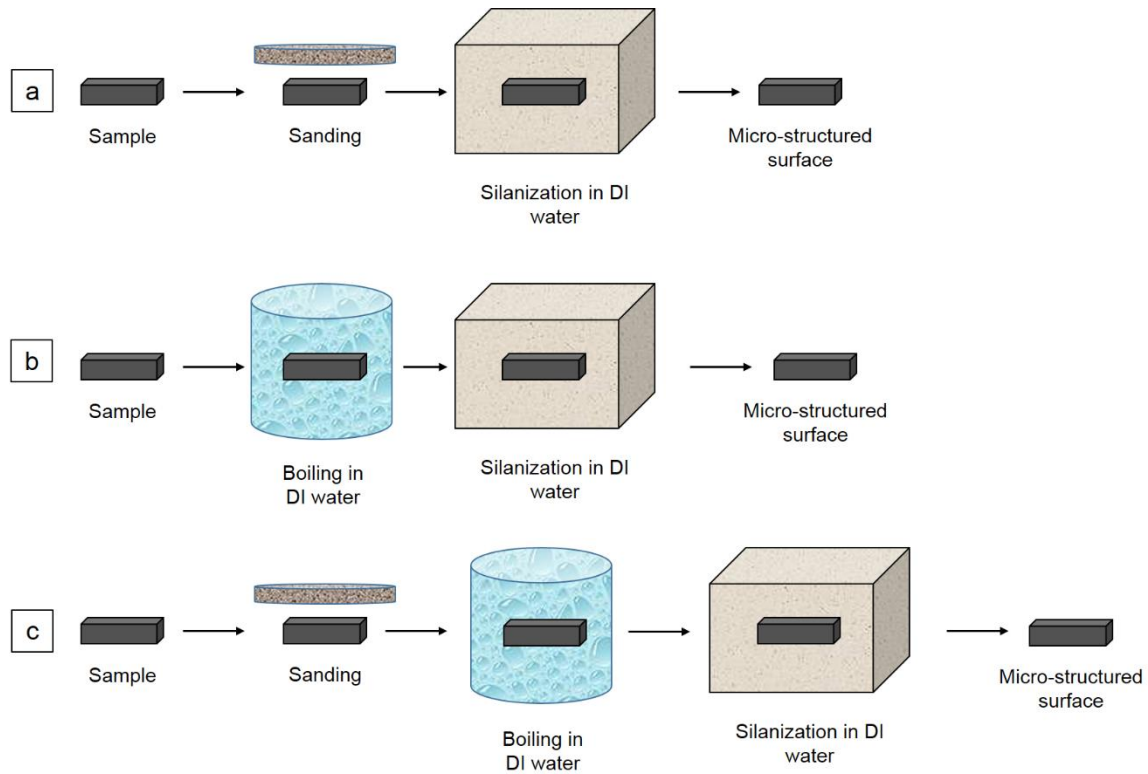
Fig.5.4. Schematic representation of the experimental procedure used to introduce a) micro-structure, b) nano-structure c) nano-micro structures (Saifaldeen, Khedir et al. 2014)

The SEM images of samples are shown in Fig.5.5 and Fig.5.6. Contact angle (CA) measurements were carried out using a VCA Optima goniometer. Liquid droplets of 5 ± 1 µl size of DI water was gently dispensed on the surfaces. The captured digital images were then analyzed for their CA measurements using the Sessile Drop method available with the software. The obtained results are shown in Table 5.2.

Table 5.2.Sample characteristics of Al 2024 plates

	#36	#1000
Contact angle (degree)	115	118
Particle diameter of sand paper (µm)	600	10
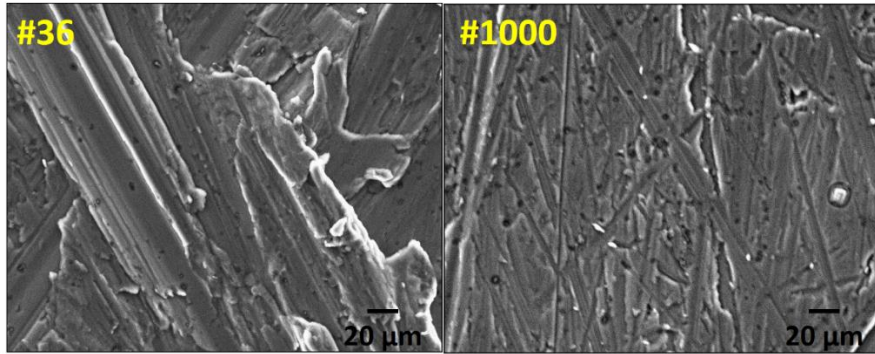
Fig.5.5. SEM image of Al-2024 alloy samples with micro-roughness
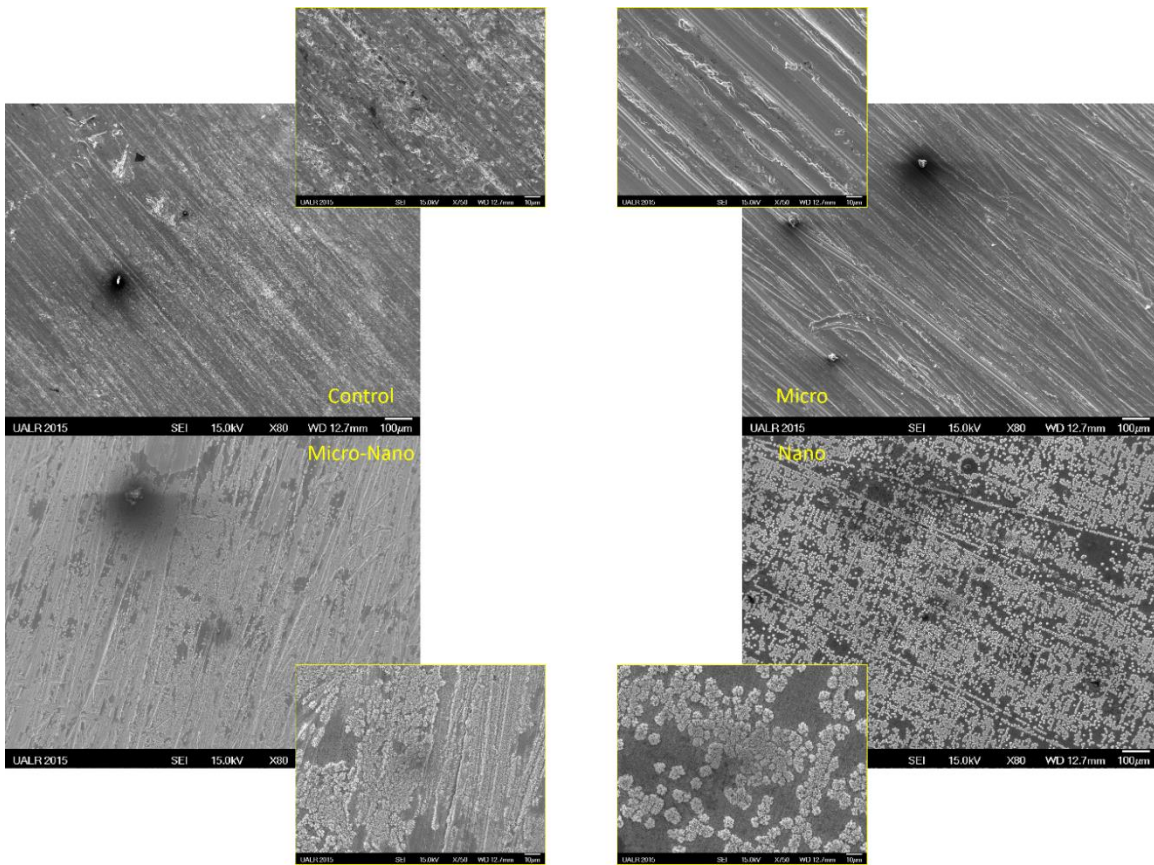
Fig.5.6. SEM image of Cu samples with micro and nano-roughness

The micro-structures of nano-treated copper samples are shown in Fig.5.7.
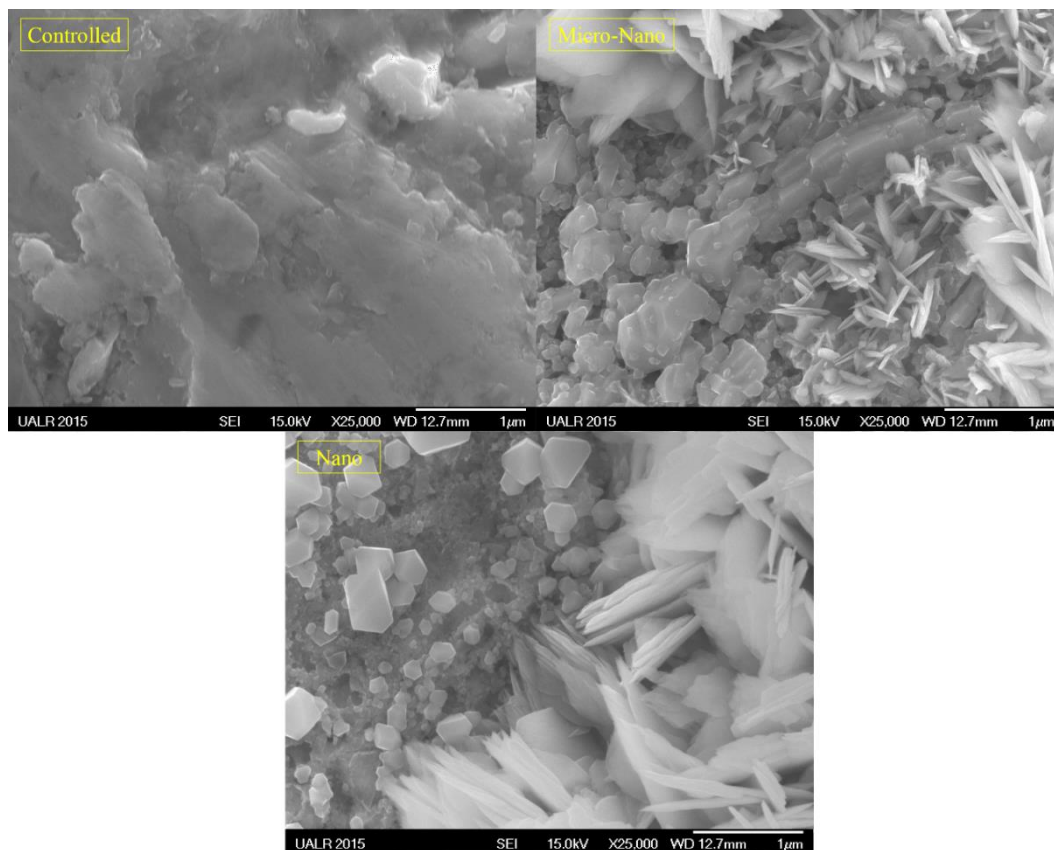
Fig.5.7. Surface morphology of different nano-treated Cu samples

Also measured contact angles of the nano-structured Cu samples are shown in Fig.5.8.
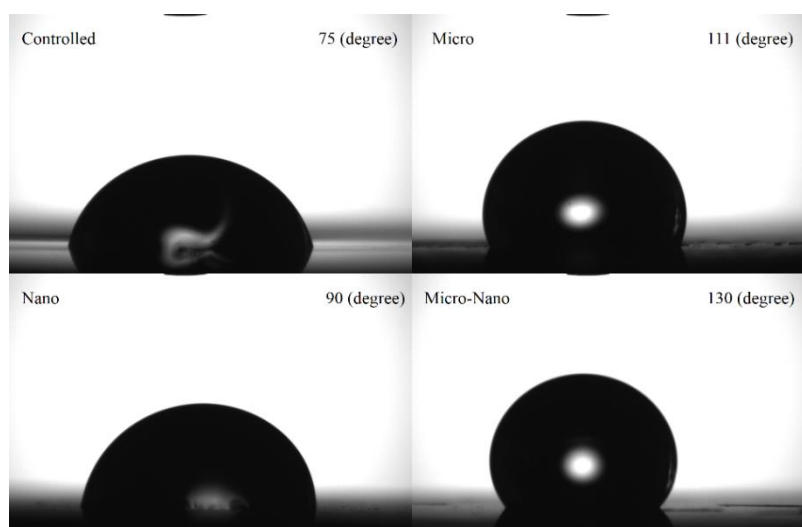
Fig.5.8. Contact angle of samples

5.4.2 Results and discussion

5.4.2.1 Micro-roughened aluminum surfaces

Flow patterns, and nucleation from roughened Al-2024 alloy samples are shown in Fig.5.9 for two different heat fluxes of 6 and 11 W/cm^2 along with those of the plain surface. The bubble departure diameter on a surface with small cavity size is generally determined by a balance between gravitational and inertia forces. As surface cavity size increases, flow inertia force decreases, thus bubble departure diameter decreases. This clarifies the smaller bubble sizes on the roughened surfaces (Hatton and Hall 1966).

At the heat flux of 6 W/cm^2, the structured surface with 1000 grid size leads to more active nucleation sites than the plain surface. The difference between the plain surface and the plate with 36 grid size is not very apparent. But the bubble size is still smaller for this plate, and more elongated bubbles are observed on the plain surface.
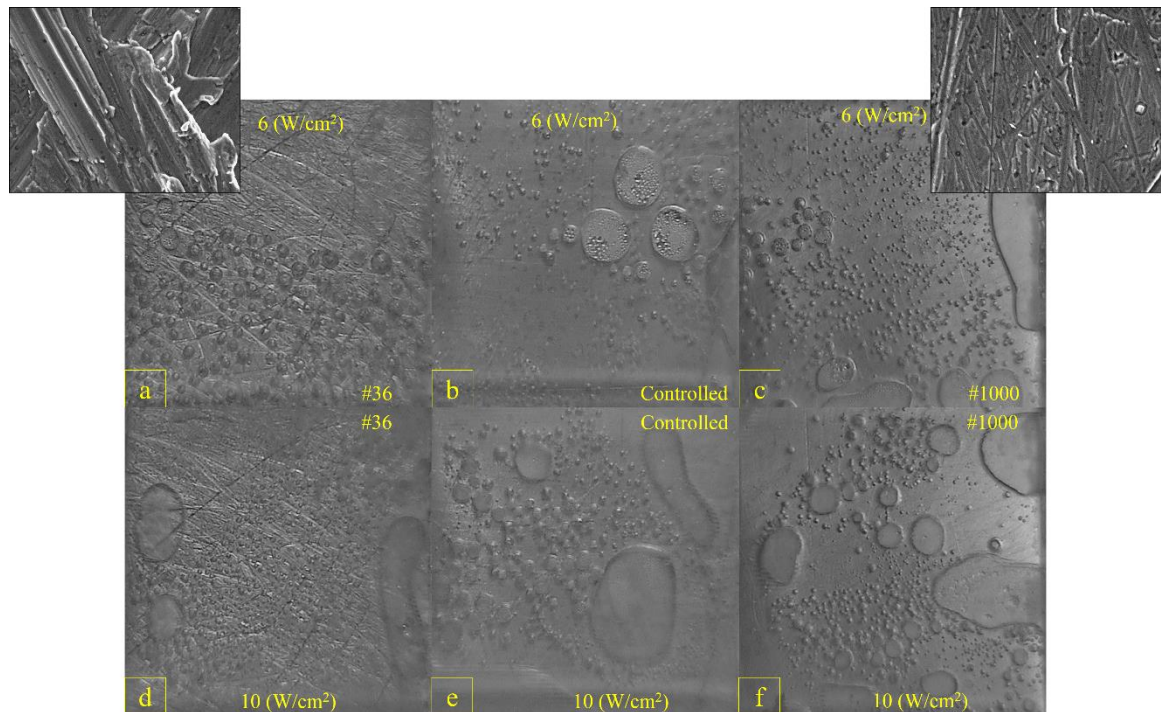
Fig.5.9. Boiling images for the mass flux of 50 kg/m^2.s and the heat fluxes of 6 W/cm^2 (a,b,c) and 10 W/ cm^2 heat flux (d,e,f).

At the higher heat flux, the flow pattern to elongated bubble pattern for the surface of # 1000 grit size. This surface again has higher nucleation site density. At higher wall temperatures, it was observed that flow regime slightly changed from bubbly to bubbly/slug at higher heat fluxes for controlled surface. As it is seen in Fig.5.9-d and Fig.5.9-f, while bubbly flow pattern exists for #1000 surface, flow pattern for untreated (controlled) surface is bubbly/slug flow pattern. The presence of different flow patterns at a fixed heat flux indicates that as surface roughness increases, bubble departure diameter decreases at detached bubbles are able to move to downstream.

Obtained wall temperatures at mass fluxes of 50 and 125 kg/m^2.s are shown in Fig.5.10. As it is seen in boiling region, #1000 surfaces have lower temperature in comparison to other surfaces. Roughen surfaces have larger active cavity sizes and higher active cavity densities, which results in lower wall superheats.
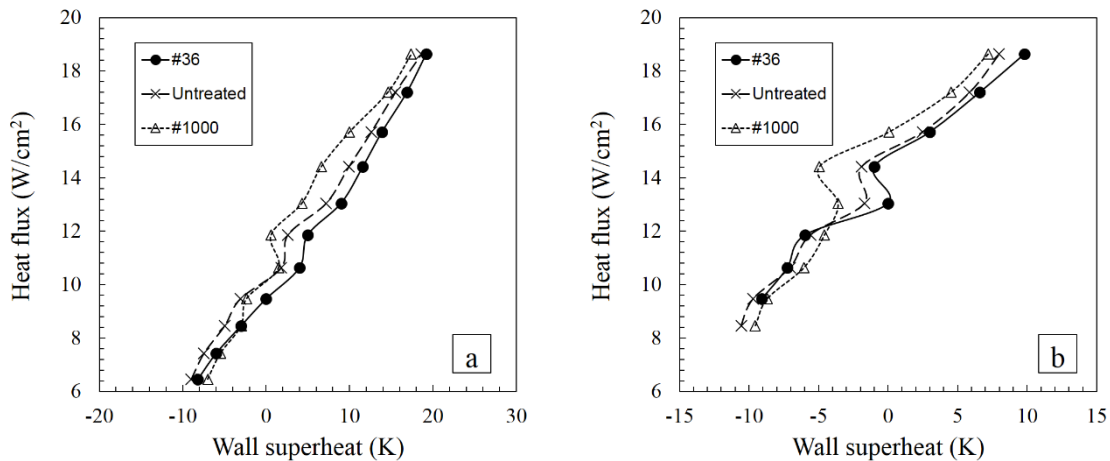
Fig.5.10. Wall superheat-heat flux profiles based the middle location of the test samples at the mass fluxes of a) 50 kg/m^2.s b) 125 kg/m^2.s

Wall superheat-heat flux profiles and heat transfer coefficients are displayed for the mass fluxes of 50 and 125 kg/m^2.s in Fig.5.11 and Fig.5.12. As mass flux increases, component, higher heat transfer coefficients are obtained due to higher convective heat transfer. Under the experimental conditions, structures have significant effect on heat transfer coefficient. Smaller bubbles, smaller bubble release frequency and more active nucleation sites result in enhancements in the microstructured surface with the grit size 1000.
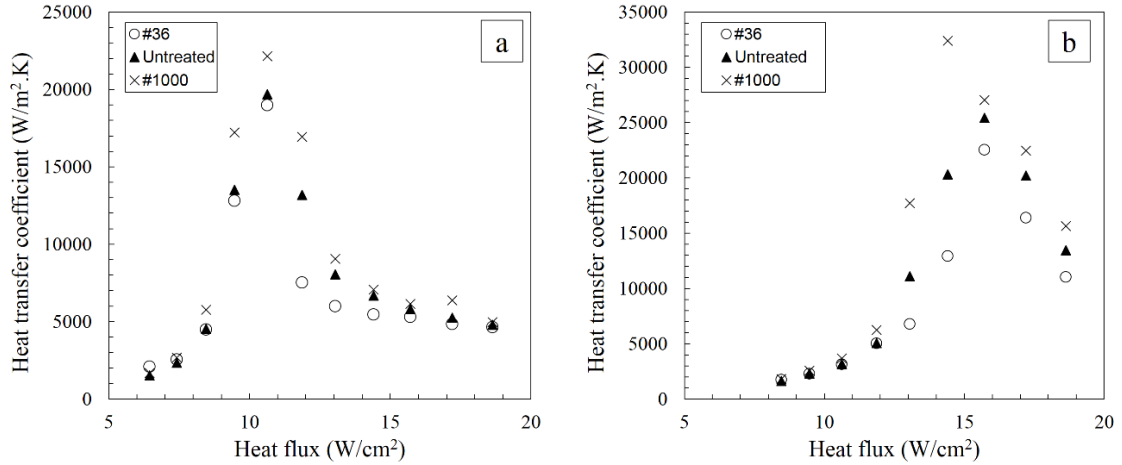
Fig.5.11. Obtained heat transfer coefficient at a) 50 kg/m^2.s b) 125 kg/ m^2.s mass fluxes

In parallel lines with the similarities of flow boiling images between the plain surface and the surface with grid size 36, no considerable difference in heat transfer coefficient profiles exists. There is an average enhancement in heat transfer of 15% and 18% for the microstructured surface of grit size 1000 at mass fluxes of 50 and 125 kg/m^2.s, respectively. Heat transfer coefficients are presented as a function of vapor quality in Fig. 1.10. As can be seen, there is first an increasing trend, while a decreasing trend is present beyond a specific vapor quality. This is due to the shift from nucleate boiling dominance to convective boiling dominance. Similar trends in heat transfer coefficient with vapor quality were also reported in the literature (Steinke and Kandlikar 2004).
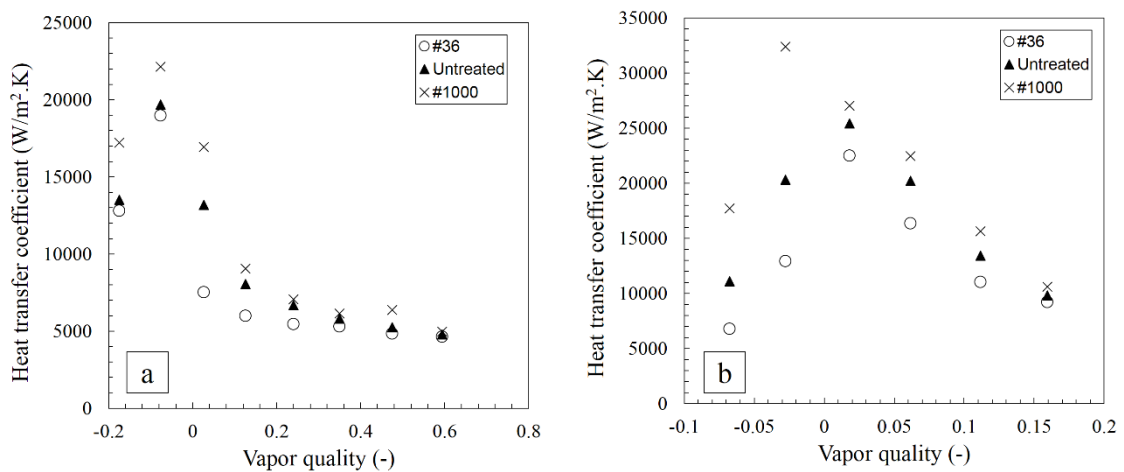
Fig.5.12. The effect of vapor quality on heat transfer coefficient at a) 50 kg/m^2.s b) 125 kg/ m^2.s mass fluxes

91

5.4.2.2 Nano-structured copper surfaces

Flow boiling images of structured copper plates are shown in Fig.5.13 for two different heat fluxes of 7 and 12 W/cm^2. As seen, nano-structured surfaces provide more active nucleation sites at a fixed applied heat flux. Although the size of cavities on nanostructured surfaces seem to be lower than the required critical cavity size at the corresponding wall superheat, nanostructures act together as a nucleation site (Li, Wang et al. 2008). Furthermore, more bubbles and smaller bubble sizes are observed for plates with nano-structures, which is due to lower surface energy of the solid surface and larger density of active nucleation sites (Saifaldeen, Khedir et al. 2014). Elongated bubbles are more detected on the plain surface. Both isolated and elongated bubbles are seen for both nano- and microstructured surfaces

Heat transfer coefficient profiles are shown in Fig.5.14. As seen in the figure, heat transfer enhancements are obtained from both micro- and nanostructured surfaces. This is mainly due to more active nucleation sites in comparison to the plain surface. On the other hand, nano-structured surfaces show a better heat transfer coefficient performance compared to microstructured surfaces. Nano-structured surfaces provide enhanced quasi-periodic liquid–solid contacts, which enables enhanced local quenching of the heater surface.
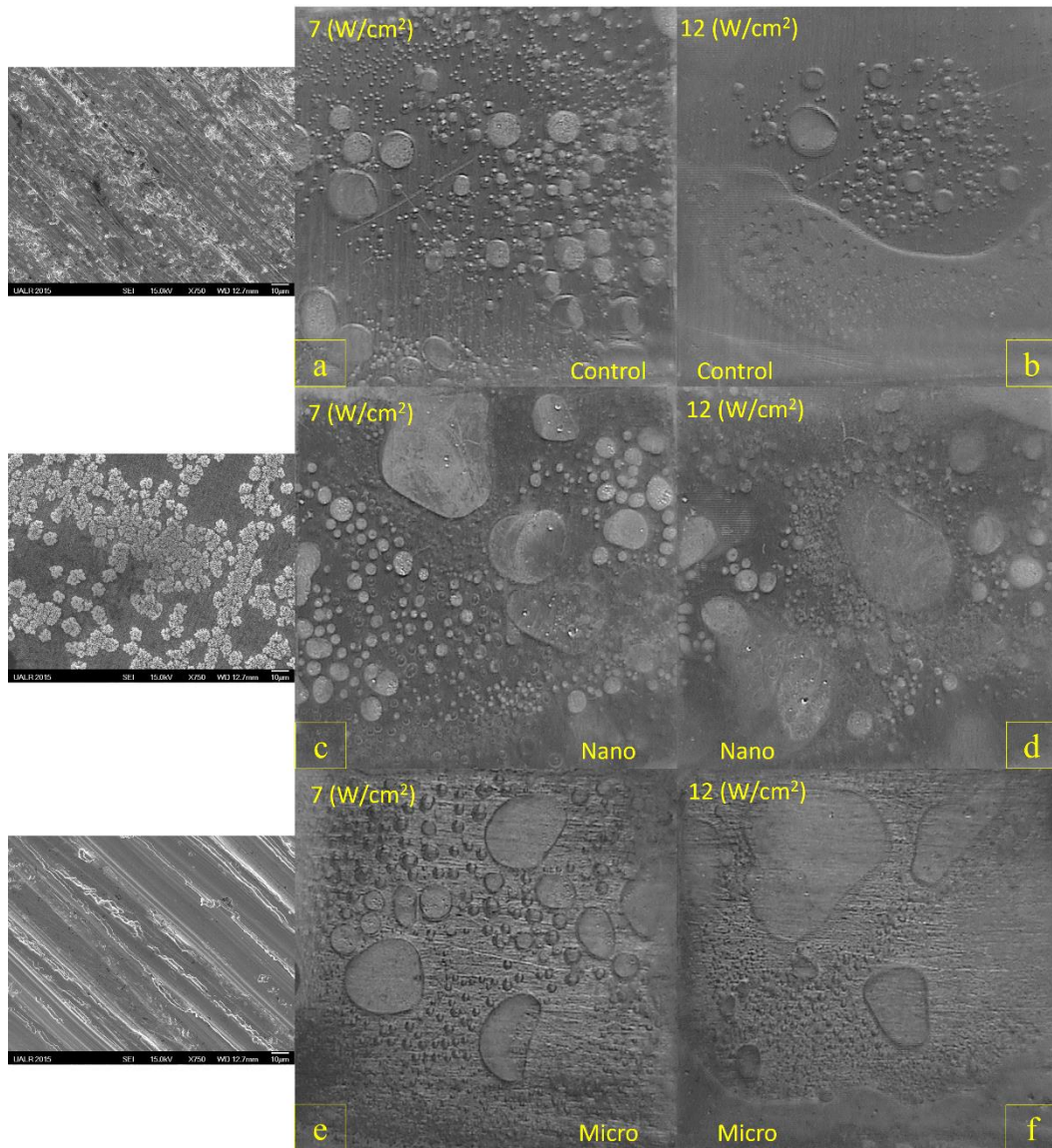
Fig.5.13. Bubble behavior for different surface treatments at 50 kg/ m^2.s flow rate and 7 W/cm^2 heat flux (a,c,e) and 12 W/ cm^2 heat flux (b,d,f)

Furthermore, flow visualization reveals that on nano-structured surfaces (namely Nano and Micro-Nano surfaces) bubbles move at higher velocities than the other surfaces (plain and microstructured) (Fig.5.15). The bubble release frequency of such surfaces is also higher than the micro-structured and plain surfaces. The average increases in heat transfer coefficients are 15%, 7%, and 22% for microstructured, nanostructured, micro-nanostructured surfaces at the mass flux of 50 (kg/ m^2.s), respectively, while they are 24%, 13%, and 30% at the mass flux of 125 (kg/ m^2.s), respectively.
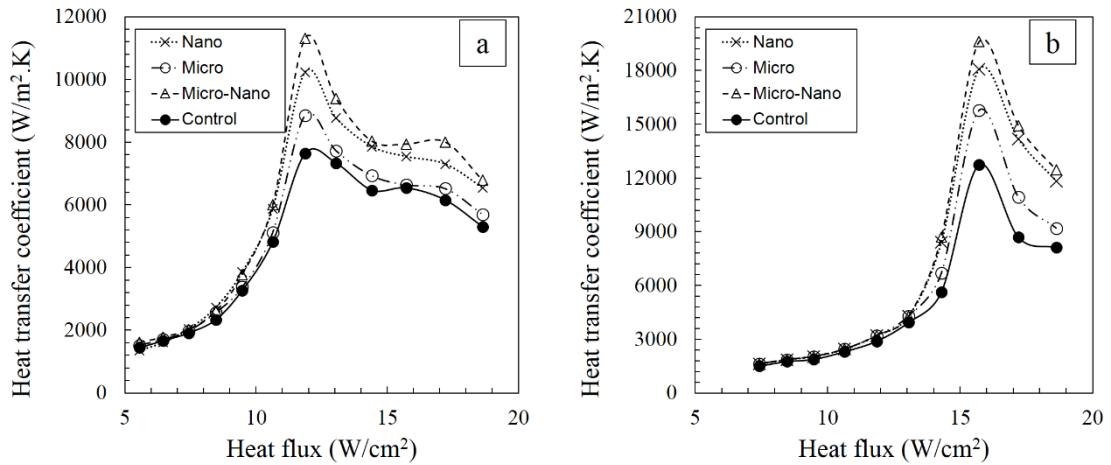
Fig.5.14. Heat transfer coefficients at the mass fluxes of a) 50 kg/ m^2.s b) 125 kg/ m^2.s
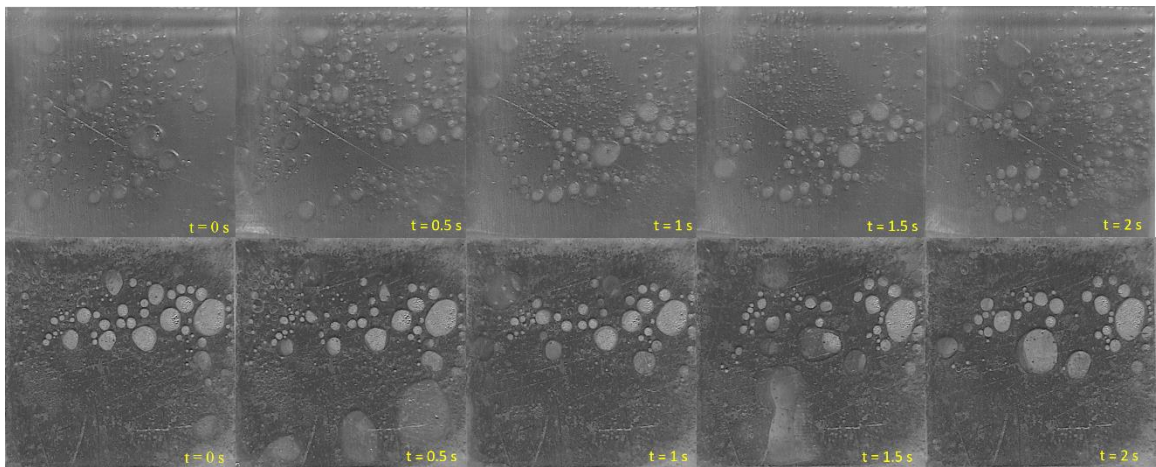
Fig.5.15. Bubble and elongated bubble motion for plain (up) and nano-micro structured plate (down) at the heat flux of 10 W/cm^2 and the mass flux of 50 kg/m^2.s

The effect of vapor quality on heat transfer coefficient at the middle position of the samples are shown in Fig.5.16. As can be seen, a decreasing trend is visible after an increasing trend. Transition from nucleate boiling dominance to convective boiling dominance is responsible for this change in the trend.
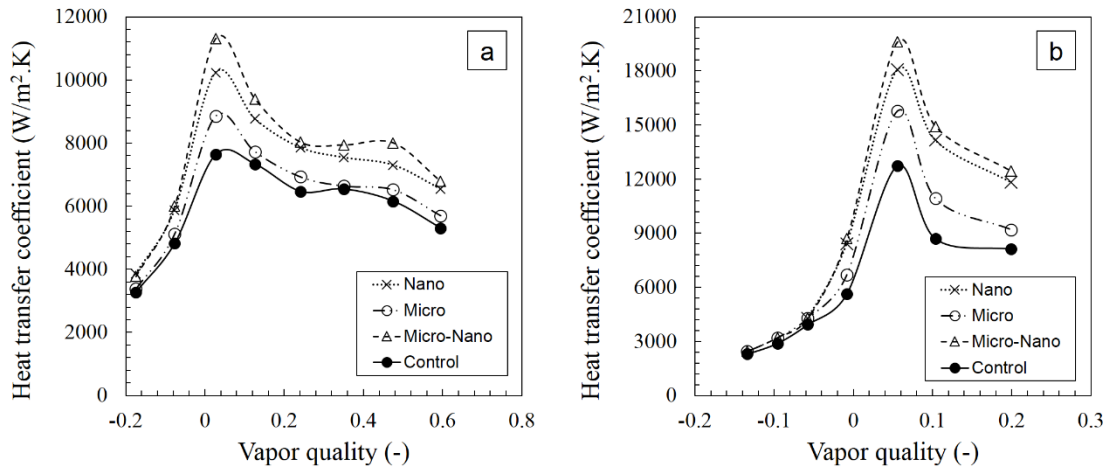
Fig.5.16. The effect of vapor quality on heat transfer coefficient at mass fluxes of a) 50 kg/ m^2.s b) 125 kg/ m^2.s

Vapor phase distribution on plain and nano-structured surfaces at the mass flux of 125 kg/m^2.s and the heat flux of 17 W/cm^2 is shown in Fig.5.17. The vapor quality is 0.1 for both cases. Bigger vapor blankets and elongated bubbles corresponding to bubbly/slug and slug/annular flow regimes exist for the plain surface, whereas smaller and more dispersed bubbles and less elongated bubbles are visible on the nano-structured surface.
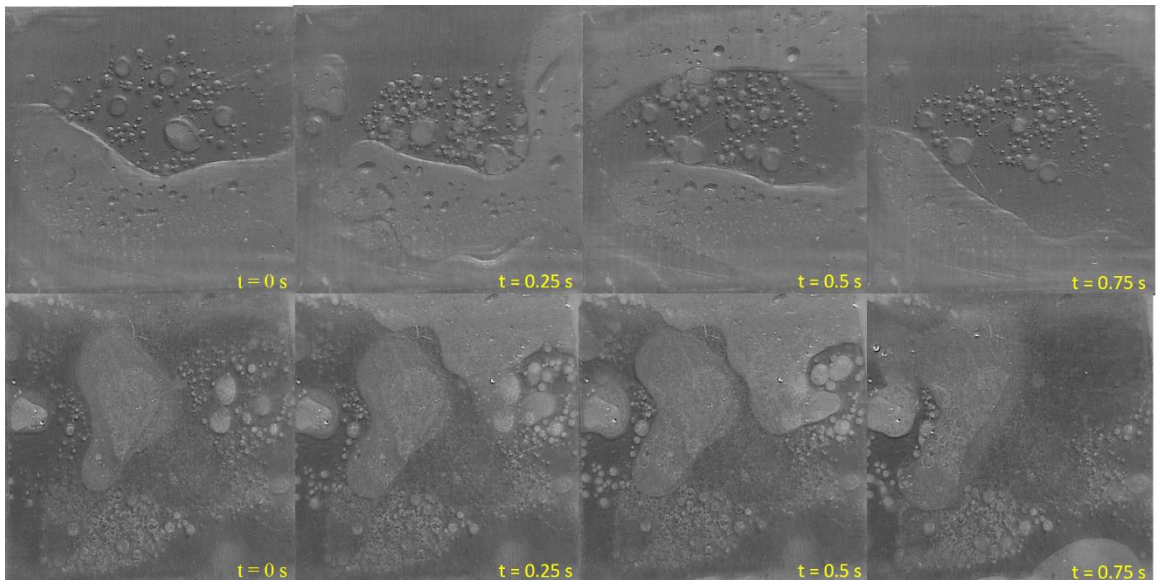
Fig.5.17. Vapor distribution on controlled surface (up) and nano-structured surface (down) at 125 kg/m^2.s mass flux and 17 W/cm^2 heat flux

5.4.3   Summary

5.5   pHEMA (Polyhydroxyethylmethacrylate) coated surfaces

5.5.1   Sample preparation and characteristics

5.5.1.1   pHEMA Deposition

One of the new techniques for polymeric thin film depositions is iCVD, and it is one type of hot-wire CVD (chemical vapor deposition). Polymeric materials do not easily deposited on the skinny structures and complex substrates. Therefore; pHEMA deposition is considered as a difficult process. Free radical polymerization is the basic principal of iCVD. Fig.5.18 shows the major elements of an iCVD system.
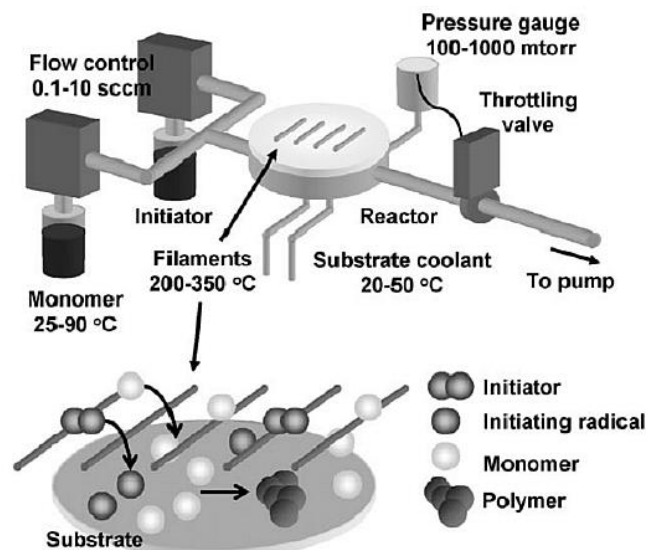
Fig.5.18. System components of the iCVD system

The desired vacuum is achieved in the vacuum chamber. Inside the vacuum chamber, a tungsten hot filament is used for initiator vapor decomposition. This starts the polymerization process, which has tree steps as starting, propagation and finalization. At first initiator is entered to the hot filaments section. Monomers and crosslinker are heated to produce the vapor. Then the process of polymerization starts by radicals that attack the adsorbed surface monomers, while the substrate temperature is kept at 295 K (this increases the adsorption

rate of gas molecules on the substrate surface). In our experiments, crosslinked pHEMA deposition duration is 75 min for 100 nm coating thickness. In comparison to the common coatings, pHEMA films have weak mechanical strengths. Therefore; in order to enhance the mechanical strength of the polymer EGDMA crosslinker agent is used (hydrophobic EGDMA agents are critical for film endurance under the experimental conditions of flow boiling). Crosslink films increase the contact angle of deposited films from 30º to 37º (ratio of crosslink is 20%) (Alf, Asatekin et al. 2010). On the other hand, polymers possess the hydrogels characteristics such as high swelling ratio. Swelling ratio gives rise to a porous coating when it is wetted. In our experiments the thickness of pHEMA increased up to 21 percent when it was in contact with the working fluid. This leads to a porous coating. Thin films swelling proportion decrease with crosslinker ratio increment, as a result stability establishment between swelling properties and mechanical strength of the thin films is achieved with an optimum crosslinker (Trujillo, Baxamusa et al. 2009).

5.5.2   Results and discussion

Fig.5.19 shows the wall superheats as a function of the applied heat flux for uncoated and coated surfaces. In the single phase region, nano-coatings have no significant effect on heat transfer. In the most of boiling region, coated surfaces exhibit s better heat transfer performance, due to lower superheats at a fixed heat flux. At higher heat flues, the deviation from the plain surface becomes smaller.

Contact angle on the coated surfaces (~45º) is lower than uncoated silicon surface (~75º), which implies that coated surfaces have more wettability compared to the plain surface. This has a negative effect on heat transfer, particularly in nucleate boiling region. On the other hand, coated surfaces provide more active nucleation sites due to their more porous structure, which enhances the bubble formation and release and more nucleation activities at the same heat flux.
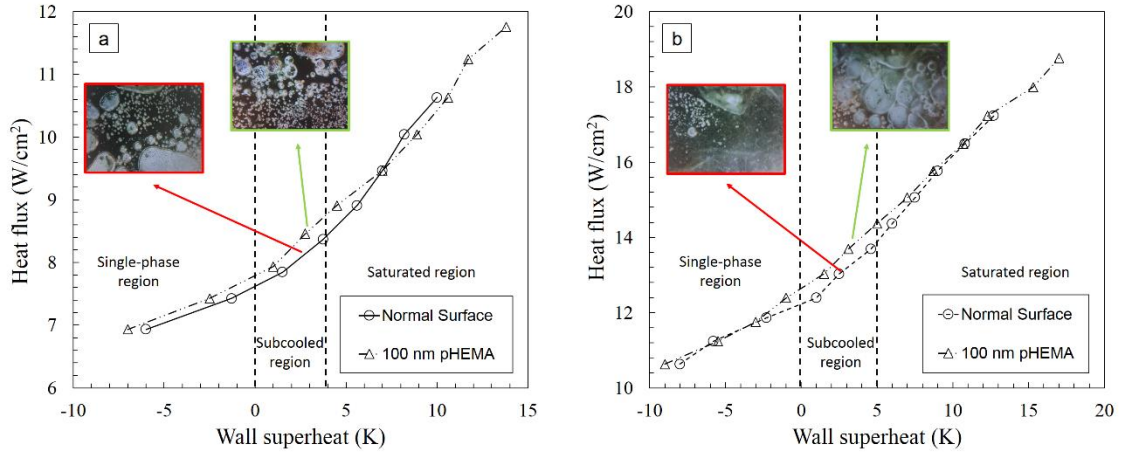
Fig.5.19. Wall superheat for a) 50 kg/m^2.s b) 125 kg/m^2.s

Local wall temperatures for two mass fluxes of 50 and 125 kg/m^2.s are shown in Fig.5.20. At low wall superheats coated surfaces have lower wall temperatures in comparison to the silicon plates. pHEMA coated surface provide more nucleation sites due to their porosity. At higher wall superheats, which is related to slug/annular flow patterns, the porous surface acts like as an insulating layer and results in higher wall temperatures.
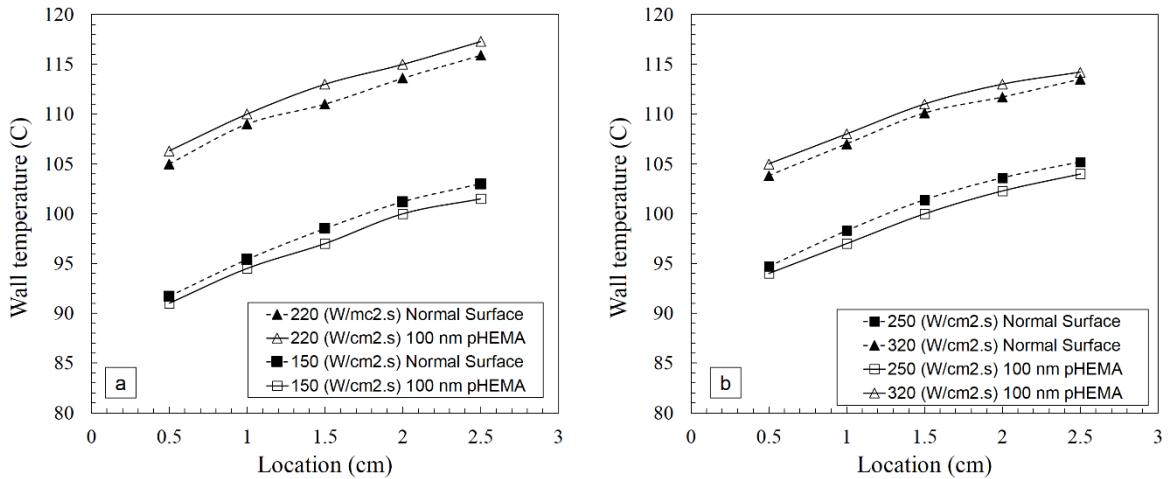
Fig.5.20. Local wall temperatures for a) 50 kg/m^2.s b) 125 kg/m^2.s

Boiling images are shown in Fig.5.21 for silicon and pHEMA coated surfaces. At low heat fluxes, more nucleation takes place on the coated surface due to the higher porosity of the

surface, which leads to enhanced heat transfer. Also, bubble sizes are bigger on the plain surface. Furthermore, it can be observed that the flow pattern change from isolated bubbles to confined bubbles is delayed for the coated surface. Confined bubbles /slug/annular flow patterns is also earlier than the plain surface
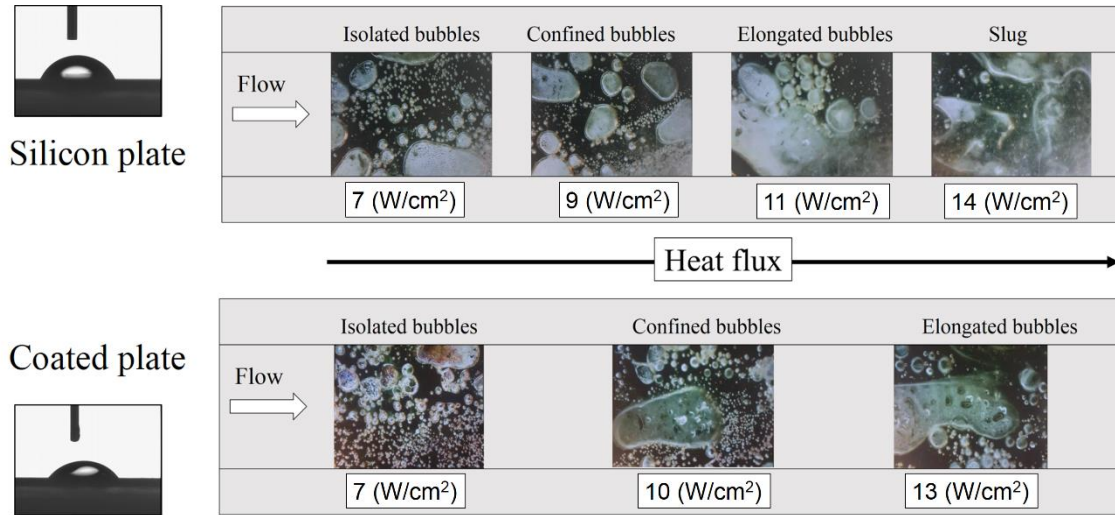
Fig.5.21. Flow map for silicon plate (up) and pHEMA coated plate (bottom)

Fig.5.22 shows heat transfer coefficients for coated and uncoated surfaces at the mass fluxes of 50 kg/ m^2.s and 125 kg/ m^2.s. Heat transfer coefficients are higher for the coated surface at low and moderate heat fluxes due to more nucleation and smaller bubble release frequency, which correspond to isolated bubble and confined bubble patterns. However, there is not any significant difference in heat transfer performance between the coated and plain surfaces, once elongated bubble pattern appears for the coated surface.

Under the condition of slug/annular flows, the functionality of nanostructures diminish, since a shift from nucleate boiling to convective boiling occurs. As a result, nanostructures start to act as an insulating layer, which results in slight lower heat transfer coefficients for the coated surface compared to the plain surface at high heat fluxes.
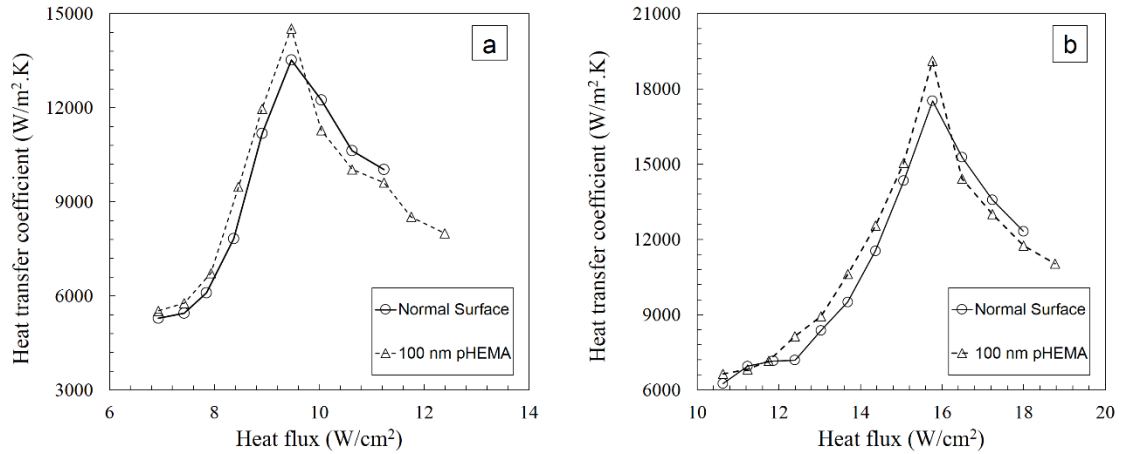
Fig.5.22. Obtained heat transfer coefficient for a) 50 kg/m^2.s b) 125 kg/m^2.s mass fluxes

5.5.3 Summary

The effect of pHEMA (Polyhydroxyethylmethacrylate) nanostructure coated surfaces on flow boiling in a rectangular microchannel is investigated. De-ionized water is considered as working fluid and flows through a microchannel with 500 μm depth. The following major conclusions are drawn from the results:

i-) pHEMA coated surfaces have lower wall temperatures at nucleate boiling region in comparison to uncoated surfaces, therefore at low wall superheats, coated surfaces have higher heat transfer coefficients.

ii-) There is not any significant difference in heat transfer performance between the coated and plain surfaces, once elongated bubble pattern appears for the coated surface. Under the condition of slug/annular flows, the functionality of nanostructures diminish, since a shift from nucleate boiling to convective boiling occurs.

iii-) It was observed that the bubble sizes are bigger on the plain surface. The flow pattern change from isolated bubbles to confined bubbles is delayed for the coated surface.

CHAPTER 6. CONCLUSIONS AND FUTURE WORK

In this thesis, numerical and experimental studies on multi-phase flows in microchannels were conducted. The effect of nanoparticles and nanotubes on convective heat transfer in horizontal microtubes, and the effect of micro and nanostructures on flow boiling in rectangular micro-channels were studied.

The major conclusions are as following:

1- The effect of heating surface is critical in multiphase flows in micro-systems. The results of MWCNT nanofluids indicated that nanotube depositions on heating surface deteriorate convective heat transfer. Furthermore, the obtained experimental results in flow boiling on enhanced and coated surfaces indicated that surface characteristics changes the flow patterns and heat removal rate. As surface roughness increases, bubble size decreases due to larger cavity sizes. Moreover, nano-structured surfaces provide more active nucleation sites which enhance surface cooling by providing more bubble nucleation. Furthermore, as surface wettability increases, bubbly flow regime extends over the wider range of applied heat flux in comparison to the un-coated surfaces. It was found that surface porosity also has a considerable effect on heat transfer coefficient.

2- The physical dimensions of microsystems have considerable effects on phase change process in microsystems. It was found as systems hydraulic diameter decreases, its heat removal ability deteriorates. On the other hand, much higher critical heat flux and lower pressure oscillations (better pressure stability) obtained for smaller microtube.

3- Although a good agreement was obtained between numerical and experimental results, at modeling of high mass flux flow boiling, the interaction force for gas phase was considered as a simple particle-particle interaction.

4- Dispersed nanotubes or nanoparticles have contradictory effects on heat transfer coefficient. According to numerical simulations, adding nanoparticles increases the mixing effect especially at wall boundaries. Adding nanoparticles reduces the hydrodynamic entry length. On the other hand, experimental results indicated that nanofluids have no considerable effect on heat transfer performance of the system at low flow rate.

101

There are several factors affecting micro-scale multiphase flows. Surface characteristics play major role on thermal characteristics of these flows. There are some recommendations for future work:

1- An investigation on the effect of different kinds of fluids such as refrigerants or different nanofluids such as gold or diamond nanofluids.

2- Using different surfaces in order to investigate the effect of surface roughness and wettability on flow boiling map.

3- A further study of flow boiling in microchannels with different hydraulic diameters.

REFERENCES

Agostini, B., M. Fabbri, J. E. Park, L. Wojtan, J. R. Thome and B. Michel (2007). "State of the art of high heat flux cooling technologies." Heat Transfer Engineering **28**(4): 258-281.

Ahn, H. S., S. H. Kang, H. Jo, H. Kim and M. H. Kim (2011). "Visualization study of the effects of nanoparticles surface deposition on convective flow boiling CHF from a short heated wall." International Journal of Multiphase Flow **37**(2): 215-228.

Ahn, H. S., S. H. Kang, C. Lee, J. Kim and M. H. Kim (2012). "The effect of liquid spreading due to micro-structures of flow boiling critical heat flux." International Journal of Multiphase Flow **43**: 1-12.

Ahn, H. S., H. Kim, H. Jo, S. Kang, W. Chang and M. H. Kim (2010). "Experimental study of critical heat flux enhancement during forced convective flow boiling of nanofluid on a short heated surface." International Journal of Multiphase Flow **36**(5): 375-384.

Akbari, M., N. Galanis and A. Behzadmehr (2011). "Comparative analysis of single and two-phase models for CFD studies of nanofluid heat transfer." International Journal of Thermal Sciences **50**(8): 1343-1354.

Akbarinia, A. (2008). "Impacts of nanofluid flow on skin friction factor and Nusselt number in curved tubes with constant mass flow." International Journal of Heat and Fluid Flow **29**(1): 229-241.

Akbarinia, A. and R. Laur (2009). "Investigating the diameter of solid particles effects on a laminar nanofluid flow in a curved tube using a two phase approach." International Journal of Heat and Fluid Flow **30**(4): 706-714.

Alajbegovic, A., D. Drew and R. Lahey Jr (1999). "An analysis of phase distribution and turbulence in dispersed particle/liquid flows." Chemical Engineering Communications **174**(1): 85-133.

Alf, M. E., A. Asatekin, M. C. Barr, S. H. Baxamusa, H. Chelawat, G. Ozaydin-Ince, C. D. Petruczok, R. Sreenivasan, W. E. Tenhaeff and N. J. Trujillo (2010). "Chemical vapor deposition of conformal, functional, and responsive polymer films." Advanced Materials **22**(18): 1993-2027.

Aminfar, H., M. Mohammadporfard and R. Maroofiazar (2013). "Eulerian simulation of subcooled boiling flow in straight and curved annuli." Journal of Mechanical Science and Technology **27**(5): 1295-1304.

Anoop, K. B., T. Sundararajan and S. K. Das (2009). "Effect of particle size on the convective heat transfer in nanofluid in the developing region." International Journal of Heat and Mass Transfer **52**(9-10): 2189-2195.

Babcock, W. Company, S. C. Stultz and J. B. Kitto (1992). Steam: its generation and use, Babcock & Wilcox.

Baffou, G., R. Quidant and F. J. G. de Abajo (2010). "Nanoscale Control of Optical Heating in Complex Plasmonic Systems." Acs Nano **4**(2): 709-716.

Bartel, M. D. (1999). Experimental investigation of subcooled boiling. M. Sc., Purdue University.

Bartel, M. D., M. Ishii, T. Masukawa, Y. Mi and R. Situ (2001). "Interfacial area measurements in subcooled flow boiling." Nuclear Engineering and Design **210**(1): 135-155.

Basu, N., G. R. Warrier and V. K. Dhir (2005). "Wall heat flux partitioning during subcooled flow boiling: Part 1-Model development." Transactions of the ASME-C-Journal of Heat Transfer **127**(2): 131-140.

Basu, N., G. R. Warrier and V. K. Dhir (2005). "Wall Heat Flux Partitioning During Subcooled Flow Boiling: Part II—Model Validation." Journal of heat transfer **127**(2): 141-148.

Behzadmehr, A., M. Saffar-Avval and N. Galanis (2007). "Prediction of turbulent forced convection of a nanofluid in a tube with uniform heat flux using a two phase approach." International Journal of Heat and Fluid Flow **28**(2): 211-219.

Bejan, A. (2013). Convection heat transfer, John wiley & sons.

Bergman, T. L. and F. P. Incropera (2011). Introduction to Heat Transfer, Wiley.

Bertsch, S. S., E. A. Groll and S. V. Garimella (2009). "A composite heat transfer correlation for saturated flow boiling in small channels." International Journal of Heat and Mass Transfer **52**(7): 2110-2118.

Betz, A. R., J. Jenkins and D. Attinger (2013). "Boiling heat transfer on superhydrophilic, superhydrophobic, and superbiphilic surfaces." International Journal of Heat and Mass Transfer **57**(2): 733-741.

Bianco, V., F. Chiacchio, O. Manca and S. Nardini (2009). "Numerical investigation of nanofluids forced convection in circular tubes." Applied Thermal Engineering **29**(17): 3632-3642.

Bianco, V., O. Manca and S. Nardini (2011). "Numerical investigation on nanofluids turbulent convection heat transfer inside a circular tube." International Journal of Thermal Sciences **50**(3): 341-349.

Bouillard, J., R. Lyczkowski and D. Gidaspow (1989). "Porosity distributions in a fluidized bed with an immersed obstacle." AIChE Journal **35**(6): 908-922.

Boulet, P. and S. Moissette (2002). "Influence of the particle–turbulence modulation modelling in the simulation of a non-isothermal gas–solid flow." International Journal of Heat and Mass Transfer **45**(20): 4201-4216.

Buongiorno, J. (2006). "Convective transport in nanofluids." Journal of Heat Transfer **128**(3): 240-250.

Cai, Y., M. Liu and L. Hui (2013). "CaCO3 fouling on microscale–nanoscale hydrophobic titania–fluoroalkylsilane films in pool boiling." AIChE Journal **59**(7): 2662-2678.

Carey, V. P. (2007). Liquid Vapor Phase Change Phenomena: An Introduction to the Thermophysics of Vaporization and Condensation Processes in Heat Transfer Equipment, Second Edition, Taylor & Francis.

Chen, C., W. Chang, K. Li, Y. Lie and T. Lin (2009). "Subcooled flow boiling heat transfer of R-407C and associated bubble characteristics in a narrow annular duct." International Journal of Heat and Mass Transfer **52**(13): 3147-3158.

Cheung, S., S. Vahaji, G. Yeoh and J. Tu (2014). "Modeling subcooled flow boiling in vertical channels at low pressures–Part 1: Assessment of empirical correlations." International Journal of Heat and Mass Transfer **75**: 736-753.

Choi, J. and Y. Zhang (2012). "Numerical simulation of laminar forced convection heat transfer of Al2O3–water nanofluid in a pipe with return bend." International Journal of Thermal Sciences **55**(0): 90-102.

Choi, S. U. S. and J. A. Eastman (1995). Enhancing thermal conductivity of fluids with nanoparticles.

Çıkım, T., E. Armağan, G. O. Ince and A. Koşar (2014). "Flow Boiling Enhancement in Microtubes With Crosslinked pHEMA Coatings and the Effect of Coating Thickness." Journal of Heat Transfer **136**(8): 081504.

Cioncolini, A., J. R. Thome and C. Lombardi (2009). "Unified macro-to-microscale method to predict two-phase frictional pressure drops of annular flows." International Journal of Multiphase Flow **35**(12): 1138-1148.

Cole, R. (1960). "A photographic study of pool boiling in the region of the critical heat flux." AIChE Journal **6**(4): 533-538.

Coleman, H. W. and W. G. Steele (2009). Experimentation, validation, and uncertainty analysis for engineers, John Wiley & Sons.

Collier, J. G. and J. R. Thome (1994). Convective Boiling and Condensation, Clarendon Press.

Cornwell, K. and P. A. Kew (1993). Boiling in small parallel channels. Energy Efficiency in Process Technology, Springer**:** 624-638.

Das, S. K., S. U. Choi, W. Yu and T. Pradeep (2007). Nanofluids: Science and Technology, Wiley.

Das, S. K., N. Putra, P. Thiesen and W. Roetzel (2003). "Temperature Dependence of Thermal Conductivity Enhancement for Nanofluids." Journal of Heat Transfer **125**(4): 567-574.

Demir, E., T. Izci, A. S. Alagoz, T. Karabacak and A. Koşar (2014). "Effect of silicon nanorod length on horizontal nanostructured plates in pool boiling heat transfer with water." International Journal of Thermal Sciences **82**: 111-121.

Drew, D. and R. Lahey (1993). "Analytical modeling of multiphase flow." Particulate two-phase flow: 509-566.

Eastman, J. A., S. U. S. Choi, S. Li, W. Yu and L. J. Thompson (2001). "Anomalously increased effective thermal conductivities of ethylene glycol-based nanofluids containing copper nanoparticles." Applied Physics Letters **78**(6): 718-720.

Einstein, A. (1906). "Eine neue bestimmung der moleküldimensionen." Annalen der Physik **324**(2): 289-306.

Fani, B., M. Kalteh and A. Abbassi "Investigating the effect of Brownian motion and viscous dissipation on the nanofluid heat transfer in a trapezoidal microchannel heat sink." Advanced Powder Technology(0).

Fard, M. H., M. N. Esfahany and M. R. Talaie (2010). "Numerical study of convective heat transfer of nanofluids in a circular tube two-phase model versus single-phase model." International Communications in Heat and Mass Transfer **37**(1): 91-97.

Fazeli, S. A., S. M. Hosseini Hashemi, H. Zirakzadeh and M. Ashjaee (2012). "Experimental and numerical investigation of heat transfer in a miniature heat sink utilizing silica nanofluid." Superlattices and Microstructures **51**(2): 247-264.

Ferjančič, K. and I. Golobič (2002). "Surface effects on pool boiling CHF." Experimental Thermal and Fluid Science **25**(7): 565-571.

Forrest, E., E. Williamson, J. Buongiorno, L.-W. Hu, M. Rubner and R. Cohen (2010). "Augmentation of nucleate boiling heat transfer and critical heat flux using nanoparticle thin-film coatings." International Journal of Heat and Mass Transfer **53**(1): 58-67.

Ganapathy, H., A. Shooshtari, K. Choo, S. Dessiatoun, M. Alshehhi and M. Ohadi (2013). "Volume of fluid-based numerical modeling of condensation heat transfer and fluid flow characteristics in microchannels." International Journal of Heat and Mass Transfer **65**: 62-72.

Garimella, S. V., V. Singhal and D. Liu (2006). "On-chip thermal management with microchannel heat sinks and integrated micropumps." Proceedings of the Ieee **94**(8): 1534-1548.

Gavriilidis, A., P. Angeli, E. Cao, K. K. Yeong and Y. S. S. Wan (2002). "Technology and applications of microengineered reactors." Chemical Engineering Research & Design **80**(A1): 3-30.

Ghiaasiaan, S. M. (2008). Two-Phase Flow, Boiling, and Condensation: In Conventional and Miniature Systems, Cambridge University Press.

Gidaspow, D. (1994). Multiphase flow and fluidization: continuum and kinetic theory descriptions, Academic press.

Gnielinski, V. (1976). "New equations for heat and mass-transfer in turbulent pipe and channel flow." International Chemical Engineering **16**(2): 359-368.

Godson, L., B. Raja, D. M. Lal and S. Wongwises (2010). "Enhancement of heat transfer using nanofluids-An overview." Renewable & Sustainable Energy Reviews **14**(2): 629-641.

Göktepe, S., K. Atalık and H. Ertürk (2014). "Comparison of single and two-phase models for nanofluid convection at the entrance of a uniformly heated tube." International Journal of Thermal Sciences **80**: 83-92.

Guo, Z. Y. and Z. X. Li (2003). "Size effect on single-phase channel flow and heat transfer at microscale." International Journal of Heat and Fluid Flow **24**(3): 284-298.

Haghighi, E. B., M. Saleemi, N. Nikkam, Z. Anwar, I. Lumbreras, M. Behi, S. A. Mirmohammadi, H. Poth, R. Khodabandeh and M. S. Toprak (2013). "Cooling performance of nanofluids in a small diameter tube." Experimental Thermal and Fluid Science **49**: 114-122.

Haghshenas Fard, M., M. N. Esfahany and M. Talaie (2010). "Numerical study of convective heat transfer of nanofluids in a circular tube two-phase model versus single-phase model." International Communications in Heat and Mass Transfer **37**(1): 91-97.

Hall, D. D. and I. Mudawar (2000). "Critical heat flux (CHF) for water flow in tubes—II.: Subcooled CHF correlations." International Journal of Heat and Mass Transfer **43**(14): 2605-2640.

Hamilton, R. and O. Crosser (1962). "Thermal conductivity of heterogeneous two-component systems." Industrial & Engineering chemistry fundamentals **1**(3): 187-191.

Harirchian, T. and S. V. Garimella (2012). "Flow regime-based modeling of heat transfer and pressure drop in microchannel flow boiling." International Journal of Heat and Mass Transfer **55**(4): 1246-1260.

Hatton, A. and I. Hall (1966). Photographic study of boiling on prepared surfaces. CHEMICAL ENGINEERING PROGRESS, AMER INST CHEMICAL ENGINEERS 345 E 47TH ST, NEW YORK, NY 10017.

Haynes, B. S. and D. F. Fletcher (2003). "Subcooled flow boiling heat transfer in narrow passages." International Journal of Heat and Mass Transfer **46**(19): 3673-3682.

Heris, S. Z., M. N. Esfahany and S. G. Etemad (2007). "Experimental investigation of convective heat transfer of Al2O3/water nanofluid in circular tube." International Journal of Heat and Fluid Flow **28**(2): 203-210.

Hiltunen, K., A. Jäsberg, S. Kallio, H. Karema, M. Kataja, A. Koponen, M. Manninen and V. Taivassalo (2009). "Multiphase flow dynamics." Theory and Numerics. Tech. Rep **722**.

Hiltunen, K. and V. t. tutkimuskeskus (2009). Multiphase Flow Dynamics: Theory and Numerics, VTT.

Hsu, Y. (1962). "On the size range of active nucleation cavities on a heating surface." Journal of Heat Transfer **84**(3): 207-213.

Hwang, G.-S. and M. Kaviany (2006). "Critical heat flux in thin, uniform particle coatings." International journal of heat and mass transfer **49**(5): 844-849.

Hwang, K. S., S. P. Jang and S. U. S. Choi (2009). "Flow and convective heat transfer characteristics of water-based Al2O3 nanofluids in fully developed laminar flow regime." International Journal of Heat and Mass Transfer **52**(1-2): 193-199.

Incropera, F. P. and D. P. DeWitt (1981). Fundamentals of heat transfer, Wiley.

Ishii, M. (1975). "Thermo-fluid dynamic theory of two-phase flow." NASA STI/Recon Technical Report A **75**: 29657.

Ishii, M. and K. Mishima (1980). Study of two-fluid model and interfacial area, Argonne National Lab., IL (USA).

J. A. Eastman, U. S. C., S. Li, L. J. Thompson and S. Lee (1996). Enhanced Thermal Conductivity through the Development of Nanofluids. MRS Proceedings, 457, 3 doi:10.1557/PROC-457-3. .

Jang, S. P. and S. U. S. Choi (2004). "Role of Brownian motion in the enhanced thermal conductivity of nanofluids." Applied Physics Letters **84**(21): 4316-4318.

Jeong, Y. H., M. S. Sarwar and S. H. Chang (2008). "Flow boiling CHF enhancement with surfactant solutions under atmospheric pressure." International Journal of Heat and Mass Transfer **51**(7): 1913-1919.

Jou, R. Y. and S. C. Tzeng (2006). "Numerical research of nature convective heat transfer enhancement filled with nanofluids in rectangular enclosures." International Communications in Heat and Mass Transfer **33**(6): 727-736.

Jung, J.-Y., H.-S. Oh and H.-Y. Kwak (2009). "Forced convective heat transfer of nanofluids in microchannels." International Journal of Heat and Mass Transfer **52**(1–2): 466-472.

Kalteh, M., A. Abbassi, M. Saffar-Avval, A. Frijns, A. Darhuber and J. Harting (2012). "Experimental and numerical investigation of nanofluid forced convection inside a wide microchannel heat sink." Applied Thermal Engineering **36**: 260-268.

Kalteh, M., A. Abbassi, M. Saffar-Avval and J. Harting (2011). "Eulerian-Eulerian two-phase numerical simulation of nanofluid laminar forced convection in a microchannel." International Journal of Heat and Fluid Flow **32**(1): 107-116.

Kandlikar, S., S. Garimella, D. Li, S. Colin and M. R. King (2005). Heat transfer and fluid flow in minichannels and microchannels, Elsevier.

Kandlikar, S. G. (1999). Handbook of Phase Change: Boiling and Condensation, Taylor & Francis.

Kandlikar, S. G. (2006). "Effect of liquid-vapor phase distribution on the heat transfer mechanisms during flow boiling in minichannels and microchannels." Heat transfer engineering **27**(1): 4-13.

Kandlikar, S. G. (2010). "A Scale Analysis Based Theoretical Force Balance Model for Critical Heat Flux (CHF) During Saturated Flow Boiling in Microchannels and Minichannels." Journal of Heat Transfer **132**(8): 081501-081501.

Kandlikar, S. G. and W. J. Grande (2003). "Evolution of Microchannel Flow Passages--Thermohydraulic Performance and Fabrication Technology." Heat transfer engineering **24**(1): 3-17.

Karimzadehkhouei, M., S. E. Yalcin, K. Şendur, M. P. Mengüç and A. Koşar (2014). "Pressure drop and heat transfer characteristics of nanofluids in horizontal microtubes under thermally developing flow conditions." Experimental Thermal and Fluid Science.

Kaya, A., R. Demiryürek, E. Armağan, G. Ozaydin-Ince, M. Sezen and A. Koşar (2013). "Boiling heat transfer enhancement in mini/microtubes via polyhydroxyethylmethacrylate (pHEMA) coatings on inner microtube walls at high mass fluxes." Journal of Micromechanics and Microengineering **23**(11): 115017.

Kaya, A., M. R. Ozdemir and A. Kosar (2013). "High mass flux flow boiling and critical heat flux in microscale." International Journal of Thermal Sciences **65**: 70-78.

Khaleduzzaman, S., I. Mahbubul, I. Shahrul and R. Saidur (2013). "Effect of particle concentration, temperature and surfactant on surface tension of nanofluids." International Communications in Heat and Mass Transfer **49**: 110-114.

Khanafer, K. and K. Vafai (2011). "A critical synthesis of thermophysical characteristics of nanofluids." International Journal of Heat and Mass Transfer **54**(19): 4410-4428.

Khanafer, K., K. Vafai and M. Lightstone (2003). "Buoyancy-driven heat transfer enhancement in a two-dimensional enclosure utilizing nanofluids." International Journal of Heat and Mass Transfer **46**(19): 3639-3653.

Khanikar, V., I. Mudawar and T. Fisher (2009). "Effects of carbon nanotube coating on flow boiling in a micro-channel." International Journal of Heat and Mass Transfer **52**(15): 3805-3817.

Kim, H. and M. Kim (2009). "Experimental study of the characteristics and mechanism of pool boiling CHF enhancement using nanofluids." Heat and Mass Transfer **45**(7): 991-998.

Kim, J., Y. T. Kang and C. K. Choi (2004). "Analysis of convective instability and heat transfer characteristics of nanofluids." Physics of Fluids **16**(7): 2395-2401.

Kocamustafaogullari, G. and M. Ishii (1983). "Interfacial area and nucleation site density in boiling systems." International Journal of Heat and Mass Transfer **26**(9): 1377-1387.

Končar, B., I. Kljenak and B. Mavko (2004). "Modelling of local two-phase flow parameters in upward subcooled flow boiling at low pressure." International Journal of Heat and Mass Transfer **47**(6): 1499-1513.

Koncar, B., E. Krepper and Y. Egorov (2005). "CFD modelling of subcooled flow boiling for nuclear engineering applications."

Kosar, A. (2009). "A model to predict saturated critical heat flux in minichannels and microchannels." International Journal of Thermal Sciences **48**(2): 261-270.

Kosar, A. (2012). FLOW BOILING IN MICROSCALE AT HIGH FLOWRATES. New York, Amer Soc Mechanical Engineers.

Koşar, A., C.-J. Kuo and Y. Peles (2005). "Boiling heat transfer in rectangular microchannels with reentrant cavities." International Journal of Heat and Mass Transfer **48**(23): 4867-4886.

Krishnamurthy, S. and Y. Peles (2010). "Flow boiling heat transfer on micro pin fins entrenched in a microchannel." Journal of Heat Transfer **132**(4): 041007.

Krishnamurthy, S. and Y. Peles (2010). "Flow Boiling on Micropin Fins Entrenched Inside a Microchannel—Flow Patterns and Bubble Departure Diameter and Bubble Frequency." Journal of Heat Transfer **132**(4): 041002.

Kuipers, J., W. Prins and W. Van Swaaij (1992). "Numerical calculation of wall-to-bed heat-transfer coefficients in gas-fluidized beds." AIChE Journal **38**(7): 1079-1091.

Kumar, C. S., S. Suresh, L. Yang, Q. Yang and S. Aravind (2014). "Flow boiling heat transfer enhancement using carbon nanotube coatings." Applied Thermal Engineering **65**(1): 166-175.

Kumaresan, V., S. Mohaideen Abdul Khader, S. Karthikeyan and R. Velraj (2013). "Convective heat transfer characteristics of CNT nanofluids in a tubular heat exchanger of

various lengths for energy efficient cooling/heating system." International Journal of Heat and Mass Transfer **60**(0): 413-421.

Kuo, C.-J., A. Kosar, Y. Peles, S. Virost, C. Mishra and M. K. Jensen (2006). "Bubble dynamics during boiling in enhanced surface microchannels." Microelectromechanical Systems, Journal of **15**(6): 1514-1527.

Kurtoğlu, E., A. Bilgin, M. Şeşen, B. Mısırlıoğlu, M. Yıldız, H. F. Y. Acar and A. Koşar (2012). "Ferrofluid actuation with varying magnetic fields for micropumping applications." Microfluidics and nanofluidics **13**(4): 683-694.

Kurtoğlu, E., A. Kaya, D. Gözüaçık, H. F. Y. Acar and A. Koşar (2014). "Experimental Study on Convective Heat Transfer Performance of Iron Oxide Based Ferrofluids in Microtubes." Journal of Thermal Science and Engineering Applications **6**(3): 034501.

Kurul, N. and M. Z. Podowski (1990). Multidimensional effects in forced convection subcooled boiling. Proceedings of the Ninth International Heat Transfer Conference.

Launder, B. E. and D. Spalding (1974). "The numerical computation of turbulent flows." Computer methods in applied mechanics and engineering **3**(2): 269-289.

Lee, J. and I. Mudawar (2008). "Fluid flow and heat transfer characteristics of low temperature two-phase micro-channel heat sinks – Part 2. Subcooled boiling pressure drop and heat transfer." International Journal of Heat and Mass Transfer **51**(17–18): 4327-4341.

Lee, P., F. Tseng and C. Pan (2004). "Bubble dynamics in microchannels. Part I: single microchannel." International Journal of Heat and Mass Transfer **47**(25): 5575-5589.

Lee, T. H., G. C. Park and D. J. Lee (2002). "Local flow characteristics of subcooled boiling flow of water in a vertical concentric annulus." International Journal of Multiphase Flow **28**(8): 1351-1368.

Lemczyk, T. and D. Molloy (1996). "Fluid Properties Research Report: Advanced Engineering NP-329." Long Manufacturing.

Lemmert, M. and J. Chawla (1977). "Influence of flow velocity on surface boiling heat transfer coefficient." Heat Transfer in Boiling **237**: 247.

Li, C., Z. Wang, P. I. Wang, Y. Peles, N. Koratkar and G. Peterson (2008). "Nanostructured copper interfaces for enhanced boiling." small **4**(8): 1084-1088.

Li, H., F. Tseng and C. Pan (2004). "Bubble dynamics in microchannels. Part II: two parallel microchannels." International Journal of heat and mass Transfer **47**(25): 5591-5601.

Li, X., W. Wei, R. Wang and Y. Shi (2009). "Numerical and experimental investigation of heat transfer on heating surface during subcooled boiling flow of liquid nitrogen." International Journal of Heat and Mass Transfer **52**(5–6): 1510-1516.

Li, Y., J. e. Zhou, S. Tung, E. Schneider and S. Xi (2009). "A review on development of nanofluid preparation and characterization." Powder Technology **196**(2): 89-101.

Lie, Y. and T. Lin (2006). "Subcooled flow boiling heat transfer and associated bubble characteristics of R-134a in a narrow annular duct." International journal of heat and mass transfer **49**(13): 2077-2089.

Liu, D. and S. V. Garimella (2007). "Flow boiling heat transfer in microchannels." Journal of Heat Transfer **129**(10): 1321-1332.

Liu, D. and L. Y. Yu (2011). "Single-Phase Thermal Transport of Nanofluids in a Minichannel." Journal of Heat Transfer,Transactions of the Asme **133**(3): 11.

Liu, Z.-h., J.-g. Xiong and R. Bao (2007). "Boiling heat transfer characteristics of nanofluids in a flat heat pipe evaporator with micro-grooved heating surface." International Journal of Multiphase Flow **33**(12): 1284-1295.

Liu, Z. and R. H. S. Winterton (1991). "A general correlation for saturated and subcooled flow boiling in tubes and annuli, based on a nucleate pool boiling equation." International Journal of Heat and Mass Transfer **34**(11): 2759-2766.

Lotfi, R., Y. Saboohi and A. Rashidi (2010). "Numerical study of forced convective heat transfer of nanofluids: comparison of different approaches." International Communications in Heat and Mass Transfer **37**(1): 74-78.

Lucas, D., J. Shi, E. Krepper and H. Prasser (2004). Models for the forces acting on bubbles in comparison with experimental data for vertical pipe flow. 3rd International Symposium on Two-Phase Flow Modelling and Experimentation, Pisa, Italy.

Luo, H. and H. F. Svendsen (1996). "Theoretical model for drop and bubble breakup in turbulent dispersions." AIChE Journal **42**(5): 1225-1233.

Magnini, M., B. Pulvirenti and J. R. Thome (2013). "Numerical investigation of hydrodynamics and heat transfer of elongated bubbles during flow boiling in a microchannel." International Journal of Heat and Mass Transfer **59**: 451-471.

Mahbubul, I., R. Saidur and M. Amalina (2012). "Latest developments on the viscosity of nanofluids." International Journal of Heat and Mass Transfer **55**(4): 874-885.

Maïga, S. E. B., S. J. Palm, C. T. Nguyen, G. Roy and N. Galanis (2005). "Heat transfer enhancement by using nanofluids in forced convection flows." International Journal of Heat and Fluid Flow **26**(4): 530-546.

Martín-Callizo, C., B. Palm and W. Owhaib (2007). "Subcooled flow boiling of R-134a in vertical channels of small diameter." International Journal of Multiphase Flow **33**(8): 822-832.

Maxwell, J. C. (1881). A treatise on electricity and magnetism, Clarendon press.

McNab, G. and A. Meisen (1973). "Thermophoresis in liquids." Journal of Colloid and Interface Science **44**(2): 339-346.

Mehendale, S., A. Jacobi and R. Shah (2000). "Fluid flow and heat transfer at micro-and meso-scales with application to heat exchanger design." Applied Mechanics Reviews **53**(7): 175-193.

Messina, A. and E. Park (1981). "Effects of precise arrays of pits on nucleate boiling." International Journal of Heat and Mass Transfer **24**(1): 141-145.

Miller, A. and D. Gidaspow (1992). "Dense, vertical gas-solid flow in a pipe." AIChE journal **38**(11): 1801-1815.

Mills, A. F. (1992). Heat Transfer, Irwin.

Minkowycz, W. J., E. M. Sparrow and J. Y. Murthy (2006). Handbook of Numerical Heat Transfer, Wiley.

Mohammed Shah, M. (1987). "Improved general correlation for critical heat flux during upflow in uniformly heated vertical tubes." International Journal of Heat and Fluid Flow **8**(4): 326-335.

Mokhtari Moghari, R., A. Akbarinia, M. Shariat, F. Talebi and R. Laur (2011). "Two phase mixed convection Al2O3–water nanofluid flow in an annulus." International Journal of Multiphase Flow **37**(6): 585-595.

Moore, G. (1965). Cramming More Components Onto Integrated Circuits, Electronics,(38) 8.

Moraga, F., F. Bonetto and R. Lahey (1999). "Lateral forces on spheres in turbulent uniform shear flow." International journal of Multiphase flow **25**(6): 1321-1372.

Moraveji, M. K. and R. M. Ardehali (2013). "CFD modeling (comparing single and two-phase approaches) on thermal performance of Al$_2$o$_3$/water

nanofluid in mini-channel heat sink." International Communications in Heat and Mass Transfer **44**: 157-164.

Morshed, A., F. Yang, M. Y. Ali, J. A. Khan and C. Li (2012). "Enhanced flow boiling in a microchannel with integration of nanowires." Applied Thermal Engineering **32**: 68-75.

Mudawar, I. and M. B. Bowers (1999). "Ultra-high critical heat flux (CHF) for subcooled water flow boiling—I: CHF data and parametric effects for small diameter tubes." International Journal of Heat and Mass Transfer **42**(8): 1405-1428.

Narumanchi, S., A. Troshko, D. Bharathan and V. Hassani (2008). "Numerical simulations of nucleate boiling in impinging jets: Applications in power electronics cooling." International Journal of Heat and Mass Transfer **51**(1): 1-12.

Narvaez, J. A., A. R. Veydt and R. J. Wilkens (2014). "Evaluation of Nanofluids as Potential Novel Coolant for Aircraft Applications: The Case of De-ionized Water-Based Alumina Nanofluids." Journal of Heat Transfer,Transactions of the Asme **136**(5): 10.

Nguyen, N. T. and S. T. Wereley (2002). Fundamentals and Applications of Microfluidics, Artech House.

Norton, D. G., E. D. Wetzel and D. G. Vlachos (2006). "Thermal management in catalytic microreactors." Industrial & Engineering Chemistry Research **45**(1): 76-84.

Ong, C. L. and J. R. Thome (2011). "Macro-to-microchannel transition in two-phase flow: Part 1-Two-phase flow patterns and film thickness measurements." Experimental Thermal and Fluid Science **35**(1): 37-47.

Ozel, B. G., A. Orum, M. Yildiz and Y. Z. Menceloglu (2014). "Experimental study on the rheology of anisotropic, flocculated and low volume fraction colloids." Korea-Australia Rheology Journal **26**(1): 105-116.

Pak, B. C. and Y. I. Cho (1998). "Hydrodynamic and heat transfer study of dispersed fluids with submicron metallic oxide particles." Experimental Heat Transfer an International Journal **11**(2): 151-170.

Palm, S. J., G. Roy and C. T. Nguyen (2006). "Heat transfer enhancement with the use of nanofluids in radial flow cooling systems considering temperature-dependent properties." Applied Thermal Engineering **26**(17): 2209-2218.

Park, S. D., S. W. Lee, S. Kang, I. C. Bang, J. H. Kim, H. S. Shin, D. W. Lee and D. W. Lee (2010). "Effects of nanofluids containing graphene/graphene-oxide nanosheets on critical heat flux." Applied Physics Letters **97**(2): 023103.

Phan, H. T., N. Caney, P. Marty and S. Colasson (2012). "Flow boiling of water on nanocoated surfaces in a microchannel." Journal of Heat Transfer **134**(2): 020901.

Piasecka, M. (2014). "The use of enhanced surface in flow boiling heat transfer in a rectangular minichannel." Experimental Heat Transfer **27**(3): 231-255.

Pierre, C. C. S. and S. G. Bankoff (1967). "Vapor volume profiles in developing two-phase flow." International Journal of Heat and Mass Transfer **10**(2): 237-249.

Podowski, R., D. Drew, R. Lahey Jr and M. Podowski (1997). A mechanistic model of the ebullition cycle in forced convection subcooled boiling. Eighth international topical meeting on nuclear reactor thermal-hydraulics.

Rafet Özdemir, M., A. Kaya and A. Koşar (2011). "Low Mass Quality Flow Boiling in Microtubes at High Mass Fluxes." Journal of Thermal Science and Engineering Applications **3**(4): 041001-041001.

Ranz, W. and W. Marshall (1952). "Evaporation from drops." Chem. Eng. Prog **48**(3): 141-146.

Rea, U., T. McKrell, L.-w. Hu and J. Buongiorno (2009). "Laminar convective heat transfer and viscous pressure loss of alumina–water and zirconia–water nanofluids." International Journal of Heat and Mass Transfer **52**(7): 2042-2048.

Ribatski, G. (2013). "A Critical Overview on the Recent Literature Concerning Flow Boiling and Two-Phase Flows Inside Micro-Scale Channels." Experimental Heat Transfer **26**(2-3): 198-246.

Ribatski, G., L. Wojtan and J. R. Thome (2006). "An analysis of experimental data and prediction methods for two-phase frictional pressure drop and flow boiling heat transfer in micro-scale channels." Experimental Thermal and Fluid Science **31**(1): 1-19.

Rogers, J. and J.-H. Li (1994). "Prediction of the onset of significant void in flow boiling of water." Journal of heat transfer **116**(4): 1049-1053.

Roy, G., C. T. Nguyen and P.-R. Lajoie (2004). "Numerical investigation of laminar flow and heat transfer in a radial flow cooling system with the use of nanofluids." Superlattices and Microstructures **35**(3–6): 497-511.

Roy, R. P., S. Kang, J. A. Zarate and A. Laporta (2002). "Turbulent subcooled boiling flow - Experiments and simulations." Journal of Heat Transfer-Transactions of the Asme **124**(1): 73-93.

Rui, Z. A. and W. Wen (2011). "Simulation of subcooled flow boiling in a micro-channel." International Journal of Refrigeration-Revue Internationale Du Froid **34**(3): 781-795.

Saeidi, D. and A. Alemrajabi (2013). "Experimental investigation of pool boiling heat transfer and critical heat flux of nanostructured surfaces." International Journal of Heat and Mass Transfer **60**: 440-449.

Saidur, R., K. Leong and H. Mohammad (2011). "A review on applications and challenges of nanofluids." Renewable and Sustainable Energy Reviews **15**(3): 1646-1668.

Saifaldeen, Z. S., K. R. Khedir, M. F. Cansizoglu, T. Demirkan and T. Karabacak (2014). "Superamphiphobic aluminum alloy surfaces with micro and nanoscale hierarchical roughness produced by a simple and environmentally friendly technique." Journal of Materials Science **49**(4): 1839-1853.

Sakanova, A., S. Yin, J. Zhao, J. Wu and K. Leong (2014). "Optimization and comparison of double-layer and double-side micro-channel heat sinks with nanofluid for power electronics cooling." Applied Thermal Engineering **65**(1): 124-134.

Sami, S. M. and T. Duong (1987). "A subcooled void model." Applied Mathematical Modelling **11**(4): 264-271.

Sarwar, M. S., Y. H. Jeong and S. H. Chang (2007). "Subcooled flow boiling CHF enhancement with porous surface coatings." International journal of heat and mass transfer **50**(17): 3649-3657.

Selvakumar, P. and S. Suresh (2012). "Convective performance of CuO/water nanofluid in an electronic heat sink." Experimental Thermal and Fluid Science **40**: 57-63.

Serrano, E., G. Rus and J. Garcia-Martinez (2009). "Nanotechnology for sustainable energy." Renewable and Sustainable Energy Reviews **13**(9): 2373-2384.

Sesen, M., W. Khudhayer, T. Karabacak and A. Kosar (2010). "Compact nanostructure integrated pool boiler for microscale cooling applications." Micro & Nano Letters **5**(4): 203-206.

Şeşen, M., W. Khudhayer, T. Karabacak and A. Koşar (2010). "Compact nanostructure integrated pool boiler for microscale cooling applications." Micro & Nano Letters **5**(4): 203-206.

Şeşen, M., Y. Tekşen, B. Şahin, K. Şendur, M. P. Mengüç and A. Koşar (2013). "Boiling heat transfer enhancement of magnetically actuated nanofluids." Applied Physics Letters **102**(16): 163107.

Shah, R. K. and A. L. London (1978). Laminar flow forced convection in ducts: a source book for compact heat exchanger analytical data, Academic Press.

Shah, R. K. and A. L. London (2014). Laminar flow forced convection in ducts: a source book for compact heat exchanger analytical data, Academic press.

Siginer, D. A., H. P. Wang, A. S. o. M. E. F. E. Division and A. S. o. M. E. M. Division (1995). Developments and applications of non-Newtonian flows, 1995: presented at the 1995 ASME International Mechanical Engineering Congress and Exposition, November 12-17, 1995, San Francisco, California, American Society of Mechanical Engineers.

Singh, P. K., P. Harikrishna, T. Sundararajan and S. K. Das (2012). "Experimental and numerical investigation into the hydrodynamics of nanofluids in microchannels." Experimental Thermal and Fluid Science **42**: 174-186.

Sohel, M., R. Saidur, N. Hassan, M. Elias, S. Khaleduzzaman and I. Mahbubul (2013). "Analysis of entropy generation using nanofluid flow through the circular microchannel and minichannel heat sink." International Communications in Heat and Mass Transfer **46**: 85-91.

Steinke, M. E. and S. G. Kandlikar (2004). "An experimental investigation of flow boiling characteristics of water in parallel microchannels." Journal of Heat Transfer **126**(4): 518-526.

Sun, Y., L. Zhang, H. Xu and X. Zhong (2011). "Subcooled flow boiling heat transfer from microporous surfaces in a small channel." International Journal of Thermal Sciences **50**(6): 881-889.

Sundar, L. S., K. Sharma, M. Naik and M. K. Singh (2013). "Empirical and theoretical correlations on viscosity of nanofluids: A review." Renewable and Sustainable Energy Reviews **25**: 670-686.

Suzuki, K., T. Kokubu, M. Nakano, H. Kawamura, I. Ueno, H. Shida and O. Ogawa (2005). "Enhancement of heat transfer in subcooled flow boiling with microbubble emission." Experimental thermal and fluid science **29**(7): 827-832.

Swamee, P. K. and A. K. Jain (1976). "Explicit equations for pipe-flow problems." Journal of the hydraulics division **102**(5): 657-664.

Syamlal, M. and D. Gidaspow (1985). "Hydrodynamics of fluidization: prediction of wall to bed heat transfer coefficients." AIChE Journal **31**(1): 127-135.

Taitel, Y. and A. E. Dukler (1976). "A model for predicting flow regime transitions in horizontal and near horizontal gas-liquid flow." AIChE Journal **22**(1): 47-55.

Tang, Y., B. Tang, Q. Li, J. Qing, L. Lu and K. Chen (2013). "Pool-boiling enhancement by novel metallic nanoporous surface." Experimental Thermal and Fluid Science **44**: 194-198.

Teng, T. P., Y. H. Hung, T. C. Teng, H. E. Mo and H. G. Hsu (2010). "The effect of alumina/water nanofluid particle size on thermal conductivity." Applied Thermal Engineering **30**(14-15): 2213-2218.

Thome, J. R. (2004). "Boiling in microchannels: a review of experiment and theory." International Journal of Heat and Fluid Flow **25**(2): 128-139.

Thome, J. R. and L. Consolini (2010). "Mechanisms of boiling in micro-channels: critical assessment." Heat Transfer Engineering **31**(4): 288-297.

Tillman, P., J. M. Hill and Ieee (2006). A new model for thermal conductivity in nanofluids. New York, Ieee.

Torregrosa, A., A. Broatch, P. Olmeda and O. Cornejo (2014). "Experiments on subcooled flow boiling in IC engine-like conditions at low flow velocities." Experimental Thermal and Fluid Science **52**: 347-354.

Trebotich, D., J. D. Zahn and D. Liepmann (2002). Complex fluid dynamics in BioMEMS devices: Modeling of microfabricated microneedles. Cambridge, Computational Publications.

Trujillo, N. J., S. H. Baxamusa and K. K. Gleason (2009). "Grafted functional polymer nanostructures patterned bottom-up by colloidal lithography and initiated chemical vapor deposition (iCVD)." Chemistry of Materials **21**(4): 742-750.

Tu, J. Y. and G. H. Yeoh (2002). "On numerical modelling of low-pressure subcooled boiling flows." International Journal of Heat and Mass Transfer **45**(6): 1197-1209.

Tuckerman, D. B. and R. Pease (1981). "High-performance heat sinking for VLSI." Electron Device Letters, IEEE **2**(5): 126-129.

Turgut, A. and E. Elbasan (2014). Nanofluids for electronics cooling. Design and Technology in Electronic Packaging (SIITME), 2014 IEEE 20th International Symposium for, IEEE.

Wang, G. D. and P. Cheng (2009). "Subcooled flow boiling and microbubble emission boiling phenomena in a partially heated microchannel." International Journal of Heat and Mass Transfer **52**(1-2): 79-91.

Wang, G. X. and V. Prasad (2000). "Microscale heat and mass transfer and non-equilibrium phase change in rapid solidification." Materials Science and Engineering a-Structural Materials Properties Microstructure and Processing **292**(2): 142-148.

Wei, J.-h., L.-m. Pan, D.-q. Chen, H. Zhang, J.-j. Xu and Y.-p. Huang (2011). "Numerical simulation of bubble behaviors in subcooled flow boiling under swing motion." Nuclear Engineering and Design **241**(8): 2898-2908.

Williams, W., J. Buongiorno and L.-W. Hu (2008). "Experimental investigation of turbulent convective heat transfer and pressure loss of alumina/water and zirconia/water nanoparticle colloids (nanofluids) in horizontal tubes." Journal of Heat Transfer **130**(4): 042412.

Woodcock, C., X. Yu, J. Plawsky and Y. Peles (2015). "Piranha Pin Fin (PPF)—Advanced flow boiling microstructures with low surface tension dielectric fluids." International Journal of Heat and Mass Transfer **90**: 591-604.

Wu, J. and J. Zhao (2013). "A review of nanofluid heat transfer and critical heat flux enhancement—Research gap to engineering application." Progress in Nuclear Energy **66**: 13-24.

Wu, X. Y., H. Y. Wu and P. Cheng (2009). "Pressure drop and heat transfer of Al2O3-H2O nanofluids through silicon microchannels." Journal of Micromechanics and Microengineering **19**(10): 11.

Xu, J., T. Wong and X. Huang (2006). "Two-fluid modeling for low-pressure subcooled flow boiling." International journal of heat and mass transfer **49**(1): 377-386.

Xuan, Y. M. and Q. Li (2003). "Investigation on convective heat transfer and flow features of nanofluids." Journal of Heat Transfer,Transactions of the Asme **125**(1): 151-155.

Yang, F., X. Dai, Y. Peles, P. Cheng, J. Khan and C. Li (2014). "Flow boiling phenomena in a single annular flow regime in microchannels (I): Characterization of flow boiling heat transfer." International Journal of Heat and Mass Transfer **68**: 703-715.

Yang, F., X. Dai, Y. Peles, P. Cheng, J. Khan and C. Li (2014). "Flow boiling phenomena in a single annular flow regime in microchannels (II): Reduced pressure drop and enhanced critical heat flux." International Journal of Heat and Mass Transfer **68**: 716-724.

Yarin, L., A. Mosyak and G. Hetsroni (2008). <u>Fluid flow, heat transfer and boiling in micro-channels</u>, Springer Science & Business Media.

Yeoh, G. and J. Tu (2004). "Population balance modelling for bubbly flows with heat and mass transfer." <u>Chemical engineering science</u> **59**(15): 3125-3139.

Yeoh, G., S. Vahaji, S. Cheung and J. Tu (2014). "Modeling subcooled flow boiling in vertical channels at low pressures–Part 2: Evaluation of mechanistic approach." <u>International Journal of Heat and Mass Transfer</u> **75**: 754-768.

Yuan, M., J. Wei, Y. Xue and J. Fang (2009). "Subcooled flow boiling heat transfer of FC-72 from silicon chips fabricated with micro-pin-fins." <u>International Journal of Thermal Sciences</u> **48**(7): 1416-1422.

Yun, B.-J., A. Splawski, S. Lo and C.-H. Song (2012). "Prediction of a subcooled boiling flow with advanced two-phase flow models." <u>Nuclear engineering and design</u> **253**: 351-359.

Zhang, W., T. Hibiki, K. Mishima and Y. Mi (2006). "Correlation of critical heat flux for flow boiling of water in mini-channels." <u>International Journal of Heat and Mass Transfer</u> **49**(5–6): 1058-1072.

Zhuan, R. and W. Wang (2010). "Simulation on nucleate boiling in micro-channel." <u>International Journal of Heat and Mass Transfer</u> **53**(1-3): 502-512.

Zhuan, R. and W. Wang (2012). "Flow pattern of boiling in micro-channel by numerical simulation." <u>International Journal of Heat and Mass Transfer</u> **55**(5-6): 1741-1753.

Zirakzadeh, H., A. Mashayekh, H. N. Bidgoli and M. Ashjaee (2012). "Experimental investigation of heat transfer in a novel heat sink by means of alumina nanofliud." <u>Heat Transfer Research</u> **43**(8).

APPENDIX

Uncertainty analysis

An uncertainty analysis of the experimental method, apparatus and data is performed in the following sections. The uncertainties were comparable with other values reported in the literature for microchannels.

Method

Method proposed by Coleman and Steele (Coleman and Steele 2009) is used as uncertainty analysis procedure. Consider a general case in which a quantity R is determined from a set of measured values, X_i :

$$R = R(X_1, X_2, X_3, ..., X_n) \quad A.1$$

where each measured value X_i has an associated uncertainty represented by the notation ∂X_i, the effect of the uncertainty in X_i on the result R is calculated by:

$$\delta R_{X_i} = \frac{\partial R}{\partial X_i} \delta X_i \quad A.2$$

Where δR_{X_i} refers to the uncertainty in R as a result of the uncertainty in the X_i measurement. Then the uncertainty in the result is given in general form as:

$$\delta R = \sqrt{\left(\frac{\partial R}{\partial X_1} \delta X_1\right)^2 + \left(\frac{\partial R}{\partial X_2} \delta X_2\right)^2 + \left(\frac{\partial R}{\partial X_3} \delta X_3\right)^2 + ... + \left(\frac{\partial R}{\partial X_n} \delta X_n\right)^2} \quad A.3$$

When R depends on a number of measured quantities and this dependence can be expressed in the form:

$$R = X_1^{C_1} X_2^{C_2} X_3^{C_3} ... X_n^{C_n} \quad A.4$$

The overall uncertainty is determined from the uncertainties of each of the individual measurements:

$$\frac{\delta R}{R} = \pm\sqrt{\left(C_1\frac{\delta X_1}{X_1}\right)^2 + \left(C_2\frac{\delta X_2}{X_2}\right)^2 + \left(C_3\frac{\delta X_3}{X_3}\right)^2 + ... + \left(C_n\frac{\delta X_n}{X_n}\right)^2} \quad A.5$$

The result of this equation is the overall uncertainty in R expressed as a percentage. The following section describes the uncertainty associated with the instrumentation and the method used in the measurements of each of the individual quantities.

Uncertainties

Fluid properties

Properties of water (liquid and vapor) were determined based on correlations of tabulated values as function of temperature presented by Lemczyk and Molloy (Lemczyk and Molloy 1996) and Babcock and Wilcox (Babcock, Company et al. 1992). The correlations deviate from the tabulated values by less than 0:4 %. Therefore, the uncertainty in the fluid properties is:

$$\frac{\partial \text{Properties}}{\text{Properties}} = \pm 4 \times 10^{-3} \quad A.6$$

Channel dimensions

The uncertainty in the microchannel dimensions were estimated based on twice the standard deviation (2σ) of several measurements taken with a surface tester as:

1. Rectangular microchannel: width 15000 ± 200 (μm), depth 500 ± 40 (μm), length 140000 ± 2000 (μm). Therefore:

$$\frac{\partial W}{W} = \frac{1000}{15000} = \pm 0.067$$

$$\frac{\partial a}{a} = \frac{20}{500} = \pm 0.08 \quad A.7$$

$$\frac{\partial L}{L} = \frac{2000}{140000} = \pm 0.015$$

2. Microtube: Inner diameters 596 ± 12.7 (μm), 889 ± 12.7 (μm), outer diameters 901.7 ± 38.1 (μm), 1066.8 ± 38.1 (μm), lengths 60000 ± 2000 (μm), 120000 ± 2000 (μm). Therefore:

118

$$\frac{\partial D_i}{D_i} = \pm 0.021, 0.014$$

$$\frac{\partial D_o}{D_o} = \pm 0.042, 0.035 \qquad A.8$$

$$\frac{\partial L}{L} = \pm 0.034, 0.016$$

Mass flow

The volumetric flow rate in the microchannel was measured using a micro gear pump and a flow turbine meter.

- Micro gear pump

  The gear pump with the maximum uncertainty of $\frac{\partial \dot{m}}{\dot{m}} = \pm 0.01$ were used for low mass flow rates.

- Turbine meter

  A turbine meter was used for calculating higher flow rates. Its maximum uncertainty was $\frac{\partial \dot{m}}{\dot{m}} = \pm 0.005$

Channel cross sectional area

The cross sectional areas of the channel and microtube are calculated as following

$$A = a \times W$$

$$A = \pi \frac{D_i^2}{4} \qquad A.9$$

Therefore, the uncertainty in the cross sectional areas are:

$$\frac{\partial A}{A} = \pm \sqrt{\left(\frac{\partial a}{a}\right)^2 + \left(\frac{\partial W}{W}\right)^2}$$

$$\frac{\partial A}{A} = \pm \sqrt{\left(2 \times \frac{\partial D_i}{D_i}\right)^2} \qquad A.10$$

Substituting the uncertainty in the channel dimensions into the general equation then the maximum uncertainties are:

$$\left.\frac{\partial A}{A}\right|_{\text{Channel}} = \pm 0.1$$

$$\left.\frac{\partial A}{A}\right|_{\text{microtube}} = \pm 0.042$$

A.11

Channel surface area

The channel surface area cannot be expressed in terms of a product of its variables. Therefore, Equation A.5 cannot be used to calculate the uncertainty. For these cases the uncertainly can be calculated using the general form:

$$A_S = (a + 2W)L$$

$$A_S = \pi D_o L$$

A.12

$$\partial A_S = \pm \sqrt{\left(\frac{\partial A_s}{\partial a} \delta a\right)^2 + \left(\frac{\partial A_s}{\partial W} \delta W\right)^2 + \left(\frac{\partial A_s}{\partial L} \delta L\right)^2}$$

$$\partial A_S = \pm \sqrt{\left(\frac{\partial A_s}{\partial D_o} \delta D_o\right)^2 + \left(\frac{\partial A_s}{\partial L} \delta L\right)^2}$$

A.13

$$\frac{\partial A_s}{\partial a} = L \quad \frac{\partial A_s}{\partial W} = 2L \quad \frac{\partial A_s}{\partial L} = a + 2W$$

$$\frac{\partial A_s}{\partial D_o} = L \quad \frac{\partial A_s}{\partial L} = D_o$$

A.14

Substituting Equation A.42 into Equation A.41

$$\partial A_S = \pm \sqrt{(L\delta a)^2 + (2L\delta W)^2 + ((a + 2W)\delta L)^2}$$

$$\partial A_S = \pm \sqrt{(L\delta D_o)^2 + (D_o \delta L)^2}$$

A.15

The relative uncertainty can be obtained dividing Equation A.43 by As then:

$$\frac{\partial A_S}{A} = \pm \sqrt{\left(\frac{L}{(a + 2W)L} \delta a\right)^2 + \left(\frac{2L}{(a + 2W)L} \delta W\right)^2 + \left(\frac{(a + 2W)}{(a + 2W)L} \delta L\right)^2}$$

A.16

120

$$\frac{\partial A_S}{A} = \pm \sqrt{\left(\frac{L}{\pi D_o L} \delta D_o \right)^2 + \left(\frac{D_o}{\pi D_o L} \delta L \right)^2}$$

Rearranging terms in Equation A.44, the uncertainty in the channel surface area can be expressed as:

$$\frac{\partial A_S}{A} = \pm \sqrt{\left(\frac{a}{(a+2W)} \frac{\delta a}{a} \right)^2 + \left(\frac{2W}{(a+2W)} \frac{\delta W}{W} \right)^2 + \left(\frac{\delta L}{L} \right)^2} \qquad \text{A.17}$$

$$\frac{\partial A_S}{A} = \pm \sqrt{\left(\frac{1}{\pi} \frac{\delta D_o}{D_o} \right)^2 + \left(\frac{1}{\pi} \frac{\delta L}{L} \right)^2}$$

Channel perimeter

The perimeter of the channel and microtube are defined as $P = 2(a+W)$ and $P = \pi D_o$, respectively. After using the general form and rearrangement of terms:

$$\frac{\partial P}{P} = \pm \sqrt{\left(\frac{a}{(a+W)} \frac{\delta a}{a} \right)^2 + \left(\frac{W}{(a+W)} \frac{\delta W}{W} \right)^2} \qquad \text{A.18}$$

$$\frac{\partial P}{P} = \pm \sqrt{\left(\pi \frac{\delta D_o}{D_o} \right)^2}$$

Hydraulic diameter

The hydraulic diameter is defined as $D_h = \dfrac{4A}{P} = \dfrac{2aW}{a+W}$. After using the general form and rearrangement of terms, the uncertainty in the hydraulic diameters are:

$$\frac{\partial D_h}{D_h} = \pm \sqrt{\left(\frac{a}{(a+W)} \frac{\delta a}{a} \right)^2 + \left(\frac{W}{(a+W)} \frac{\delta W}{W} \right)^2} \qquad \text{A.19}$$

$$\frac{\partial D_h}{D_h} = \pm \frac{\partial D_o}{D_o}$$

Mass flux

Mass flux is calculated using $G = \dfrac{\dot{m}}{A}$ equation. The uncertainty in the mass flux is:

$$\frac{\partial G}{G} = \pm \sqrt{\left(\frac{\delta \dot{m}}{\dot{m}}\right)^2 + \left(\frac{\delta A}{A}\right)^2} \quad \text{A.20}$$

Reynolds number

Reynolds number is calculated using $\text{Re} = \dfrac{G D_h}{\mu}$ equation. After applying the general form and rearrangement of terms:

$$\frac{\partial \text{Re}}{\text{Re}} = \pm \sqrt{\left(\frac{\delta G}{G}\right)^2 + \left(\frac{\delta D_h}{D_h}\right)^2 + \left(\frac{\delta \mu}{\mu}\right)^2} \quad \text{A.21}$$

Heat flux

Single-phase: The heat flux during single-phase testing was calculated from $q_W = \dfrac{\dot{m} c_p \left(T_{out} - T_{in}\right)}{A_s}$. After applying the general form and rearrangement of terms:

$$\frac{\partial q_W}{q_W} = \pm \sqrt{\left(\frac{\delta \dot{m}}{\dot{m}}\right)^2 + \left(\frac{\delta c_p}{c_p}\right)^2 + \left(\frac{T_{out}}{T_{out} - T_{in}} \frac{\delta T_{out}}{T_{out}}\right)^2 + \left(\frac{T_{in}}{T_{out} - T_{in}} \frac{\delta T_{in}}{T_{in}}\right)^2 + \left(\frac{\delta A_s}{A_s}\right)^2} \quad \text{A.22}$$

Flow boiling: The heat flux in the microchannel is defined as $q_W = \dfrac{Q_{fluid}}{A_s}$, where the heat removed by the uid (Q_{fluid}) is determined by (Liu and Garimella 2007):

$$Q_{fluid} = Q_{total} - Q_{loss}(T_W) = Q_{total} - \left(m(T_W) + b\right) \quad \text{A.23}$$

The total heat transfer rate (Q_{total}) is calculated base on the voltage, current and resistance according to $Q_{total} = V I$. Therefore, the heat transfer rate by the fluid Q_{fluid} is:

$$Q_{fluid} = V I - \left(m(T_W) + b\right) \quad \text{A.24}$$

Neglecting the uncertainties in the slope m and intercept b, and applying the general form, the uncertainty in the heat removed by the uid reduces to:

$$\partial Q_{fluid} = \pm \sqrt{(I\delta V)^2 + (V\delta I)^2 + (m\delta T_w)^2} \quad A.25$$

Then relative uncertainty in the heat rate for two-phase flow is:

$$\frac{\partial Q_{fluid}}{Q_{fluid}} = \pm \sqrt{\left(\frac{1}{1-\frac{(mT_W+b)}{VI}}\frac{\partial V}{V}\right)^2 + \left(\frac{1}{1-\frac{(mT_W+b)}{VI}}\frac{\partial I}{I}\right)^2 + ... \left(\frac{1}{\frac{VI}{mT_W}-1-\frac{b}{mT_W}}\frac{\partial T_W}{T_W}\right)^2} \quad A.26$$

The relative uncertainty in the heat flux q_W can be calculated from:

$$\partial q_W = \pm \sqrt{\left(\frac{\delta Q_{fluid}}{Q_{fluid}}\right)^2 + \left(\frac{\delta A_S}{A_s}\right)^2} \quad A.27$$

Heat transfer coefficient

The local heat transfer coefficient for saturated two-phase flow was calculated as $h = \frac{q_W}{(T_W - T_{sat})}$. After applying the general form and rearrangement of terms:

$$\frac{\partial h_{tp}}{h_{tp}} = \pm \sqrt{\left(\frac{\partial q_W}{q_W}\right)^2 + \left(\frac{T_W}{T_W - T_{sat}}\frac{\partial T_W}{T_W}\right)^2 + \left(\frac{T_{sat}}{T_W - T_{sat}}\frac{\partial T_{sat}}{T_{sat}}\right)^2} \quad A.28$$

The uncertainty of the heat transfer coefficient for subcooled flow boiling (sfb) and single-phase (sp) flow can be obtained from saturated flow boiling equation, just substituting the saturated temperature with the fluid temperature. Estimated uncertainty in the heat transfer coefficient is as follows:

$$\frac{\partial h_{sp,\&sfb}}{h_{sp\&sfb}} = \pm \sqrt{\left(\frac{\partial q_W}{q_W}\right)^2 + \left(\frac{T_W}{T_W - T_{sat}}\frac{\partial T_W}{T_W}\right)^2 + \left(\frac{T_f}{T_W - T_f}\frac{\partial T_f}{T_f}\right)^2} \quad A.29$$

Nusselt number

The local signle phase Nusselt number was calculated as $Nu = \dfrac{h D_h}{k_f}$. After applying the

general form and rearrangement of terms:

$$\frac{\partial Nu}{Nu} = \pm \sqrt{\left(\frac{\partial h_{sp}}{h_{sp}}\right)^2 + \left(\frac{\partial D_h}{D_h}\right)^2 + \left(\frac{\partial k_f}{k_f}\right)^2} \quad \text{A.30}$$

Friction factor

The friction factor of single-phase flow was calculated as $f = \dfrac{\Delta P\, D_h}{L\,\rho V^2} = \dfrac{\Delta P\, D_h\, \rho}{L\, G^2}$. After

applying the general form and rearrangement of terms:

$$\frac{\partial f}{f} = \pm \sqrt{\left(\frac{\partial \Delta P}{\Delta P}\right)^2 + \left(\frac{\partial \rho}{\rho}\right)^2 + \left(\frac{\partial L}{L}\right)^2 + \left(2\frac{\partial G}{G}\right)^2 + \left(\frac{\partial D_h}{D_h}\right)^2} \quad \text{A.31}$$

Vapor quality

The vapor quality at the exit of the channel was calculated based on an energy balance as

$x = \dfrac{\left[\dfrac{Q}{\dot{m}} - c_p\left(T_{sat} - T_{in}\right)\right]}{h_{fg}}$. After applying the general form and rearrangement of terms, the

uncertainty of the vapor quality reduces to:

$$\frac{\partial x}{x} = \pm \sqrt{ \begin{array}{l} \left(\frac{\partial h_{fg}}{h_{fg}}\right)^2 + \left(\frac{1}{1 - \frac{\dot{m}c_p(T_{sat}-T_{in})}{Q_{fluid}}}\frac{\partial Q_{fluid}}{Q_{fluid}}\right)^2 + \left(\frac{1}{1 - \frac{\dot{m}c_p(T_{sat}-T_{in})}{Q_{fluid}}}\frac{\partial \dot{m}}{\dot{m}}\right)^2 + ... \\ ... \left(\frac{1}{\frac{Q_{fluid}}{\dot{m}c_p(T_{sat}-T_{in})}-1}\frac{\partial c_p}{c_p}\right)^2 + \left(\frac{c_p T_{sat}}{\frac{Q_{fluid}}{\dot{m}}-c_p(T_{sat}-T_{in})}\frac{\partial T_{sat}}{T_{sat}}\right)^2 + ... \\ ... \left(\frac{c_p T_{in}}{\frac{Q_{fluid}}{\dot{m}}-c_p(T_{sat}-T_{in})}\frac{\partial T_{in}}{T_{in}}\right)^2 \end{array} } \qquad \text{A.32}$$

PUBLICATIONS

JOURNAL PUBLICATIONS

Abdolali Khalili Sadaghiani, Ali Koşar, "Experimental Study on Subcooled Flow Boiling in Horizontal Microtubes and Effect of Heated Length" Heat Transfer Engineering, (2015). (under review)

Abdolali Khalili Sadaghiani, Ali Koşar, "Numerical and experimental investigation on the effects of diameter and length on high mass flux subcooled flow boiling in horizontal microtubes", International Journal of Heat and Mass Transfer, (2015). (under review)

Abdolali Khalili Sadaghiani, Mehmet Yildiz, Ali Koşar, "Numerical modeling of heat transfer characteristics of nanofluid flow in a horizontal microtube", International Journal of Thermal Sciences, (2015). (under review)

Abdolali Khalili Sadaghiani, Ali Koşar, "Numerical investigation of first and second order slip flow in microchannel heat sinks with pin fins", ASME Journal of Heat Transfer, (2015). (under review)

CONFERENCE PRESENTATIONS

Abdolali Khalili Sadaghiani, Yağmur Şişman, Gözde Özaydın İnce and Ali Koşar, "An Experimental Study on Flow Boiling Characteristics of pHEMA Nano-coated Surfaces in a Microchannel", ASME 2016 5th Micro/Nanoscale Heat and Mass Transfer International Conference, (MNHMT2016, Biopolis, Singapore), (January 2016).

M. Karimzadehkhouei, **A. Khalili Sadaghiani**, K. Şendur, M. P. Mengüç and A. Koşar, "Experimental Study on Heat Transfer of Multi-Walled Carbon Nanotubes/water Nanofluid in Horizontal Microtubes", ASME 2016 5th Micro/Nanoscale Heat and Mass Transfer International Conference, (MNHMT2016, Biopolis, Singapore), (January 2016).

Yağmur Şişman, **Abdolali Khalili Sadaghiani**, Khedir R. Khedir, Tansel Karabacak and Ali Koşar "Nucleate Boiling Heat Transfer Augmentation Using Nanostructured Al-Alloy Plates", ASME 2016 5th Micro/Nanoscale Heat and Mass Transfer International Conference, (MNHMT2016, Biopolis, Singapore), (January 2016).

Abdolali Khalili Sadaghiani, Yağmur Şişman, Efe Armağan, Gözde Özaydın İnce and Ali Koşar, "On the effect of crosslinked pHEMA nano coating on flow boiling in a rectangular microchannel", 11th Nanoscience and Nanotechnology Conference, (NanoTR-11, Ankara, Turkey), (June-2015).

M. Karimzadehkhouei, **A. Khalili Sadaghiani**, K. Şendur, M. P. Mengüç and A. Koşar, "Effect of Multi-Walled Carbon Nanotubes on Single-Phase Heat Transfer", 11th Nanoscience and Nanotechnology Conference, (NanoTR-11, Ankara, Turkey), (June-2015).

Abdolali Khalili Sadaghiani, Sinan Eren Yalçin, Ali Koşar, "Experimental study of subcooled flow boiling in horizontal microtubes", 9th International Conference on Boiling and Condensation Heat Transfer, (Boiling and Condensation 2015, Boulder, Colorado), (April-2015).

Abdolali Khalili Sadaghiani, Ali Koşar, "Numerical investigation of slip flow in microchannel heat sinks with pin fins", ASME International Mechanical Engineering Congress and Exposition (IMECE2014, Montreal, Canada), (November-2014). **(Recipient of the Best Paper Award)**